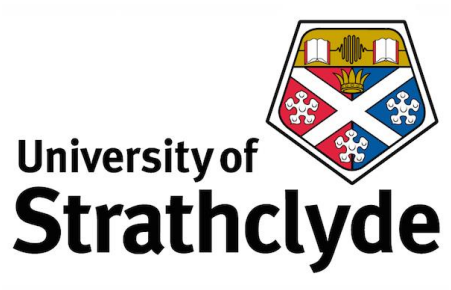

Investigating state-dependent pontine cholinergic activity during REM sleep and P-waves *in vivo*

Amisha Patel

A thesis submitted to the University of Strathclyde in accordance with the requirements for award of the degree of Doctor of Philosophy at the Strathclyde Institute of Pharmacy and Biomedical Sciences

2020

Declaration of authenticity and author's rights

This thesis is the result of the author's original research. It has been composed by the author and have not been previously submitted for examination which has led to the award of a degree.

Signed: Amisha Patel Date: 23rd March 2020

Published Work

The following papers were published during the course of this PhD:

Héricé, C., **Patel, A. A.**, & Sakata, S. (2019). Circuit mechanisms and computational models of REM sleep. *Neuroscience research*, *140*, 77-92.

Tsunematsu, T., **Patel, A. A**., Onken, A., & Sakata, S. (2020). State-dependent brainstem ensemble dynamics and their interactions with hippocampus across sleep states. *Elife*, *9*, e252244.

Patel A. A, McAlinden, N., Mathieson K., and Sakata, S. (2020). Simultaneous electrophysiology and fiber photometry in freely behaving mice. *Frontiers in Neuroscience*, 14:148.

International conference poster presentations

Amisha Patel, Niall McAlinden, Keith Mathieson, Shuzo Sakata. Functional role of brainstem cholinergic neurons in REM sleep regulation. (FENS, Berlin, 2018)

Amisha Patel, Niall McAlinden, Keith Mathieson, Shuzo Sakata. Monitoring cell-type-specific population activity of brainstem cholinergic neurons with fibre photometry. (OPTOGEN, Glasgow, 2018)

Amisha Patel, Niall McAlinden, Keith Mathieson, Shuzo Sakata. Monitoring cell-type-specific population activity of brainstem cholinergic neurons with fibre photometry. (Sculpted Light in the Brain, London, 2019)

Acknowledgements

I would like to first and foremost, thank my supervisor, Dr Shuzo Sakata for his guidance, expertise and mentoring throughout my PhD. I would also like to thank him for giving me the opportunity to carry out this research and for the encouragement to improve and refine my technical and professional abilities. I am also grateful to the Sakata Lab members (old and new) and collaborators for their expertise, training and most importantly, their friendship.

Thank you to my dearest friends and family for their patience, words of encouragement and solace when it got tough and the celebrations when the tide turned in my favour.

A special thanks goes to the animal unit technical staff, who advised and helped care for all of the mice featured in this thesis.

Last but not least, I am indebted to all the mice used in this study. Without them, this research would not have been possible. An extra special thank you goes to: Dobby, Elsa, Kilmonger, Obi-wan, Ariel, Bellatrix, Hermione, Mulan, Faraday and Goldilocks for providing the data to create the graphs presented here and being the backbone of this thesis.

Table of contents

Table of figures

List of tables

List of abbreviations

AAV	Adeno-associated virus
ACh	Acetylcholine
AD	Alzheimer's Disease
ANOVA	Analysis of variance
APP	Amyloid precursor protein
ChAT	Choline acetyltransferase
AW	Awake
BF	Basal forebrain
C-PBL	Caudo-lateral peribrachial
DAPI	4′,6-diamidino-2-phenylindole
DBS	Deep brain stimulation
DMH	Dorsomedial hypothalamus
DRN	Dorsal raphe nucleus
EEG	Electroencephalogram
EMG	Electromyography
ERP	Event related potentials
FAD	Familial Alzheimer’s Disease
FRET	Förster resonance energy transfer
GABA	Gamma-aminobutyric acid
GAT	GABA transporter
GECI	Genetically encoded calcium indicator
GEVI	Genetically encoded voltage indicator
GFP	Green fluorescent protein
GUI	Graphical user interface
ISF	Interstitial fluid
LC	Locus coeruleus
LDT	Laterodorsal tegmental nucleus
LED	Light emitting diode
LFP	Local field potential
LGB	Lateral geniculate body
LPG	Lateral paragigantocellular nucleus
LPT	Lateral pontine tegmentum
MCH	Melanin concentrating hormone
MnPO	Median preoptic
MRI	Magnetic resonance imaging

NA	Noradrenaline
NFT	Neurofibrillary tangles
NMDA	N-methyl-D-aspartate
NREM	Non rapid eye movement
OH	Orexin/hypocretin neurons
ORX	Orexin
OSA	Obstructive sleep apnea
PAG	Periaqueductal gray
PB	Parabrachial nucleus
PBS	Phosphate buffer solution
PD	Parkinson's Disease
PGO	Ponto-geniculo-occipital
PPI	Pre-pulse inhibition
PPT	Pedunculopontine tegmentum
PS1	Presenilin 1
PS2	Presenilin 2
RBD	REM sleep behaviour disorder
REM	Rapid eye movement
RMS	Root mean square
RSWA	REM sleep without atonia
SCN	Suprachiasmatic nucleus
SEM	Standard error of mean
SLD	Sublaterodorsal nucleus
TMN	Tuberomammillary nucleus
VLPO	Ventrolateral preoptic
VTA	Ventral tegmental area

Abstract

Rapid eye movement (REM) sleep is a behavioural state during which phasic deflections in pontine LFP, known as pontine waves (P-waves), occur most prominently. Cholinergic pedunculopontine and laterodorsal tegmental nucleus (PPT/LDT) neurons have been implicated in the generation mechanisms of both REM sleep and P-waves. However, given that the PPT/LDT also contains glutamatergic and GABAergic neurons, and is surrounded by other sleep-wake regulating structures, the functional role of cholinergic PPT/LDT neurons has been difficult to discern with traditional electrophysiological, lesion and pharmacological studies. Consequently, contradictory results have been reported and a clear understanding of cell-type specific neural dynamics during REM sleep and P-waves is still lacking. Based on previous studies, it was hypothesised that cholinergic PPT/LDT neuronal activity is correlated with REM sleep initiation and P-waves. To investigate this, a fibre photometry system was designed and built to simultaneously monitor GCaMP6s fluorescence activity from cholinergic PPT/LDT neurons, EEG/EMG signals for polysomnography and pontine LFP for P-wave detection during the sleep-wake cycle in freely moving mice. Results show that cholinergic PPT/LDT activity is greatest during REM sleep, with underlying rhythmic fluctuations. P-waves were more frequent during REM sleep and for the first time, this study shows that P-waves during REM sleep coincide with larger increases in calcium transients compared to NREM sleep in mice. Additionally, peaks in GCaMP6s fluorescence peaks co-occur with P-wave during REM sleep. As sleep disturbances and cholinergic degeneration are associated with Alzheimer's Disease (AD), a pilot study was carried out to investigate the effects of AD pathology on sleep, PPT/LDT cholinergic activity and P-waves. Preliminary results show that sleep disturbances were more profound in aging 5XFAD mice, a mouse model of AD, compared to controls. It is concluded that cholinergic PPT/LDT activity coincides with REM sleep initiation and P-waves, however functional studies are required to determine the causal relationship for both phenomena.

1 Introduction

This chapter will explore the key themes underlying this thesis. I will briefly introduce sleep research in general and then focus on the neurobiology of REM sleep, specifically the contributions of brainstem cholinergic neurons. I will then explore the literature on how cholinergic neurons play a role in sub-second brain waves thought to be important for memory consolidation. Finally, an overview of the technology and tools developed for cell-type specific monitoring of neuronal activity will be provided to help readers understand the nature of this research thesis.

1.1 General Introduction

Sleep is a physiological phenomenon observed throughout the animal kingdom (Siegel, 2008). Although variations in architecture and electroencephalographic patterns have been reported between species, sleep-wake cycles have been identified in birds, fish, reptiles and some insects, to name but a few (Rechtschaffen, 1998, Siegel, 2008, Cirelli and Tononi, 2008). While the function of sleep is not fully understood, it appears to be a critical part of life. In rats, chronic sleep deprivation has been shown to have several negative physiological effects. These include the inability to regulate body temperature, weight loss, increases in food intake, increases in metabolic rate and even death (Rechtschaffen and Bergmann, 1995, Rechtschaffen and Bergmann, 2002). Sleep deprivation has also been linked to cognitive deficits, obesity and emotional dysregulation in both laboratory animals and humans (Knutson et al., 2007, Brown et al., 2012). Sleep appears to also be important for memory consolidation (Stickgold and Walker, 2005) and sleep disruptions have been reported in patients with cognitive disorders such as Alzheimer's disease, Parkinson's Disease and depression (Wetter et al., 2000, Wulff et al., 2010). The cognitive symptoms associated with Alzheimer's disease, for example, may also be influenced by the sleep disturbances observed in patients (Ju et al., 2014).

The modulation of the sleep-wake cycle can be investigated on three timescales. First, by the 24-hour circadian rhythm, which is controlled primarily by the suprachiasmatic nucleus within the hypothalamus (Stephan and Zucker, 1972). Second, on a timescale of hours (in humans) or minutes (in rodents), is the ultradian rhythm. This involves the recurrent cycling of sleep/wake states. Finally, on the second and sub-second scale is the gating of brain states, where behavioural states rapidly switch from one to the next. This thesis will focus on the ultradian rhythm, the second and sub-second modulation of sleep states.

1.2 Sleep architecture in mammals

1.2.1 History of sleep characterisation in humans

The first EEG recordings in humans were carried out in 1929 by a German psychiatrist, Hans Berger, and consisted of placing electrodes on the scalp to measure macroscopic brain signals (Berger, 1929). This subsequently led to the discovery that there were variations in EEG signals between sleep and wakeful states in humans (Loomis et al., 1935a, Loomis et al., 1935b). Signals during wake were characterised by low amplitude, high frequency oscillations, while EEG during NREM sleep typically consisted of high amplitude, low frequency EEG signals (Davis et al., 1937, Steriade, 1993). NREM sleep in humans can be divided into electrophysiologically distinct sub-states, which are defined and labelled slightly differently depending on the naming system. While NREM sleep was originally split into 4 stages (S1 to S4) by Rechtschaffen and Kales (R&K) (Rechtschaffen and Kales, 1968), updated modifications by the American Academy of Sleep Medicine (AASM) (Iber et al., 2007) resulted in 3 NREM sleep stages (N1, N2 and N3), where S3 and S4 from the R&K manual were combined to reflect N3. Briefly, stage 1 of NREM sleep (N1) indicates drowsy wakefulness or the onset of sleep and is dominated with theta oscillations (4-7 Hz). Stage 2 (N2) comprises of sleep spindles and K-complexes (7-15 Hz), while stages 3 and 4 (N3) signify deep sleep and is characterised by delta waves (1-4 Hz) and slow oscillation (0.5-1 Hz) (Brown et al., 2012).

An additional sleep state, REM sleep, was identified in humans in 1953 and then in cats in 1958 (Aserinsky and Kleitman, 1953, Dement, 1958). This state is characterised by rapid eye movements, muscle atonia and changes in cortical EEG, heart rate and breathing rate. EEG signals are similar to those observed during wakefulness (low amplitude and high frequency oscillations) and was therefore, also termed paradoxical sleep by Jouvet (Jouvet, 1962). In contrast to NREM sleep, REM sleep is also dominated by theta and gamma oscillations, particularly in rodents (figure 1.1).

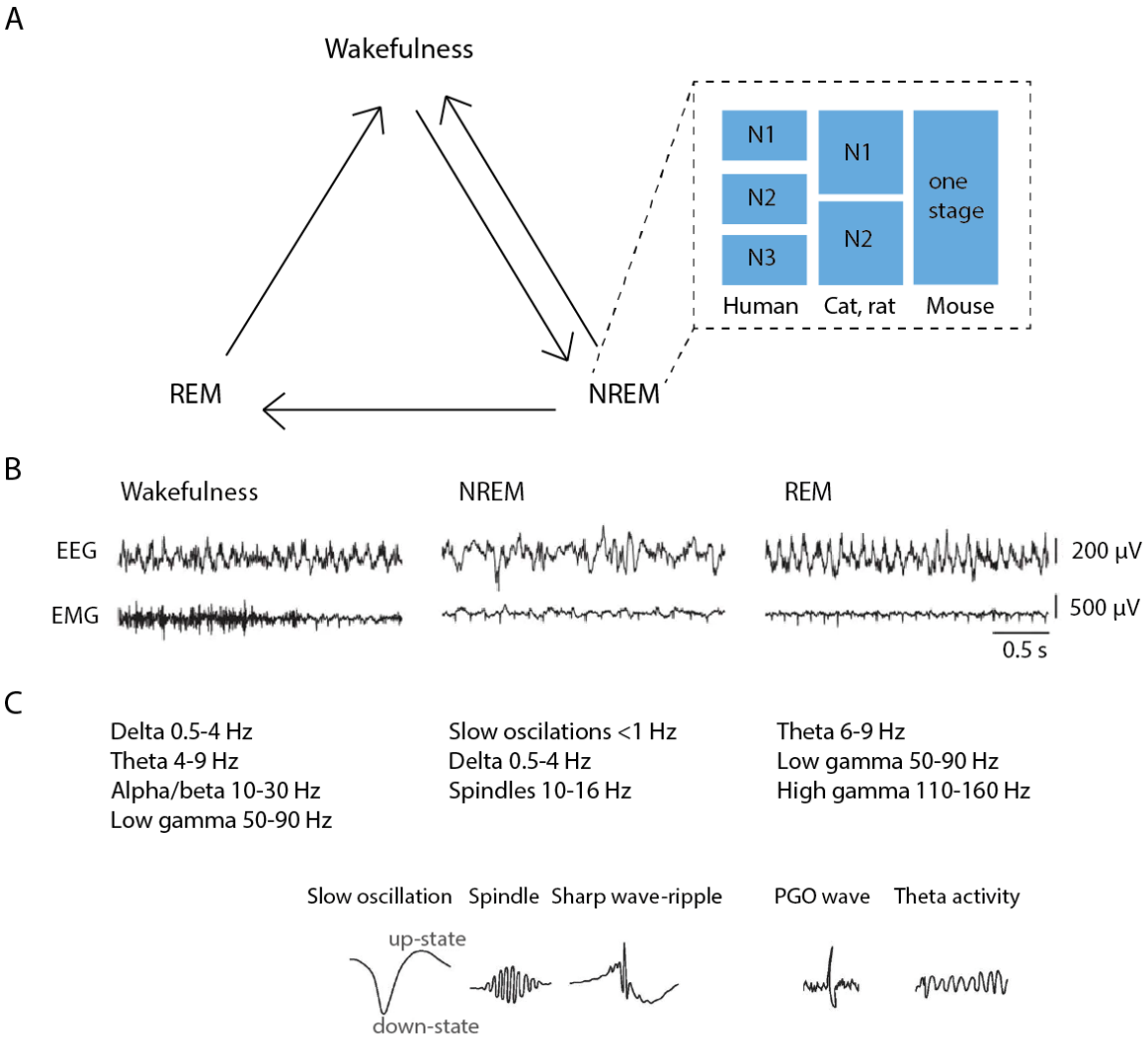

Figure 1.1: Electrophysiological characteristics of sleep.

(A) *Schematic of a sleep-wake states and NREM sub-states in human and common animal models used for sleep research, such as cats, rats and mice.* ***(B)*** *Example EEG and EMG traces during individual sleep-wake states from a mouse. Traces have been obtained from Weber et al. (2016).* ***(C)*** *Dominating EEG frequencies during wakefulness, NREM sleep and REM sleep. Frequencies were obtained from Adamantidis et al. (2019) and traces were extracted from Rasch & Born (2013).*

1.2.2 Sleep architecture in humans

Although there are differences between individuals, humans typically sleep for a single extended period (7-9 hours) during the night. Nightly sleep in normal adults begins with the first stage of NREM sleep (N1) and progresses through the deeper stages of NREM sleep (N2 and N3). After approximately 80 to 100 minutes, people normally transition into their first REM sleep episode of the night. After this, NREM and REM sleep alternate in approximately 90-

minute cycles. There is more NREM sleep at the beginning of the night and REM sleep episodes typically get longer as the night progresses (Carskadon and Dement, 2017) (figure 1.2a). REM sleep follows NREM sleep, which is preceded by wakefulness. Deviations from this results in disorders such as narcolepsy, where people transition from wakefulness to REM sleep.

There are several models for the control of sleep timing and duration. One of which is the two-process model, which consists of the interactions between circadian (process C) and homeostatic (process S) mechanisms (Borbely, 1982, Daan et al., 1984). The circadian rhythm indicates the time of day and is controlled by pacemaker neurons within the suprachiasmatic nucleus (SCN) (Welsh et al., 2010). The homeostatic process, on the other hand is controlled by the amount of time before the last sleep episode. As more time elapses, the homeostatic pressure increases, and the more likely humans and other animals are to fall asleep. Figure 1.3 shows Borbely's two-process model. The regulation of circadian rhythms on sleep-wake states can be investigated through forced desynchrony, where environmental cues such as the timing and duration of lights are altered to disrupt the endogenous circadian clock. Equally, lesioning SCN neurons in animal models help decipher the role of the circadian rhythm (Mistlberger et al., 1983, Edgar et al., 1993). Conversely, the contribution of homeostatic mechanism can be investigated though altering the time between consecutive sleep states through sleep deprivation. A study exploring the effect of SCN lesions and 24 hr REM sleep deprivation in rats by Wurts and Edgar (2000), reported that REM sleep is in fact influenced by both circadian and homeostatic processes. Here, REM sleep deprived rats had a greater tendency to transition to REM sleep during the rest phase compared to SCN lesioned rats, but, the amount of REM sleep did not depend on circadian timing. This suggests that transitions to REM sleep are regulated by the SCN and circadian process, while the amount of REM sleep is influenced by homeostatic processes.

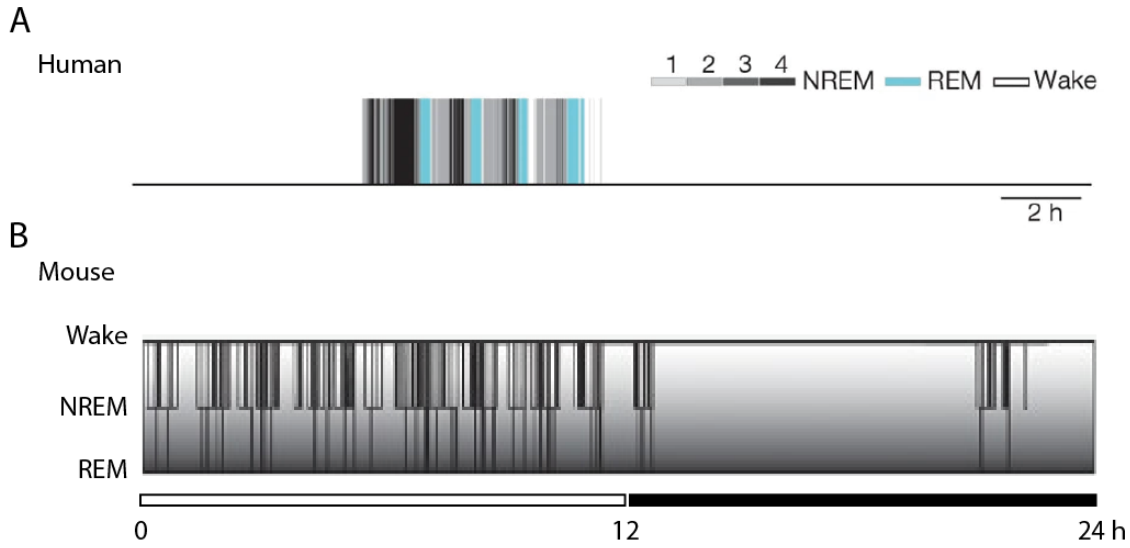

Figure 1.2: Sleep-wake architecture in humans and mice.

A) *An example hypnogram from a healthy human subject during a 22-hour recording. Trace from Weber et al (2016).* ***(B)*** *An example of the sleep-wake architecture from a mouse during a 24-hour recording. Sleep in mice is more fragmented compared to humans. They also tend to sleep more during the light cycle. Trace from Genzel et al (2014).*

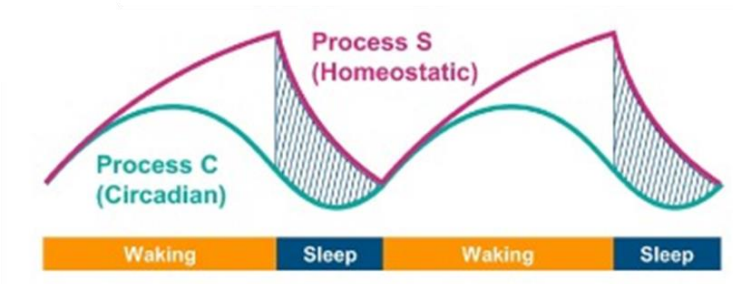

Figure 1.3: Borbely's two-process model.

From Herice et al (2019)

1.2.3 Importance of sleep research

The fact that the average human being spends a third of their life asleep makes the search for the function and mechanisms of sleep interesting. We know both humans and animal experience age-related changes in sleep. New born infants and murine pups spend disproportionately more time in REM sleep compared to other sleep-wake states (Roffwarg et al., 1966, Jouvet-Mounier et al., 1970, Carskadon and Dement, 2017). After approximately 10 days of age, the total amount of REM sleep gradually decreases while NREM sleep increases

in rat pups and stabilises to 7-8.5% REM sleep and 45-48% NREM sleep during a 24 hr period in adulthood (Jouvet-Mounier et al., 1970, Ibuka, 1984). A similar pattern is also observed in humans, where the ratios of REM and stage 2 NREM sleep stabilise at approximately 12 months of age (Louis et al., 1997). On the other hand, ageing humans tend to exhibit reduced total time in sleep, sleep fragmentation and more wakefulness (Mander et al., 2017). Age-dependent effects in rodent studies, however, are inconsistent, with some studies reporting reductions in sleep in older mice, and others observing an increase in total sleep (McKillop et al., 2018, Soltani et al., 2019, McKillop and Vyazovskiy, 2020).

More importantly, sleep disorders such as insomnia and obstructive sleep apnea (OSA), to name but a few, have been cited to have a negative impact on people's health and wellbeing. One example of this is OSA, where there is a complete or impartial reduction in airflow through the upper airways, leading to reduced blood oxygen saturation, poor sleep and excessive daytime sleepiness. OSA has been strongly associated with cardiovascular diseases such as stroke (Punjabi et al., 2009, Redline et al., 2010) and has been correlated with cognitive dysfunctions (Beebe et al., 2003). Sleep disorders in general have also been linked with depression where patients with a sleep disorder commonly reported some form of depression (Vandeputte and de Weerd, 2003). Daytime sleepiness resulting from these disorders have also been attributed to motor vehicle accidents, work related accidents and loss of production, which have both financial and nonfinancial costs to society (Hillman et al., 2018).

Sleep disturbances have also been associated with psychiatric diseases. For example, there is a reduction in the number and amplitude of NREM sleep spindles in schizophrenia patients medicated with atypical antipsychotics, which has been linked to poor sleep dependent memory consolidation associated with a motor sequence task (Ferrarelli et al., 2007, Wamsley et al., 2012). In fact, patients who received the drug eszopiclone, a non-benzodiazepine hypnotic used to treat insomnia, had more sleep spindles but did not result in significant improvements in motor procedural memory where participants performed a motor sequence task before and after sleeping. They did however, show that there was a correlation between the number of sleep spindles and degree of improvement in the task (Wamsley et al., 2013).

Furthermore, sleep disruptions have been linked to a range of other comorbidities and disorders, making research into the neurobiology of sleep ever more pressing. Patients with neurodegenerative diseases such as Alzheimer's Disease (AD) and Parkinson's Disease (PD) exhibit sleep disorders such as insomnia, disturbances in circadian rhythms and excessive daytime sleepiness (Rothman and Mattson, 2012). Sleep disturbances have been found to be a risk factor in the development of dementia (Lim et al., 2013, Ju et al., 2014, Hahn et al.,

2014, Irwin and Vitiello, 2019, Xu et al., 2020) and the severity of these disturbances increase with disease progression (Bliwise et al., 1995, Kumar et al., 2002). While neurodegenerative diseases are multifactorial and have several symptoms, sleep disruptions are thought to be, in part, due to pathological damage to sleep-wake regulating circuitry, but these disruptions may also have a bidirectional effect on disease progression (Ju et al., 2014).

As discussed, chronic sleep disruptions through sleep disorders or other diseases has a great impact on individual wellbeing, quality of life and is a burden on society as it is often the reason for institutionalisation (Knapp et al., 2007, Belger et al., 2019). Uncovering the neurobiological mechanisms underpinning sleep is therefore critical to help find therapeutic targets to alleviate the negative symptoms resulting from sleep disturbances.

1.2.4 Sleep in mammals

Sleep has also been observed throughout the animal kingdom, but sleep-wake durations and architecture vary between species (Siegel, 2009). A review by Jerome Siegel (2005) discusses some of these interspecies differences where animals such as opossums and bats sleep for up to 20 hours a day, but other animals such as elephants and giraffes only sleep for 3-4 hours. Carnivores in general slept more than herbivores, suggesting that diet may be correlated with sleep durations (Siegel, 2005). Additionally, aquatic mammals, such as cetaceans (whales, dolphins and porpoises) and even birds, exhibit unihemispheric slow-wave sleep, where only one hemisphere sleeps at a time (Rattenborg et al., 2000, Lyamin et al., 2008). This is thought to be an adaptive mechanism to detect predators (for birds) and to allow marine mammals to surface and breath.

While non-invasive EEG recordings from humans are valuable for investigating sleep, the spatial resolution of the signals are very coarse. To uncover the sleep regulating brain circuits, more invasive approaches with better spatial resolution and circuitry manipulation are required. As a result, early sleep research was predominantly carried out on cats in the mid- to late- 1900s. The use of rats became increasingly popular in the late 1900s to the present day due to their smaller size, easier animal husbandry and standardised anatomical and histological maps. With the advent of genetic manipulations in rodents through transgenics and viral vectors, rats and mice have now become the standard animal model used for both sleep research and basic research in general (Manger et al., 2008, Herice et al., 2019).

Unlike in humans, cats, rats and mice undergo several sleep-wake cycles throughout a 24-hour period (Sterman et al., 1965, Lucas and Sterman, 1974, Stephenson et al., 2012, Soltani

et al., 2019). In cats and rats, NREM sleep is broken down into two stages, while it remains a single state in mice (figure 1.1a). Both rats and mice are also nocturnal, where they are most active in the dark. Hypnograms showing the differences between typical human and mouse sleep-wake architecture can be seen in figure 1.2.

1.3 General sleep regulating circuitry

There has been extensive research into the mechanisms underlying sleep and scientists have been able to characterise a myriad of networks, brain regions and neurotransmitters that contribute to sleep-wake states and their transitions (Brown et al., 2012, Weber and Dan, 2016, Scammell et al., 2017). Although complex and orchestrated interactions between brain regions and neurotransmitters are required throughout the sleep-wake cycle, both NREM and REM sleep are generated and maintained by distinct areas of the brain. While the anterior hypothalamus, preoptic and basal forebrain areas are known to contain NREM active neurons, REM sleep is thought to be primarily generated by neurons within the brainstem (Jouvet, 1962, Saper et al., 2001, Brown et al., 2012, Weber and Dan, 2016, Herice et al., 2019, Adamantidis et al., 2019).

Briefly, slow oscillations, delta wave, thalamocortical spindles and hippocampal sharp waves-ripples are dominant features of NREM sleep (Brown et al., 2012, Adamantidis et al., 2019). Slow oscillations (<1 Hz) are a result of reverberating thalamic and cortical feedback loops, where membrane potentials of these neurons synchronously switch between depolarised (UP) and hyperpolarised (DOWN) states (Steriade et al., 1993). As a result, both thalamocortical and corticothalamic neurons undergo a period of burst activity during UP states and quiescence during DOWN states (Steriade et al., 2001, Steriade and Timofeev, 2003). These can be recorded from thalamocortical neurons, thalamic relay areas, the thalamic reticular nucleus and primary sensory and motor cortices with both EEG and LFP recordings (Adamantidis et al., 2019). Both slow oscillation and delta waves (1 - 4.5 Hz) are thought to originate from layer 5 cortical neurons (Sanchez-Vives and McCormick, 2000, Lorincz et al., 2015). Sleep spindles are 11-15 Hz oscillations that occur for 0.5-2 seconds during NREM sleep (Adamantidis et al., 2019). Spindles are generated from within the thalamic reticular nucleus, where neurons typically burst during slow wave UP states (Steriade et al., 1985, Steriade, 2000, Klinzing et al., 2016). Pacemaker GABAergic neurons within the thalamic reticular nucleus are thought to generate bursting activity in thalamocortical glutamatergic neurons through post inhibitory rebound (Steriade, 2000, Bazhenov et al., 2000, Halassa et al., 2011). Sharp wave ripples, on the other hand are observed in hippocampal CA1 neurons but also occur in other regions of the hippocampus (Chrobak and Buzsaki, 1996, Khodagholy

et al., 2017). They consist of a transient, high amplitude increase in field potentials (sharp wave), which is then followed by a 150-200 Hz oscillation (the ripple) (Ylinen et al., 1995). Not only do thalamocortical and hippocampal neurons play an active role in generating the oscillations distinct to NREM sleep states, but hypothalamic neurons, and ventrolateral and median preoptic (VLPO and MnPO, respectively) neurons have also been proposed to initiate and maintain NREM sleep (Zhang et al., 2015, Chung et al., 2017, Kroeger et al., 2018).

The discovery of distinct sleep- and wake-promoting areas of the brain led to the proposal of the 'flip-flop switch' model (Saper et al., 2001, Lu et al., 2006). Here, sleep- and wake-promoting circuits inhibit each other, which means that as one system turns on, the other turns off, creating a flip-flop circuit. The advantage of this is that state transitions are rapid, and animals can immediately wake from sleep to avoid predators (figure 1.4). Sleep-promoting VLPO neurons and wake-promoting nuclei mutually inhibit each other, while wake-on neurons inhibit REM-promoting nuclei. Orexin from the lateral hypothalamus has an excitatory effect on wake-on and REM-off neurons (Lu et al., 2006, Saper et al., 2010).

A variety of cell types reside in the brainstem area and their functions with respect to REM sleep are still widely debated. While research into REM sleep circuitry was active in the late 1900s, with the advent of novel technology, the mysteries of the mechanisms underlying REM sleep can be readdressed.

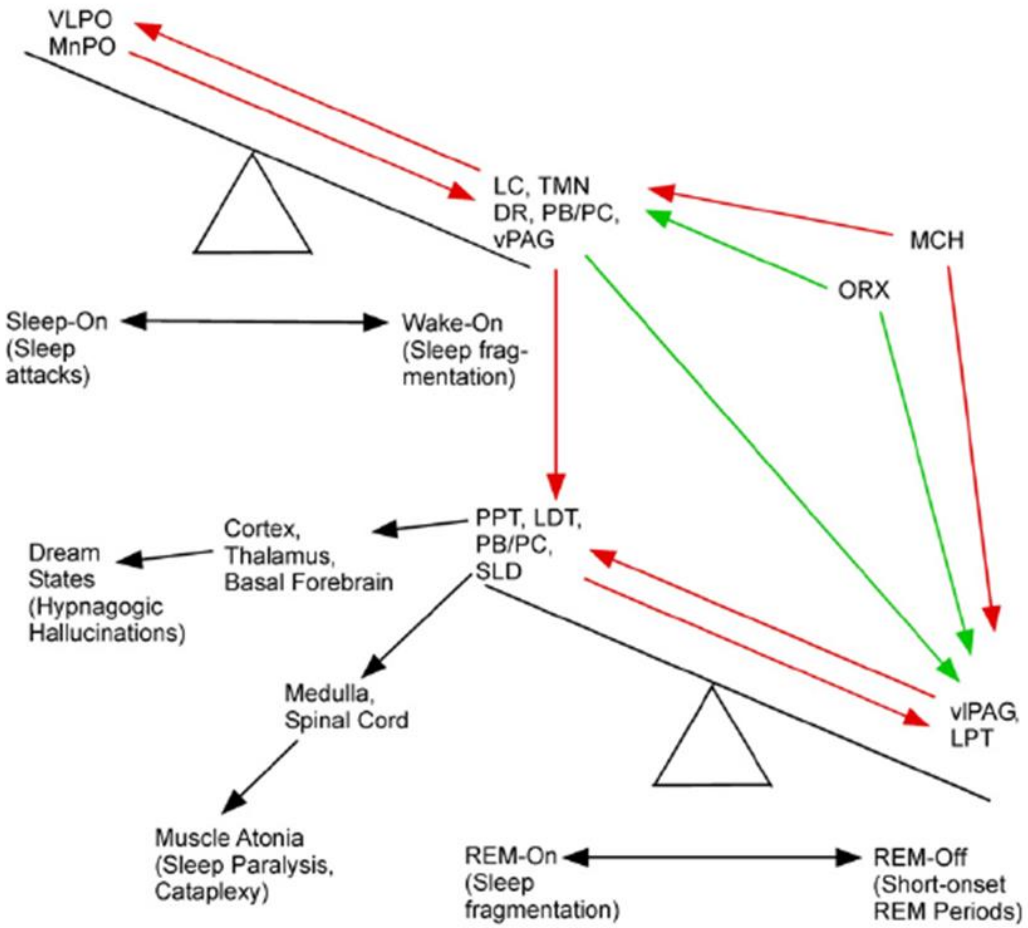

Figure 1.4: Schematic of the flip-flop model of sleep.

Model proposed to explain the rapid transitions between sleep-wake states through mutual inhibition between sleep-, wake- and REM sleep-promoting circuitry. The relationship between sleep in general and wake states was first described by Saper et al (2001). The addition of REM sleep was presented in Lu et al (2006). Red arrows represent inhibitory connections and green arrows represent excitatory projections. Abbreviations: VLPO, ventrolateral preoptic nucleus; MnPO, median preoptic area; LC, locus coeruleus; TMN, tuberomammillary nucleus; DR, dorsal raphe nucleus; PB/PC, parabrachial nucleus/precoeruleus area; vPAG, ventral periaqueductal gray; PPT, pedunculopontine tegmentum, LDT, laterodorsal tegmental nucleus; SLD, sublaterodorsal nucleus; LPT, lateral pontine tegmentum; ORX, orexin; MCH, melanin concentrating hormone. From Saper et al (Saper et al., 2010)

1.4 Brainstem regulation of REM sleep

There are multiple structures and cell-types within the brainstem and hypothalamus that are maximally active during REM sleep (REM-on) or silent during REM sleep (REM-off) (for a comprehensive review on the circuit mechanisms underlying REM sleep, see Herice *et al.* 2019) (figure 1.5). While there are still gaps in our knowledge of REM sleep regulating circuitry, REM promoting neurons can be found in the sublaterodorsal nucleus (SLD) and pedunculopontine tegmentum nucleus and laterodorsal tegmental nucleus (PPT/LDT). Glutamatergic SLD neurons have been found to influence muscle atonia and a subset of glutamatergic neurons control REM sleep (Boissard et al., 2002, Krenzer et al., 2011). Cholinergic neurons in the PPT/LDT have been found to promote the initiation of REM sleep through electrical and optogenetic stimulation studies (Thakkar et al., 1996, Van Dort et al., 2015). The ventral medulla (vM) and ventrolateral periaqueductal gray (vlPAG), on the other hand contain distinct populations of neurons that both promote and supress REM sleep (Sapin et al., 2009, Weber et al., 2015, Weber et al., 2018).

Although the regulation of REM sleep is complex and not restricted on one particular brain structure, it is important to review each structure individually to piece together the underlying circuit mechanisms. I will, therefore, focus on reviewing the literature around the influence of the PPT/LDT on REM sleep regulation. PPT/LDT neurons have been chosen to be investigated further because, although several studies have provided valuable insights into the role of this structure on REM sleep, there are inconsistencies between findings. This could, in part, be due to differences in animal models and species used, but it could also be due to limitations in experimental techniques previously used. There is, therefore, a potential for novel tools such as cell-type specific optical interrogation of neural circuits to provide more detail on the role of these neurons on sleep.

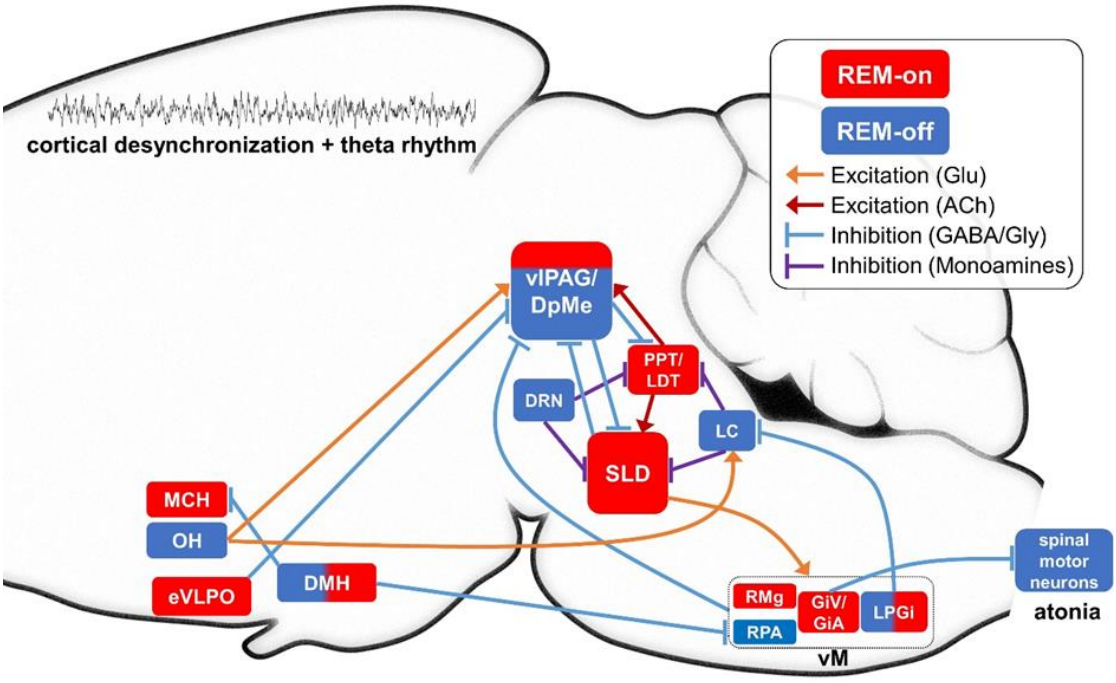

Figure 1.5: REM sleep modulating structures in the brainstem and hypothalamus. *Schematic shows some of the functional connections between REM sleep modulating areas. Abbreviations: 'DMH, dorsomedial hypothalamus; DpMe, dorsal part of the deep mesencephalic reticular nuclei; DRN, dorsal raphe nucleus; eVLPO, extended area of the ventrolateral preoptic area; GiA, alpha gigantocellular nucleus; GiV, ventral gigantocellular nucleus; LC, locus coeruleus; LDT, laterodorsal tegmental nucleus; LPGi, lateral paragigantocellular nucleus; MCH, melanin concentrating hormone neurons; OH, orexin/hypocretin neurons; PPT, pedunculopontine tegmental nucleus; RMg, raphe magnus; RPA, nucleus raphe pallidus; SLD, sublaterodorsal nucleus; vlPAG, ventrolateral periaqueductal gray. Glu, glutamate; ACh, acetylcholine; GABA, γ-aminobutyric acid; Gly, glycine. From Herice et al. (2019).*

1.5 PPT/LDT influences on REM sleep

The pedunculopontine tegmental nucleus (PPT) and laterodorsal tegmental nucleus (LDT) are the main source of brainstem acetylcholine and are located in the caudal cholinergic column (Ch5 and Ch6). PPT/LDT neurons have been found to play a role in the startle response, reward, stress, posture and gait (Jones and Shannon, 2004, Janickova et al., 2017, Fernandez et al., 2018, Azzopardi et al., 2018, Janickova et al., 2019). Additionally, the PPT/LDT has long been implicated in REM sleep, arousal and cortical desynchronization (McCarley, 2007, Weber and Dan, 2016, Mena-Segovia and Bolam, 2017, Scammell et al., 2017). Although pontine cholinergic neurons were originally thought to play a causal role in REM sleep

induction, the exact role of the PPT/LDT in REM sleep remains unknown (Grace and Horner, 2015, Grace, 2015, Van Dort et al., 2015, Kroeger et al., 2017).

1.5.1 PPT/LDT anatomy

Although the boundaries of the PPT/LDT structures are defined by the spread of cholinergic neurons, they contain a heterogeneous population of cholinergic, glutamatergic and GABAergic neurons (Clements and Grant, 1990, Ford et al., 1995, Wang and Morales, 2009). While PPT/LDT neurons are highly innervated by several brain areas, they receive inputs and project to other sleep/wake regulating areas, suggesting that they are a part of the sleep modulating circuitry. Inputs include the cortex, thalamus, hypothalamus, pons, cerebellum, medulla, spinal cord, the basal ganglia, DRN and LC (Saper and Loewy, 1982, Semba and Fibiger, 1992, Mena-Segovia et al., 2008, Martinez-Gonzalez et al., 2011, Mena-Segovia and Bolam, 2017). Outputs include, but are not limited to the thalamus, basal ganglia, basal forebrain (BF), hypothalamus, LC, pontine reticular formation, ventral tegmental area (VTA), SLD and DRN (Cornwall et al., 1990, Semba et al., 1990, Ford et al., 1995, Luppi et al., 1995, Martinez-Gonzalez et al., 2011, Mena-Segovia and Bolam, 2017).

1.5.2 PPT/LDT neuronal activity

Studies investigating the activity of LDT/PPT neurons with *in vivo* electrophysiology, juxtacellular recordings and calcium imaging have shown that different cell types have different state-dependent firing patterns. Cholinergic neurons are maximally active during wakefulness and REM sleep, but glutamatergic and GABAergic neurons are most active either during wakefulness, REM sleep or during both wake and REM sleep (McCarley and Hobson, 1971, El Mansari et al., 1989, Steriade et al., 1990a, Datta and Siwek, 2002, Boucetta et al., 2014, Cox et al., 2016). Consistent with these findings, Fos mapping studies have also shown that both cholinergic and GABAergic neurons are active during REM sleep in cats and rats (Maloney et al., 1999, Torterolo et al., 2001, Verret et al., 2005). C-Fos is an immediate early gene (IEG) and its expression is used as an indirect marker for neuronal activity. This method has been widely used to indicate whether neurons have been recently activated and can be used with relative ease. For sleep studies, animals are sleep deprived and then allowed to transition into rebound sleep for a short period of time before being euthanised. Brain sections are then prepared to be immunostained for c-fos and can also be combined with other markers to provide additional information on cell-type specificity, which is lacking in electrophysiology studies (Verret et al., 2005, Lu et al., 2006). However, one of the limitations to this technique is that neither c-fos nor other IEGs are expressed in chronically active neurons and neuronal activation can occur without fos expression (Kovács, 1998, Kovács, 2008). The poor temporal

resolution of fos mapping studies and inability to quantify changes in activity from baseline, make interpreting results from these studies difficult.

1.5.3 PPT/LDT function in REM sleep

There is an ongoing debate on the functional role of the PPT/LDT in the initiation and maintenance of REM sleep. Lesion (Sastre et al., 1981, Webster and Jones, 1988, Shouse and Siegel, 1992, Petrovic et al., 2013) and pharmacological (George et al., 1964, Amatruda et al., 1975, Baghdoyan et al., 1984a, Gnadt and Pegram, 1986, Deurveilher et al., 1997, Boissard et al., 2002, Coleman et al., 2004, Pollock and Mistlberger, 2005) studies have provided inconsistent and contradictory results (table 1.1). While Webster & Jones (1988) reported an elimination of REM sleep for the first few weeks following neurotoxic lesion in cats, Shouse & Siegel (1992) only observed a reduction in the duration of REM sleep episodes. Bilateral PPT lesions also had little effect on rat sleep-wake architecture and REM sleep (Petrovic et al., 2013) and in one case, PPT lesions, surprisingly increased the percentage of REM sleep (Lu et al., 2006). Interpreting results from these studies is difficult as lesions can encompass additional sleep/wake promoting structures around the PPT/LDT areas.

Similarly, microinjections of cholinergic agonist carbachol or acetylcholinesterase inhibitor, neostigmine, into the brainstem reticular formation increased the duration of REM-like sleep in cats (George et al., 1964, Baghdoyan et al., 1984a) but results from murine species have been varied. On one hand, both Gnadt and Pegram (1986) and Coleman *et al.* (2004) report an increase in REM sleep following respective carbachol (in rats) and neostigmine (in mice) microinjections into the brain stem reticular formation. However, in another study only 13% of the carbachol injections in rats significantly increased the number of REM sleep episodes (Deurveilher et al., 1997) or had no effect at all (Boissard et al., 2002). Similarly, the neostigmine-induced potentiation of REM sleep was also not observed in mice (Pollock & Mistlberger 2005). One possible explanation for the discrepancies between cat and murine species could be that the mechanisms controlling REM sleep are different in both species. Additionally, variations in the volumes of pharmacological agents administered could have resulted in differences in the diffusion area of the agents. While too small a volume may not influence all cells, volumes that are too large could modulate neurons in the surrounding areas, outside the target area.

Electrical stimulation of LDT neurons in cats increased the number and duration of REM sleep episodes (Thakkar et al., 1996). Here, cats were unilaterally implanted with a stimulating bipolar electrode targeting the LDT. Baseline sleep-wake recordings were carried out a day

before continuous stimulation (0.5 ms square pulse at 8 Hz), followed by a second day of baseline recordings. In line with this, cell-specific optogenetic stimulation of cholinergic PPT or LDT neurons in mice resulted in immediate NREM-to-REM transitions (Van Dort et al., 2015). Although there were no changes in the duration of REM sleep, the number of REM sleep episodes increased in ChR2 expressing mice compared to control mice (not expressing ChR2), suggesting that cholinergic neurons within the PPT and LDT may play role in the initiation but not the maintenance of REM sleep. Longer term stimulation of glutamatergic, GABAergic and cholinergic PPT neurons through chemogenetics, however, resulted in varying effects on the sleep-wake architecture of mice (Kroeger et al., 2017). Glutamatergic activation increased the duration of wakefulness, while GABAergic activation moderately reduced the duration of REM sleep. Activation of cholinergic neurons had no effect on REM sleep but did promote light NREM sleep. A limitation of both studies is that they did not record activity from the neurons to know their responses to optogenetic or chemogenetic manipulation (Van Dort et al., 2015, Kroeger et al., 2017). Cholinergic PPT neurons have been reported to fire in phase with slow oscillations and nested gamma oscillations (Mena-Segovia et al., 2008), which could explain the inconsistencies observed in the optogenetic and chemogenetic stimulation protocols. While optogenetic stimulation depolarises neurons in a time-locked fashion, chemogenetic activation increases cholinergic tone over a longer period of time. This suggests that coordinated firing of the PPT/LDT neurons may be required to modulate REM sleep induction.

Taken together, it appears that the neural dynamics within the PPT and LDT are more complex than previously thought. It is also possible that the technology used to investigate the function of these neuron are not refined enough to tease out the intricacies involved. While the current consensus is that PPT/LDT neurons play a modulatory role in REM sleep generation (Grace and Horner, 2015), state-dependent coordination of PPT/LDT neuronal firing and its influence on REM sleep are still not known.

Table 1.1: Summary of functional studies of pontine cholinergic neurons on REM sleep.

Species	Drugs/Cell types	Influence on REM sleep	Reference
Lesion			
Cat		No REM sleep for first few weeks	Webster & Jones (1988)
Cat		Reduction in duration of REM	Shouse & Siegel (1992)
Rat		No effect	Petrovic et al (2013)
Rat		Increase total duration of REM	Lu et al (2006)
Pharmacology			
Cat	Carbachol	Increase REM	George et al (1964)
Cat	Neostigmine	Increase REM	Baghdoyan et al (1984)
Rat	Carbachol	Increase REM	Gnadt & Pegram (1989)
Rat	Carbachol	Only 13% of injections increased number of REM	Deurveilher et al (1997)
Rat	Carbachol	No effect	Boissard et al (2002)
Mice	Neostigmine	Increase REM	Coleman et al (2004)
Mice	Neostigmine	No effect	Pollock & Mistlberger (2005)
Electrical stimulation			
Cat		Increase duration of REM	Thakker et al (1996)
Optogenetic activation			
Mice	ChAT+	NREM-to-REM transitions. Increased number of REM sleep episodes	Van Dort et al (2015)
Chemogenetic activation			
Mice	ChAT+	No effect on REM	Kroeger et al (2017)
	vGluT2+	Increase duration of wakefulness	
	vGAT+	Reduction in duration of REM	

1.6 P-waves: memory and underlying mechanisms

As well as cortical desynchronization, REM sleep is also associated with the presence of ponto-geniculo-occipital (PGO) waves. PGO waves are a result of the synchronous firing of neurons that propagate from the pons to the lateral geniculate body and occipital cortex, with the pontine component of PGO waves being referred to as P-waves (Datta and Siwek, 1997). PGO waves have been identified in humans, however, to measure local field potentials (LFP), invasive implantation of electrodes in the brain are required. As a result, the direct measurement of PGO waves are rare in humans and has been limited to a few patients who have undergone neurosurgery. An example of this is a study that confirmed the pontine component of PGO waves in a 67 year old patient with Parkinson's Disease who was implanted with a DBS electrode in the left PPT (Lim et al., 2007).

The first studies to report PGO waves were carried out in cats as they were a common animal model used for sleep research (Jouvet et al., 1959, Mikiten et al., 1961, Mouret et al., 1963, Brooks and Bizzi, 1963). Several electrophysiological, lesion and pharmacological studies in cats also showed that PGO waves originated from the pons and had different patterns during different behavioural states (Jouvet, 1962, Brooks and Bizzi, 1963, Bizzi and Brooks, 1963, McCarley et al., 1978, Sakai and Jouvet, 1980, Baghdoyan et al., 1984a, Callaway et al., 1987, Steriade et al., 1990b). For example, PGO waves occurred at higher frequencies during REM sleep compared to NREM (Brooks and Bizzi, 1963, Thomas and Benoit, 1967). As rodent models became more popular, due to their size and maintenance costs, research into the underlying mechanisms of these waves became more common in rats. PGO waves in rats also occurred most frequently during REM sleep (Marks et al., 1980, Farber et al., 1980), however a key difference between cats and rats was that PGO waves could be measured from the lateral geniculate body of cats but they are not present in rats. The phasic waves observed in the rat pons are analogous to the pontine element of PGO waves in cat and are, therefore, referred to as P-waves (Marks et al., 1980, Datta et al., 1998). For the purposes of this thesis, when making general comments, I will refer to these waves as P-waves.

There are two main reasons for investigating the mechanisms underlying P-waves. First is that P-waves occur just before the onset of REM sleep and at higher frequencies during REM sleep in humans, cats and rats, suggesting that there may be causal link between P-waves and the initiation and duration of REM sleep (Datta and Hobson, 1994, Lim et al., 2007). Second, while the function of P-waves is unknown, they may be the mechanism by which REM sleep dependent learning and memory takes place (Datta and Siwek, 1997). Considering

the phasic activation of neurons start at the pons and have been confirmed in humans, cats and rodents, P-waves are an appealing phenomenon to investigate.

1.6.1 P-waves and their implications in learning and memory

Sleep in general has historically been implicated in learning and memory (Rasch & Born 2013). The role of REM sleep on memory consolidation was first hypothesised to be through a process called 'reverse learning' or 'unlearning' in 1983 (Crick & Mitchison 1983). Crick and Mitchison proposed that synaptic connections were weakened during REM sleep rather than being strengthened. This has often been interpreted as forgetting, but Crick and Mitchison suggest that unwanted connections are dampened down. They theorised that if these connections were not removed, the brain would eventually be saturated and neural networks would over connect. Consequently, any new information traces, would excite the entire circuit indiscriminately. They suggested that P-waves during REM sleep enable this 'unlearning' by activating the neural networks in a random fashion.

During development, neural plasticity is critical for the formation of neural circuits. Indeed, young humans and mammals spend more time in REM sleep, suggesting that REM sleep is critical for development (Roffwarg et al. 1966). REM sleep deprivation in developing cats and rats impaired cortical plasticity and delayed the critical period for visual cortex development, respectively (Shaffery et al., 2002, Dumoulin Bridi et al., 2015). Equally, sleep deprivation and the reduction in P-waves resulted in abnormal visual experiences in developing cats (Marks et al., 1995). In another study, dendritic calcium transients were monitored from layer 5 pyramidal neurons in the motor cortex of 30-day old (P30) mice before and after a motor learning task. (Li et al., 2017). Here, Li and colleagues report that more newly formed dendritic spines during the motor task were actively pruned when mice were allowed to transition to REM sleep compared to REM sleep deprived mice. Additionally, the size of a fraction of the newly formed spines increased following learning, with a significantly larger proportion of growing spines in mice with more REM sleep. This suggests that REM sleep not only prunes unwanted synapses but also maintains new synapses after learning in mice.

An increase in REM duration and P-wave density have also been linked to memory consolidation in avoidance tasks, where rats that were successful in consolidating fear extinction memory, had an increased density of P-waves following training (Datta, 2000, Datta and O'Malley, 2013). Neurotoxic lesions to P-wave generator cells (within the subcoeruleus) reduced both the number of P-waves and the performance in avoidance learning (Mavanji et al., 2004), while carbachol (a cholinergic agonist) injections to the area enhanced P-wave

density and improved performance in the learning task (Mavanji and Datta, 2003). Additionally, injecting carbachol during NREM sleep has been reported to eliminate the memory impairing effects of REM sleep deprivation (Datta et al., 2004). Although P-waves have been implicated in memory consolidation, the mechanisms by which this occurs is still unknown.

1.6.2 Neural mechanisms underlying P-waves

Early lesion studies found that lesioning neurons at various locations within the brainstem area (PPT, pontomesencephalic tegmentum and peribrachial area) greatly reduced the frequency of P-waves and disrupted sleep in cats (Sakai et al., 1976, Webster and Jones, 1988, Shouse and Siegel, 1992, Datta and Hobson, 1995). To add to these studies, several studies examined brainstem firing patterns in relation to P-waves and identified neurons that were active in phase with P-waves and were labelled as PGO-on cells (Saito et al., 1977, Sakai and Jouvet, 1980, El Mansari et al., 1989, Datta and Hobson, 1994, Datta, 1995). These PGO-on cells were not confined to a particular area or nucleus, but were identified in the LDT, PPT, locus coeruleus, sub coeruleus and caudo-lateral peribrachial area.

Two functional groups of neurons have been identified in the generation of P-waves; triggering neurons and transferring neurons. Triggering neurons generate the P-waves and are located in the caudo-lateral peribrachial (C-PBL) area in cats and dorsal subcoeruleus in rats (Datta and Hobson, 1995, Datta et al., 1998). Transferring neurons, on the other hand are located within the rostral peribrachial (R-PBL) area and receive direct inputs from the C-PBL which in turn, propagate the P-waves to the thalamic LGB in cats (McCarley et al., 1978, Nelson et al., 1983, Steriade et al., 1990a, Steriade et al., 1990b).

Many PGO-on neurons are located in the cat PPT/LDT (Saito et al., 1977, El Mansari et al., 1989). Considering that the main nuclei within the brainstem cholinergic system are PPT/LDT neurons, it has been proposed that cholinergic neurons play a causal role in P-wave generation. PPT lesions reduced the total amount time spent in REM sleep and PGO-wave density in cats (Shouse and Siegel, 1992). However, microinjection of carbachol in the cat peribrachial area, increased PGO wave density for up to 5 days but did not affect the duration of REM sleep (Quattrochi and Hobson, 1999), suggesting that P-waves may not play a causal role in the maintenance of REM sleep.

Overall, P-waves are an interesting phenomenon that still needs to be fully characterised. Although previous studies have been valuable in gaining an insight into the importance of P-

waves, with the use of modern technological advancements, we can gain cell-specific insights into the mechanisms underlying P-wave generation and how they may affect REM sleep.

1.7 Cell-type specific neuronal monitoring

A great deal of knowledge on the firing patterns and coordination of neurons during the sleep-wake cycle have been gained over the past few decades (Brown et al., 2012, Scammell et al., 2017). However, the non-laminar nature of the hypothalamic and brainstem structures discussed previously, make it difficult to physically isolate individual nuclei. We, therefore, still lack a clear understanding of the cell-type specific neural dynamics occurring during REM sleep. Although previous studies have been beneficial to our understanding of REM sleep regulation, the techniques used have their limitations. For example, c-fos mapping studies were used to identify neurons that were active during REM sleep but has poor temporal resolution (Maloney et al., 1999, Verret et al., 2005). Equally, juxtacellular recording experiments have good temporal resolution but are difficult to utilise for long sleep/wake recordings (Boucetta et al., 2014). *In vivo* extracellular electrophysiological recordings provide invaluable information on both multiunit activity and single neurons over longer periods of time and from multiple brain regions with good temporal resolution. However, electrophysiology cannot target specific genetic cell types, has difficulty recording from sparsely activating neurons and has limitations with recording the same neurons over several days or week.

To address these issues, an optical approach to monitor cell-type specific activity has potential to be a powerful tool for sleep research. While the neurophotonics toolbox is rapidly expanding, there are two main components that need to be taken into consideration when designing optical experiments. The first is deciding which sensor to use and the other is determining which imaging technique is most appropriate for the scientific question. Both factors are discussed below.

1.7.1 Optical sensor toolbox

Genetically encoded optical indicators are becoming increasingly popular in *in vivo* research. This is because optical indicators can be genetically encoded to report activity changes that traditional electrophysiology cannot report. These include indicators that report changes in neurotransmitter concentration, pH, intracellular calcium concentrations and transmembrane voltage membranes (Lin and Schnitzer, 2016).

Properties of optical reporters for neural activity

There are several factors that need to be considered when deciding which optical indicator to use for *in vivo* experimentation. One of these include biocompatibility. To accurately monitor neuronal activity, reporters need to be non-toxic and have a limited effect on normal cell physiology. Reporters also need to be sufficiently bright (high signal-to-noise ratio) in order to detect optical signals and to distinguish neural activity from general background noise. The ability to monitor activity over several days, weeks or even months is also an extremely valuable factor for scientific research. An ideal indicator would be photostable and have minimal photobleaching. Other factors include the absorption/emission spectra and kinetics of the reporter. Absorption/emission spectra dictate the illumination and detection wavelengths required to successfully capture an optical readout while the kinetics of the reporter need to match the physiological signal being monitored to allow for accurate interpretation of results.

Genetically encoded calcium indicators (GECIs)

While there are several types of reporters being developed and used by the scientific community, genetically encoded calcium indicators (GECIs) are the most widely used reporters to date, primarily due to their superior brightness and signal-to-noise ratio compared to other indictors. Action potentials open voltage-gated calcium (Ca^{2+}) channels, which lead to reversible and rapid increases in cytoplasmic Ca^{2+} concentrations. Intracellular calcium concentrations then slowly decay through buffer mechanisms and pump-channels over 100-500 ms (Helmchen et al., 1996, Koester and Sakmann, 2000). GECIs report the changes in intracellular calcium concentrations and therefore, give an indirect measure of neuronal activity and action potentials. It should also be noted that calcium signalling in cells is not limited to just voltage-dependent increases but consists of several intracellular processes that function on different time scales and can be unique to different cell types (Berridge et al., 2003).

There are two classes of GECI based on their molecular mechanisms. One involves Förster resonance energy transfer (FRET), which involves the transfer of energy between two fluorophores in close proximity (Jares-Erijman and Jovin, 2003). Example GECIs based on this mechanism include variants from the Yellow Cameleon family such as YC2.60, YC3.60 and YC-Nano (Miyawaki et al., 1999, Nagai et al., 2004, Horikawa et al., 2010) as well as Twitch (Thestrup et al., 2014). The other class of GECI contain a single fluorescence protein (FP), which emits changes in fluorescence intensity (can increase or decrease depending of the specific FP) with increases in cytosolic Ca^{2+}. This includes the GCaMP family of reporters, which are also widely used. With successive improvements and optimisations to reporter brightness, photostability, dynamic range and kinetics, the GCaMP6 and jGCaMP7 series are

the latest and superior GCaMP editions (Akerboom et al., 2012, Chen et al., 2013, Dana et al., 2019).

To facilitate imaging from multiple types of neurons or for combining imaging with optogenetics, each indicator and actuator needs to be monitored and activated independently without influencing the other. One way to do this is to develop indicators with different excitation/emission wavelengths. While there have been promising developments with red-shifted GECIs, variants such as R-GECO1 (Zhao et al., 2011) and R-CaMP2 (Inoue et al., 2015) experience spectral cross-talk and photoswitching with blue light (Akerboom et al., 2013, Wu et al., 2013), limiting their use with optogenetics. Improved variants of these include jRCaMP1a, jRCaMP1b and jRGECO1a (Dana et al., 2016). A recently published study expanded the toolbox further by developing a suite of GECIs with four different excitation wavelengths (blue, green, yellow and red) called xCaMPs (Inoue et al., 2019). This study even demonstrated simultaneous monitoring of three populations of neurons in the medial prefrontal cortex using three colour variants of xCaMP (XCaMP-B, XCaMP-Gf and XCaMP-R) (Inoue et al., 2019).

Even though GECIs have been widely used and enabled scientific advancements, there are some limitations to using calcium indicators that need to be taken into consideration. One of these is the fact that calcium transients are an indirect measure of neuronal activity and they are intrinsically slow. Additionally, the slow decay of Ca^{2+} concentrations following depolarisation make it difficult to extrapolate spike rates, especially when neurons exhibit burst or fast firing rates (Chen et al., 2013, Theis et al., 2016).

Genetically encoded voltage indicators (GEVIs)

Genetically encoded voltage indicators (GEVIs) have the potential to mitigate the limitations that GECIs pose. They report changes in membrane potential which include depolarisation, hyperpolarisation and subthreshold potentials which are intrinsically faster than calcium dynamics. Since the development of the first GEVI, FlaSh in 1997 (Siegel and Isacoff, 1997), there has been a growth in the number of GEVIs engineered, which has simultaneously been facilitated by advancements in protein screening technology. They vary in their molecular structure and have had varied success.

Early generations of GEVIs had poor membrane localisation and were not tested in *in vivo* models (Siegel and Isacoff, 1997, Sakai et al., 2001, Dimitrov et al., 2007, Tsutsui et al., 2008, Baker et al., 2008). Brightness has also been a problem for GEVIs. The faster kinetics of both the voltage indicators and voltage dynamics than calcium transients mean that faster

acquisition frame rates are required for imaging, which result in fewer photons detected per frame. Increasing illumination intensities can compensate for the reduced photon capture, but this also increases the risk of photobleaching and phototoxicity. Although QuasAr1 and QuasAr2 were red-shifted GEVIs and capable of optogenetic stimulation without spectral crosstalk they were not bright enough. GEVIs with the same rhodopsin-based backbone required more than 100 W/cm^2 illumination intensity for *in vivo* imaging (Kralj et al., 2011, Hochbaum et al., 2014). To put this into perspective, *in vivo* GCaMP6 imaging typically requires tens of mW/cm^2 illumination intensity (Chen et al., 2013).

With the requirements stated previously in mind, ArcLight and ASAP1, ASAP2f and Ace2N-mNeon have been promising candidates for *in vivo* voltage imaging (Cao et al., 2013, Gong et al., 2015, Yang et al., 2016). Though measurements varied between the individual indicators, all were biocompatible, had good membrane localisation and had kinetics that were fast enough to detect individual action potentials and subthreshold potentials in Drosophila and/or mouse neurons. The photostability of the indicators were improved allowing all indicators to be used *in vivo* to measure voltage signals in response to sensory stimuli in flies and mice (Cao et al., 2013, Gong et al., 2015, Yang et al., 2016). There were also improvements in brightness compared to the QuasAr series, where indicators typically required 3-25 mW/mm^2 illumination intensities (Gong et al., 2015, Yang et al., 2016). However, photobleaching was still a major problem. Recording times were limited to a maximum of 1.5 hours and continuous imaging resulted in a stable signal for just 10 minutes (Yang et al., 2016).

As with GECIs, spectral diversity has also been engineered in GEVIs. Red-shifted GEVIs such as VARNAM and ASAP3 have been developed (Kannan et al., 2018, Chavarha et al., 2018). An additional chemigenetic voltage indicator, Voltron, has also been engineered. It comprises of a rhodopsin protein inserted into the transmembrane, which is then fluorescently tagged with a synthetic dye (Abdelfattah et al., 2019). The advantages of this is that the synthetic dyes are brighter and photostable, allowing for longer recordings to be carried out. Synthetic dyes with different excitation/emission wavelengths can also be used, resulting in an expanded optical toolbox with the ability to monitor spiking activity from distinct populations of neurons. A disadvantage of Voltron, however, is that the fluorescent dyes need to be delivered to the brain. Recently, two different groups also developed red-shifted GEVIs, which were both compatible with optogenetic stimulation and could monitor neural activity from multiple neurons (Piatkevich et al., 2019, Adam et al., 2019), providing powerful tools for both monitoring neural activity and functionally investigating neural systems with behavioural and optogenetic manipulation.

Overall, the ability to optically monitor voltage dynamics has the potential to be an extremely valuable tool for investigating the functions of the brain. As a result, great advancements in the development of GEVIs has been made since the late 1990s. A summary comparing the main properties of GECIs and GEVIs is shown in figure 1.6.

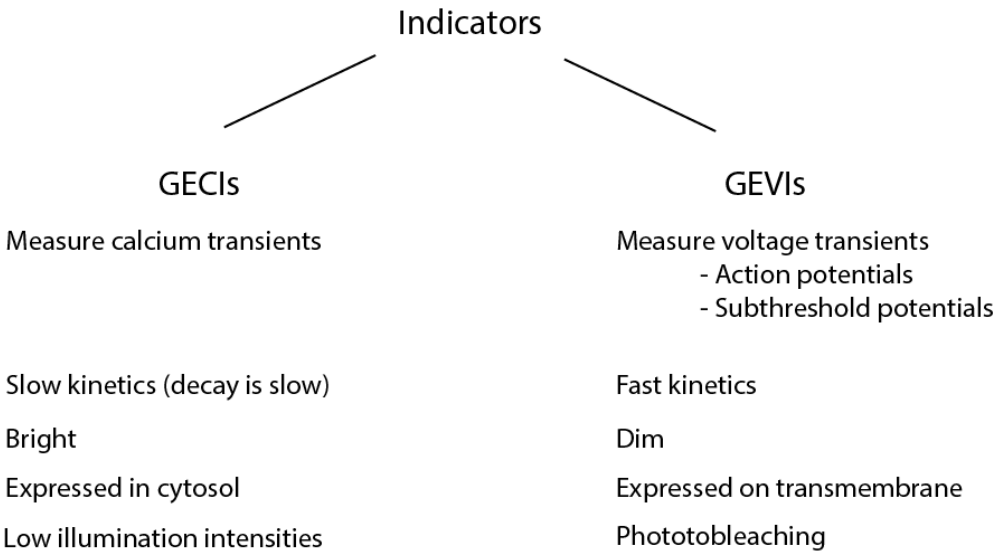

Figure 1.6: Summary of advantages and disadvantages of GECIs and GEVIs for monitoring neuronal activity in vivo.

Methods for expressing optical reporters

There are three methods for expressing optical reporters in the brain. These include, transgenesis, viral gene delivery and *in utero* electroporation. Transgenic mice lines are commonly used in neuroscience and those that express optical reporters include GCaMP2 (Diez-Garcia et al., 2005), YC 3.60 (Atkin et al., 2009) and GCaMP3 (Zariwala et al., 2012). Although transgenic mouse lines take time to develop, recent advances by the Allen Institute for Brain Science have also resulted in several more reporter mouse lines being available, such as mice expressing the GCaMP6 series reporters (Ai93, Ai94, Ai95 and Ai96) and voltage indicators ASAP2s (Ai69 and Ai70) (Madisen et al., 2015, Daigle et al., 2018). Expression is stable over several generations and is valuable for studies that require the expression of the construct throughout the brain.

Another strategy for expressing indicators includes viral injection that involves the direct injection of a genetic construct into a specific region of the brain. To selectively express optical

reporters in a cell-type specific manner, recombinase expressing (e.g. Cre/loxP or FLP/FRT) animal lines in conjunction with recombinase-dependent viruses can be used (Knopfel, 2012, Zeng and Madisen, 2012, Huang and Zeng, 2013). Although this approach is somewhat invasive, it is one of the most common strategies used as several combinations of transgenic mouse lines and viral constructs can be implemented to address individual scientific questions.

The final method, *in utero* electroporation, comprises of the injection of a plasmid into the ventricles of prenatal embryos. This is useful for developmental studies and because there is a temporal and spatial pattern for cortical layer and cell type development, the time and location at which plasmids are injected can used to restrict expression to particular layers and cell types (Tabata and Nakajima, 2001, Borrell et al., 2005).

1.7.2 Techniques to monitoring cell-type specific activity

In conjunction with the optical indicator, an appropriate imaging technique is required to measure optical readouts from the indicators. There are a variety of imaging tools that can be used and choosing an appropriate tool is largely dictated by the scientific question, the location of imaged neurons and weighing up of the advantages and disadvantages of the technique. Imaging tools typically either monitor individual neuronal activity or population activity, synonymous to single cell recordings and local field potentials (LFP) recordings with *in vivo* electrophysiology. One of the main limitations of using light to monitor neuronal activity is that brain tissue scatters light, making it difficult to monitor neuronal activity deep in the brain.

To monitor single cell activity, one-photon and multiple-photon (two- and three- photon) fluorescence microscopy has been developed. Two-photon excitation has better spatial resolution and can image deeper (~500 µm) in the brain compared to one-photon imaging (~100 µm) (Helmchen and Denk, 2005). In fact, two-photon imaging provides a good enough resolution to monitor individual dendritic and soma activity (Chen et al., 2013, Dana et al., 2019, Kerlin et al., 2019). However, imaging is still limited to superficial layers of the brain. To image deeper in the brain, one- and two-photon imaging with implanted endoscopes can be used, or superficial tissue can be aspirated, but this can cause large amounts of damage which can affect the neurons and circuitry being monitored (Jung et al., 2004, Barretto et al., 2011). Using indicators that are excited by longer wavelengths of light, such a red-shifted GECIs or GEVIs, results in less optical scattering and deeper imaging (Jacques, 2013).

Another limitation of two-photon microscopy is that the conventional imaging hardware is heavy and bulky. This meant that animals needed to be head-fixed to monitor neuronal activity.

However, advancements in the miniaturisation of imaging hardware has resulted in head mounted, freely moving recordings from rats (Helmchen et al., 2001).

Fibre photometry, on the other hand, can record population activity from deep brain regions through an implanted optic fibre. Calcium-based fibre photometry to measure aggregate calcium activity has been widely used by the neuroscience community and is compatible with freely moving animals (Lutcke et al., 2010, Gunaydin et al., 2014, Zalocusky et al., 2016, Li et al., 2016). Although cellular resolution is lost, the technique can be scaled up to measure from multiple brain regions (Guo et al., 2015, Kim et al., 2016).

1.8 Hypothesis and aims

As discussed, a great amount of research has been carried out into the mechanisms underlying P-waves and REM sleep. However, the function of P-waves with respect to REM sleep are still unknown. Although cholinergic neurons in the peribrachial area (of which the PPT and LDT are the largest cholinergic nuclei) have been shown to play a role in REM sleep initiation and the transferring of P-waves (Saito et al., 1977, El Mansari et al., 1989), the PPT/LDT contain heterogeneous populations of neurons and the temporal contributions of these neurons to P-waves still needs to be fully explored.

We hypothesise that the synchronous firing of cholinergic PPT/LDT neurons are correlated with P-wave generation and the initiation of REM sleep. To address this, there are two main aims of this project; first, is to observe the activity profile of cholinergic PPT/LDT neurons during the sleep/wake cycle. Second is to investigate the activity profile of cholinergic PPT/LDT neurons in relation to P-waves.

To do this cell-type specific population calcium activity was measured in mice. A fibre photometry system was designed and assembled to measure GCaMP6s activity in freely moving mice. The system was first optimised to measure from a small population of neurons and then used *in vivo* to show state-dependent cholinergic activity during the sleep-wake cycle. GCaMP6s was the chosen indicator because it is the brightest in the GCaMP6 family and is compatible with long illumination periods required for sleep-wake recordings.

To the best of my knowledge, an optical approach to monitor cell-type specific activity has not been used to investigate P-wave generation mechanisms before. There are a few reasons for using a fibre photometry to monitor neuronal activity over techniques that provide single cell resolution. First, considering P-waves are a result of population activity, single cell resolution

is not required. Secondly, PPT/LDT neurons are situated deep in the brain. This means that large amounts of brain tissue would need to be aspirated to get an appropriate field of view with single or multi-photon microscopy. Finally, fibre photometry systems are affordable, do not need specialist expertise in photonics and can be used in freely moving mice.

The next chapter in this thesis will be the materials and methods used to characterise population cholinergic PPT/LDT activity during sleep-wake states and P-waves. Here, the assembly and optimisation of the fibre photometry system will be described. Chapter 3 will present results on the activity of PPT/LDT neurons during sleep-wake states while chapter 4 covers their activity during P-waves. The final results chapter, chapter 5, presents a pilot study into the effects of disease on sleep, cholinergic PPT/LDT activity and P-waves. Here, a short literature review on Alzheimer's Disease and its effect on sleep is included with preliminary results from a mouse model of AD.

2 Materials and Methods

This chapter describes the materials and methods used to carry out experiments and analysis for this thesis. First a brief summary of the animals used in this study will be described. Next, as the fibre photometry system was designed and assembled for this study, details of the system architecture and steps taken to assess its performance and optimise its use for *in vivo* experiments are described. Implant assembly and surgical protocols are then described, followed by experimental methods for *in vivo* recordings. Finally, methods used for data analysis and histology are detailed.

2.1 Animals

All experiments and procedures were performed in accordance with the Animals Scientific Procedures Act of 1986 and with the consent of the Home Office and the University of Strathclyde's Ethical Committee.

Transgenic mice expressing Cre-recombinase specifically in cholinergic neurons (ChAT-Cre) were used (ChAT-IRES-Cre, JAX006410). A total of 37 mice (22 males and 15 females) were used in this study (20 mice were implanted with a bare optic fibre, while 17 mice were implanted with bipolar electrodes to measure P-wave activity). Ages of these mice upon surgery ranged between 8 and 41 weeks (figure 2.1). Mice were injected with a Cre-dependent adeno-associated virus (AAV5-CAG-flex-GCaMP6s-WPRE-SV40 or AAV5-Syn-flex-GCaMP6s-WPRE-SV40, Penn Vector Core; titre $8.3x10^{12}$ GC/ml) to transduce GCaMP6s in ChAT-expressing neurons. Three adeno-associated viral vector (AAV) serotypes were available for GCaMP6s (AAV1, 5 and 9). With the use of a Cre-Lox system, as used in this study, the expression of GCaMP6s can be restricted in a cell-type specific manor with all three serotypes. As a result, any of the three available serotypes would be appropriate for this study. Population calcium transients were then monitored using an implanted optic fibre (20 mice, FP) or an optrode consisting of a bipolar electrode attached to the optic fibre (17 mice, FPpw) (figure 2.1) (also see sections 2.3.3 & 2.4, below).

Where possible, mice were group housed (pairs) but if litter mates were not available, mice were single housed. Mice were housed in high-roofed cages with ad libitum access to food and water, on a 12-hour dark/12-hour light cycle with lights on between 07:00 and 19:00.

A

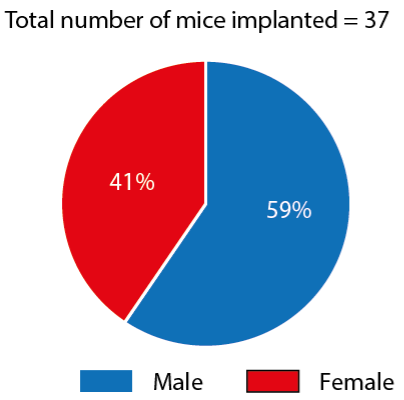

B

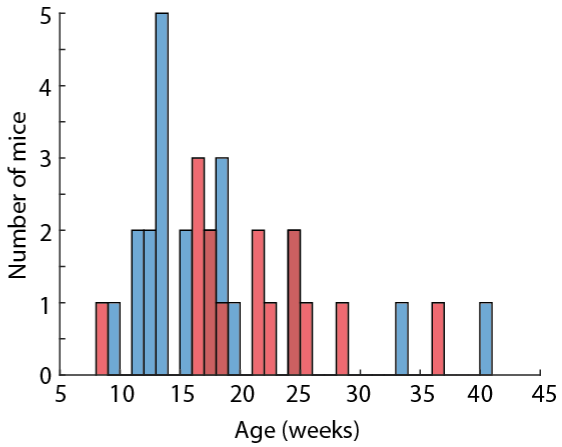

C

	FP	FPpw
Male	15	7
Female	5	10
Total	20	17

Figure 2.1: Sex, age and implant configuration of mice.

(A) *Percentage of male (blue) and female (red) mice.* ***(B)*** *Histogram showing the ages of mice when they were surgically implanted for males (blue) and females (red).* ***(C)*** *Total number of mice implanted with a bare optic fibre (FP) and those implanted with a bipolar electrode attached to the optic fibre (optrode, FPpw). Both FP and FPpw mice feature in chapter 3 analysis while on FPpw mice feature in chapter 4 analysis*

2.2 Fibre photometry

2.2.1 System setup

The fibre photometry system was designed and put together with the advice and help of Dr Niall McAlinden (figure 2.2, figure 2.3 & table 2.1). The system was based on illumination protocols established by the Deisseroth lab (Kim et al., 2016), where one wavelength of light was used to optimally excite GCaMP6s fluorophores (470 nm LED; M470L3, Thorlabs) and another was used to obtain a Ca^{2+}-independent isosbestic signal (405 nm LED; M405L3, Thorlabs). Both LEDs were connected to individual LED drivers (LEDD1B) and were independently controlled with a National Instruments DAQ (NI USB-6211) using custom written Labview software (written by Dr Niall McAlinden). Light from the LEDs passed through aspheric lenses (AL2520M-A, Thorlabs), into an open space, through excitation filters and a dichroic mirror (FB470-10, FB405-10 and DMLP425R, respectively). Light from the illumination path then reached a fibre launch system (KT110/M, Thorlabs) and into a multimode patch cable, which was subsequently connected to an implantable optic fibre on

the mouse (M82L01 and CFM14L05, respectively, Thorlabs). The patch cable and implantable optic fibre were connected using a ceramic 2.5 mm diameter mating sleeve (ADAF1, Thorlabs). Light emissions from GCaMP6s expressing neurons were then collected back through the optic fibre, and directed through a detection path, passing a dichroic mirror (MD498, Thorlabs) to reach a photodetector (NewFocus 2151, Newport). The photodetector was connected to the DAQ for data acquisition (1000 Hz). Light paths were manually aligned by changing the angle of the mirrors and measuring light output at the end of the patch cable with a light meter (PM100A and S120C, Thorlabs).

Electrophysiology signals (EEG and EMG) were recorded using an interface board (RHD2000, Intan Technologies) and an amplifier connecting to the mouse via a tether (RHD2132, intan Technologies). Data was digitised at a sampling rate of 1000 Hz, amplified at 1030V/V and saved with the optical data using the DAQ and Labview program to conserve timings.

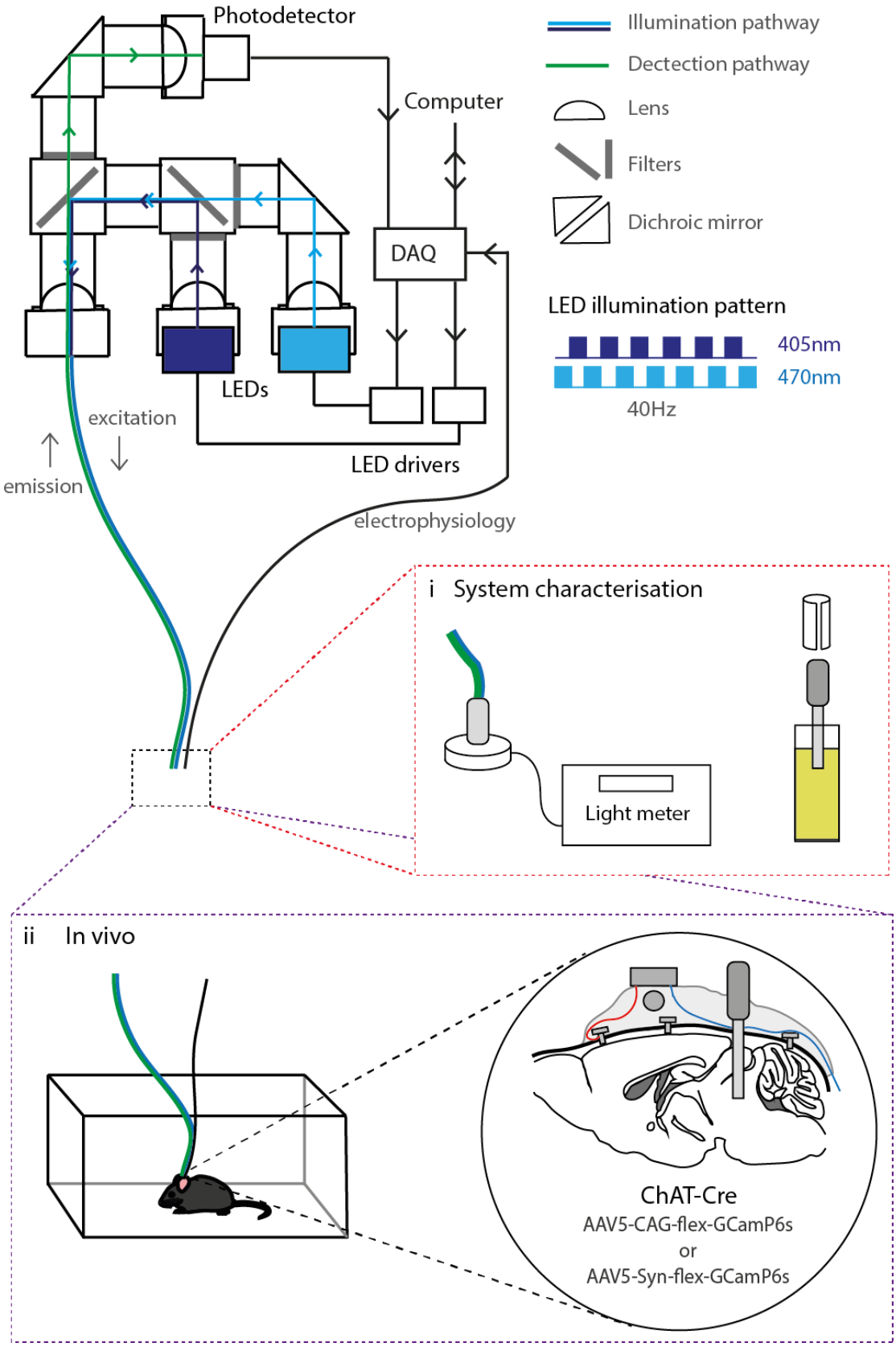
Photodetector
Computer
DAQ
LEDs
excitation
emission
LED drivers
electrophysiology
Illumination pathway
Dectection pathway
Lens
Filters
Dichroic mirror
LED illumination pattern
405nm
470nm
40Hz
i System characterisation
Light meter
ii In vivo
ChAT-Cre
AAV5-CAG-flex-GCamP6s
or
AAV5-Syn-flex-GCamP6s

Figure 2.2: Schematic of fibre photometry system and experimental set up.

Diagram of the fibre photometry system. Both LEDs were independently controlled at 40Hz in a square pulse pattern by the National Instruments DAQ (programmed through Labview software). Light from each LED passed through excitation filters and down the patch cable (illumination pathway, blue), which connected to an implantable multimode optic fibre via a ceramic sleeve. Emitted light was collected back through the optic fibre, patch cable and emission filters to the photodetector (detection pathway, green). Electrophysiology signals were recorded through an Intan Technologies interface board (not shown), which then connected to the DAQ. ***(Insert i)*** *Several measurements were taken to characterise the system. First the light output at the end of the patch cable was measured using a light meter (left). The sensitivity of the system was assessed by placing an optic fibre (connected to the system) in different concentrations of fluorescein solutions (right). Measurements at the detector were taken with different illumination intensities for each LED. The third characterisation (not shown) was to measure the amount of baseline light reaching the detector in the absence of fluorescent molecules. To do this, the patch cable was left to hang in the air and measurements at the detector were taken as light intensities for each LED was increased.* ***(Insert ii)*** *Schematic of the in vivo experimental set up. Mice were tethered to the fibre photometry system and placed in an open-topped Perspex box. Insert shows surgical implantation. Please see figure 2.5 for more details on implant configurations.*

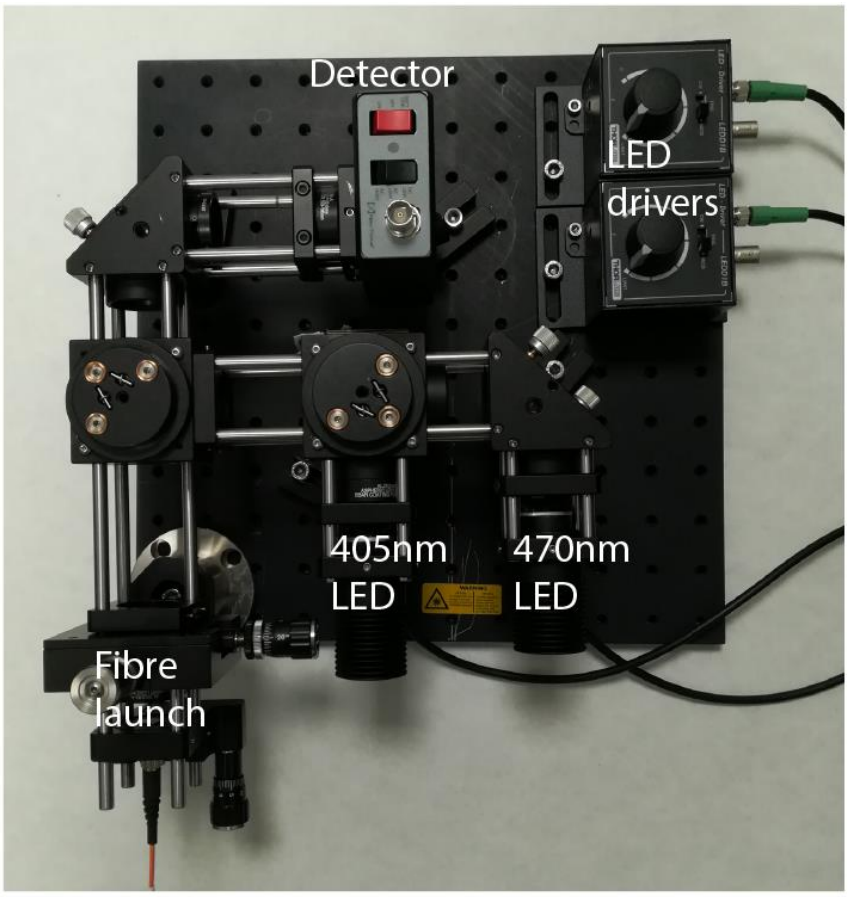

Figure 2.3: Photograph of the optical component of the of the fibre photometry system.

Filters and dichroic mirrors are held in place with mirror mounts and filter holders. All components were secured in place to an optical breadboard (Thorlabs)

Table 2.1: Parts list for fibre photometry system.

Cage rods, post holders and optical mounts were also used to hold optical components (ER2-P4; ER2.5-P4; ER1-P4; UPH50/M & TRM0/M-P5)

Component	Supplier	Product Code	Quantity
Photodetector	Newport	NewFocus 2151	1
470nm LED	Thorlabs	M470L3	1
405nm LED	Thorlabs	M405L3	1
LED driver	Thorlabs	LEDD1B	2
LED power source	Thorlabs	KSP101	2
LED holder	Thorlabs	CP12	2
Dichroic mirror	Thorlabs	DMLP425R	1
Dichroic mirror	Thorlabs	MD498	1
Excitation filter	Thorlabs	FB470-10	1
Excitation filter	Thorlabs	FB405-10	1
Bandpass filter	Thorlabs	MF525-39	1
Broadband dielectric mirror	Thorlabs	BB1-E02	2
Mirror mount	Thorlabs	KCB1C/M	2
Aspheric lens	Thorlabs	AL2520M-A	4
Cage plate for lens	Thorlabs	CP08/M	4
Lens tubes	Thorlabs	SM103-P5	5 pack
Filter holder	Thorlabs	C4W	2
Filter holder	Thorlabs	B4C/M	2
Filter holder	Thorlabs	FFM1	2
Fibre launch	Thorlabs	KT110/M	1
Patch cable	Thorlabs	M82L01	1
Optic fibre implant	Thorlabs	CFM14L05-10	10 pack
Mating sleeve	Thorlabs	ADAF1-5	5 pack

2.2.2 *System characterisation*

Two types of measurements were taken to characterise the fibre photometry system, light output and the systems' ability to detect a fluorescence signal. The brightness of both LEDs were driven by an input voltages between 0 V (off) and 5 V (brightest). To investigate the relationship between the voltage input and light output, the driving voltage for each LED was increased systematically and the light output at the end of the patch cable was measured using a light meter (PM100A and S120C, Thorlabs) (figure 2.2, insert i). All measurements were taken in a dark room (with the lights off).

To assess the sensitivity of the system, fluorescein, a fluorophore with a similar excitation/emission profile as GFP (peak excitation/emission of fluorescein and GFP are around 460nm/515nmm and 475nm/509nm, respectively), was used. An optic fibre (connected to the patch cable) was immersed into different concentrations of fluorescein solution (water, 0.1 µM,0.5 µM, 1 µM, 5 µM and 10 µM) and the average reading over a second was taken at the detector (figure 2.2, insert i). Readings were repeated at various LED input voltages.

Fluorescein cannot give insights into biological correlates; however, it can be used as a valuable tool to assess and optimise the system. Different concentrations of fluorescein can be thought of as being analogous to different expression levels of GCaMP and/or GCaMP-positive neurons *in vivo*. As the PPT/LDT is comprised of a small number of cholinergic neurons, it was predicted that *in vivo*, GCaMP6s signals would also be relatively small. The ideal system should, therefore, be sensitive enough to distinguish between water and the lowest concentration of fluorescein (0.1 µM). Additionally, if the optic fibre is positioned at a slight distance from the GCaMP6s expressing neurons, more light power would be required to excite GCaMP6s proteins. To account for the variability in optic fibre positioning in individual mice, the functional range of the input power from the LEDs should also be as large as possible.

2.2.3 *Photometry system optimisation*

After assembling the photometry system, two initial measurements were taken. The first was to quantify the amount of light reaching the end of the patch cable to identify the illumination intensity range. The second, was to measure the amount of light reaching the detector at different light intensities to provide a baseline threshold. Measurements showed that when the LEDs were turned on to their maximum power (5 V), light output at the end of the patch cable was 1.62 mW/mm^2 and 2.32 mW/mm^2 for the 405 nm and 470 nm LEDs, respectively (figure

2.4a). However, there was a lot of light reaching the detector. The detector saturated at 2 V (405 nm) and 1.6 V (470 nm) LED power, meaning that a maximum of 0.62 mW/mm^2 405 nm and 0.9 mW/mm^2 470 nm of light could be delivered to detect a fluorescence signal. To reduce the amount of light leaking back to the detector and improve the discernibility between water and 0.1 µM, several modification steps were trialled. First, an additional filter (FF01-405/150-25, Semrock) was added to the detection path in the hope of eliminating blue light from the LEDs reaching the detector. This modification had no recognisable effect on the light output at the end of the patch cable (figure 2.4b), but did, improve the functional light input range. The 405 nm LED could be turned on to 4 V and the 470 nm LED to 3 V before the detector saturated when the patch cable was left to hang in the air (figure 2.4c & d). However, the system performed poorly for distinguishing between low concentrations of fluorescein (0.1 µM) and water.

Next, the illumination path was aligned to enter the fibre launch at an angle. The premise of this was that any blue light from the LEDs reflected at the junction between the free space and the optic fibre would be reflected at an angle and therefore, not be aligned with the detection path. This increased the amount of light at the end of the patch cable but did not improve the functional light input range. The detector saturated when both LEDs were turned on to 2 V.

The third approach was to leave both LEDs on at full power for several hours to burn away a reflective coating on the patch cable. After leaving the LEDs on for several days, both the functional range (detector saturated at 4 V and 5 V for 405 nm and 470 nm LEDs, respectively) and difference between the reading at the detector for water and 0.1 µM fluorescein were notably improved (figure 2.4f). Thus, with the third approach, it was predicted that the system was sensitive enough to detect fluorescent calcium signals from a small number of neurons *in vivo*.

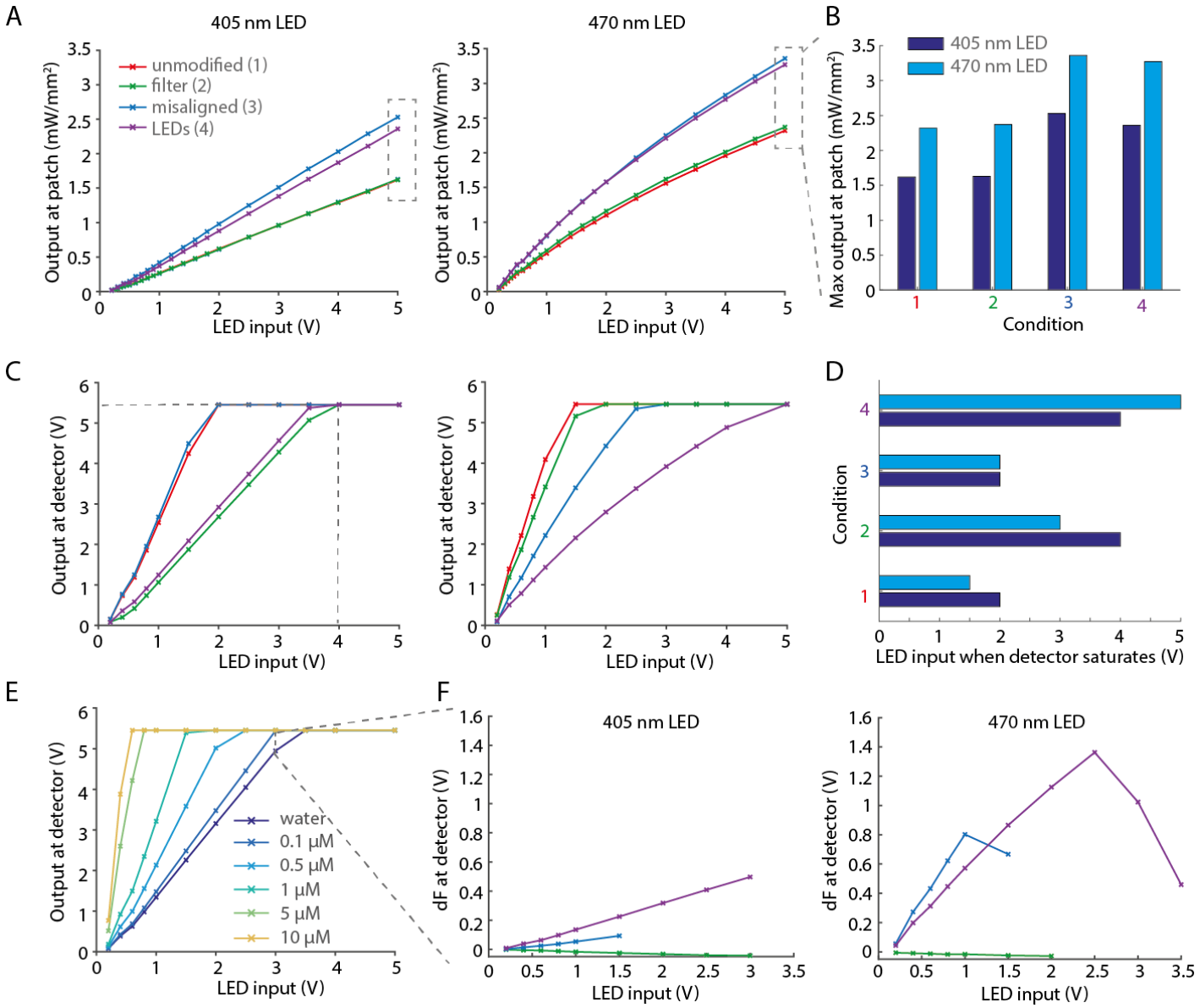
A
405 nm LED
470 nm LED
unmodified (1)
filter (2)
misaligned (3)
LEDs (4)
Output at patch (mW/mm²)
LED input (V)
B
405 nm LED
470 nm LED
Max output at patch (mW/mm²)
Condition
C
Output at detector (V)
LED input (V)
D
Condition
LED input when detector saturates (V)
E
water
0.1 µM
0.5 µM
1 µM
5 µM
10 µM
Output at detector (V)
LED input (V)
F
405 nm LED
470 nm LED
dF at detector (V)
LED input (V)

Figure 2.4: Optimisation of the fibre photometry system.

Several modifications were made to the fibre photometry system to improve the functional range and sensitivity for detecting low fluorescent signals. ***(A)*** *Light output at the end of the patch cable for the 405 nm (left) and 470 nm (right) LEDs. Modification steps include the original set up (red), adding an additional filter (Semrock, FF01-405/150-25, green), misaligning the light illumination path at the fibre launch junction (blue) and leaving the LEDs on for several days (purple).* ***(B)*** *Maximum light output at the end of the patch cable for 405 nm and 470 nm illumination. Condition numbers refer to those in (A).* ***(C)*** *Reading at the detector as LED illumination is increased for the 405 nm LED (left) and 470 nm LED (right). The patch cable was left hanging in the air so readings show the amount of light from the LEDs alone reaching the detector. Colours represent system modifications as specified in (A). Dashed line indicates the minimum illumination required from the 405 nm LED to saturate the detector when the additional filter was added to the system.* ***(D)*** *Minimum LED illumination power when the detector saturates for both LEDs.* ***(E)*** *Reading at the detector with varying concentrations of fluorescein. Data shows the system's sensitivity to detecting fluorescein after leaving the LEDs on for several days with the 405 nm LED.* ***(F)*** *The differences in the readings at the detector between water and 0.1 µM fluorescein with the different optimisation steps (filter, green; misaligned, blue; and leaving LEDs on, purple). Measurements at different illumination intensities, for both the 405 nm LED (left) and 470 nm LED were taken.*

2.3 Fabricating implants for *in vivo* electrophysiology

2.3.1 EEG and EMG connectors

All mice were implanted with skull screw electroencephalogram (EEG) and electromyography (EMG) wires. To make the EEG implants, 3 copper wires (0.2 mm diameter, 357-918, RS-Pro) were cut to length (1.2 cm, 1.2 cm and 2 cm) and the insulation removed from both ends. One end of the wire was wrapped around a skull screw (M1X2, Yahata Neji) and the other end was soldered to a single channel on a 2-by-3 piece connector (SDL-112-T-12, Semtec). EMG implants were made from two 2 cm long multicore copper wires (2840/7, Alpha Wire). Each wire was stripped of insulation at both ends and one end was soldered to a channel on the 2-by-3 connector. Electrical connections from the exposed end of the wire to the connector were checked with an impedance meter and secured with dental cement.

2.3.2 Optrode fabrication

While a cohort of mice (20 mice) were implanted with an unmodified optic fibre (5 mm long 400 µm diameter, 0.39NA, CFM14L05, Thorlabs) to measure transient calcium activity alone, a subset of mice (17 mice) were implanted with an optrode to simultaneously measure calcium transients and P-waves. Optrodes consisted of a bipolar electrode (pair of electrodes) glued to the optic fibre and were fabricated though a multistep process. First two 1.5 cm long (0.1

mm diameter) stainless steel wires (FE205850/2, Goodfellow) were glued together (offset by approximately 0.5 - 1 mm at the tip). Insulation was removed at one end and connected to a 2-piece connector (SS-132-T-2-N, Semtec) using conductive paint (186-3593, RS-Pro). The conductive epoxy was left to dry for 10 minutes and then secured in place with dental cement. Impedances were checked by connecting the bipolar electrodes to the Intan system (RHD2132 16-channel amplifier board and RHD2000, Intan Technologies) with a custom-made connector, and placing the tips of the bipolar electrodes in saline. Electrodes with impedances between 200 kΩ and 1 MΩ at 1 kHz were folded (as shown in figure 2.5c) and positioned alongside the optic fibre. The electrodes were fixed in place 500 µm below the tip of the optic fibre with superglue (473-455, RS-Pro), taking care not to get glue on the tips of either the optic fibre or bipolar electrode. Dental cement was then used to secure and stabilise the structure. Impedances were checked again and optrodes were ready for implantation.

2.4 Surgeries

Aseptic technique was upheld as best as possible with the use of sterile surgical gloves, disinfected surfaces (with 70% ethanol) and autoclaved gowns and surgical equipment. Mice were first anaesthetised with isoflurane in an anaesthetic chamber (5% until they stopped moving and then maintained at 2% for a further 5 minutes). Fur on the incision site, covering the top of the skull, was shaved and cleaned with a damp cotton bud. The mouse was then head fixed into a stereotaxic frame (SR-5M-HT, Narishige) with an incisor bar and blunt ear bars. Anaesthetic (isoflurane) was delivered through a breather via a nose cone and maintained between 1.5% and 1%, with 0.8 L/min air flow. Breathing and pinch reflexes were monitored throughout the surgery and levels of anaesthetic were adjusted accordingly. Mice were maintained at 37°C by being placed on a temperature feedback heat mat. Eye gel was applied over the eyes to protect the eyes from the bright surgical lights.

The shaved skin was cleaned with betadine and local anaesthetic, lidocaine (2%, 0.1-0.3 mg), was injected subcutaneously at the incision site. Rimadyl, a non-steroidal anti-inflammatory drug, was also injected subcutaneously into the small of the back (10ml/kg, 0.01% rimadyl diluted in injecting saline). A vertical incision was made along the midline to gain access to the skull. Skin and connective tissue were cleared with the successive use of 70% ethanol, 3% H_2O_2 and a surgical blade. Bregma and lambda were identified, and the tilt of the skull was adjusted so that the heights of bregma and lambda were within ±150 µm of each other using a motorised stereotaxic micromanipulator (Narishige).

A total of 6 burr holes were made, one targeting the PPT/LDT (right hemisphere), two over both frontal bones, two over both parietal bones and one over the cerebellum (figure 2.2 & figure 2.5). The surgical coordinates were modified during this study due to unsuccessful attempts at measuring GCaMP6s signals and P-waves. The initial coordinates for the PPT/LDT were -4.5 mm posterior and 1 mm medial from bregma while the second set of coordinates were slightly posterior at -4.8 mm posterior and 0.75 mm medial from bregma (table 2.2). The AAV5-CAG-flex-GCaMP6s-WPRE-SV40 or AAV5-Syn-flex-GCaMP6s-WPRE-SV40 virus was injected into the PPT/LDT (3.25 mm and 3 mm deep from the surface of the brain, for the first and second set of coordinates, respectively) using a microinjection pump (500 nl, at a speed of 30 nl/min; Sys-Micro4 and nanoliter2010, World Precision Instruments). Following injection, the micropipette was left in the brain for a further 10 minutes and then slowly raised up.

EEG, anchor, and ground screws were then implanted (over the frontal cortices, parietal cortices and cerebellum, respectively). Part of a drinking straw was horizontally positioned between the screws and the connector to provide mechanical support when plugging mice to the recording system. EMG wires were placed in the upper trapezius muscle and optic fibre (CFM14L05-10, Thorlabs) or optrode implanted over the PPT/LDT (3 mm and 2.7 mm deep from surface of the brain for the first and second set of coordinates, respectively) using the motorised stereotaxic micromanipulator. The headcap was secured in place with dental cement.

The success rate with both sets of surgical coordinates are discussed in chapter 3, section 3.2.1, and section 3.3.4; and chapter 6.

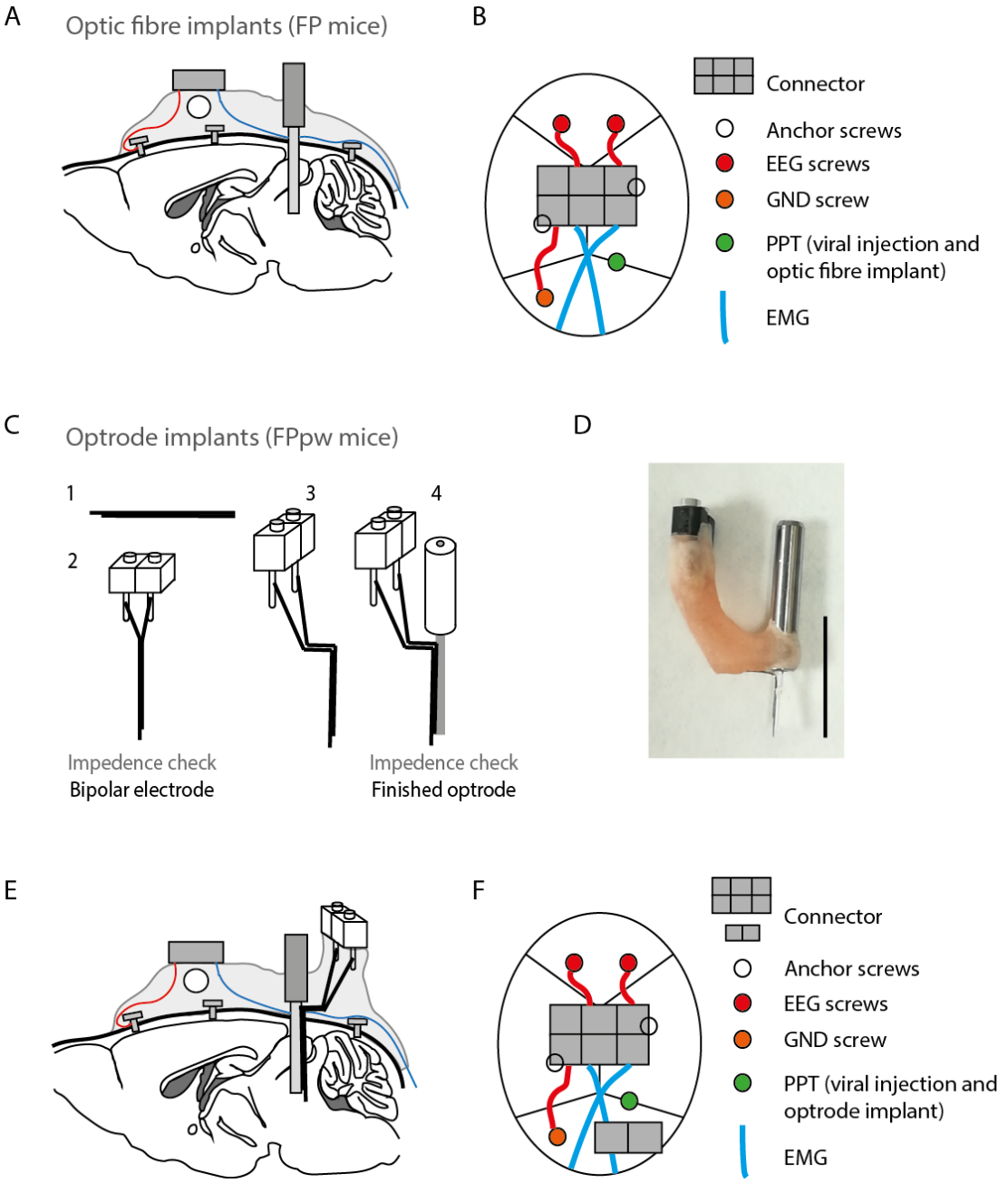

Figure 2.5: Schematic of surgical implants used to measure EEG, EMG, GCaMP6s signals and P-waves.

(A & B) *Profile from the side (A) and the top (B) of implants for mice implanted with a bare optic fibre (FP mice). This consisted of an optic fibre targeting the PPT/LDT nucleus, EEG, ground and anchor screws, EMG wires and a connector.* ***(C)*** *Fabrication process for making optrodes. 1) Two wires are glued together with a 0.5-1 mm offset. 2) Insulation is removed from one end of the bundle and attached to a connector with conductive epoxy. Impedances are checked and electrodes folded as shown in step 3. 4) Bipolar electrodes are fixed to the optic fibre with glue and dental cement.* ***(D)*** *Image of a complete optrode. Scale bar represents 1 cm.* ***(E & F)*** *Schematic of surgical implants for mice implanted with an optrode from the side (E) and from the top (F).*

Table 2.2: First and second set of surgical coordinates.

	Anterior – posterior	Medial-lateral	Depth (injection)	Depth (implant)
1	-4.5	1	3.25	3
2	-4.8	0.75	3	2.7

2.5 Habituation and sleep/wake recordings

Mice were allowed 5 days to recover, during which time, their weight and well-being was closely monitored. Two stages of habituation then followed. The first was being habituated to the recording box, being handled and scruffed. The second habituation stage took place 2-3 weeks after surgery to habituate the mice to the experimental setup and being tethered to both the electrophysiology and fibre photometry systems. Mice were scruffed and the straw in the headcap was placed into a custom-made clamp to keep the head still and absorb any vertical forces while connecting and disconnecting the tethers. Once connected, mice were placed in a Perspex box (21.5 cm x 47 cm x 20 cm depth) lined with absorbent paper, bedding and food pellets. During this habituation stage, short recordings (20 – 30 minutes) were taken to test whether a GCaMP6s fluorescence signal could be detected.

Cholinergic PPT/LDT neurons have been known to be active during the startle response (Koyama et al., 1994, Fendt et al., 2001, Azzopardi et al., 2018). To test if the injection site and optic fibre locations were on target, mice were presented with bursts of sound (60 dB, 100 ms pulse, generated by a real-time processor RP2.1, Tucker-Davis Technologies) through a speaker (ES1, Tucker-Davies Technologies) located next to the perspex box. Sound was presented manually at random intervals. If a stimulus evoked change in fluorescence signal was detected, longer (4-5 hour) recordings were taken to allow for multiple sleep/wake transitions. Illumination power was adjusted at the tip of the patch cable to 0.4 - 0.94 mW/mm^2 for the 405 nm LED and 0.7 - 1.37 mW/mm^2 for the 470 nm LED. The LEDs on the fibre photometry system were alternatively turned on at 40Hz.

Sleep/wake recordings typically started between 9:00 and 10:30 am during the light phase of the 24hr light/dark cycle. These sleep/wake recordings were repeated over multiple days (typically 3 days). Both 405 nm and 470 nm LEDs were alternately turned on and off at 40 Hz in a square pulse fashion. These illumination parameters were the same for all recordings (during habituation and sleep/wake recordings). Both electrophysiological and fluorescence data was obtained at a sampling rate of 1000Hz.

2.6 Data analysis

All data and signal processing were analysed using MATLAB (R2016b, Mathworks). Plots were made with MATLAB and figures consisting of several plots were assembled with Adobe Illustrator.

2.6.1 Electrophysiology

Sleep scoring

Sleep/wake states were manually scored offline and in accordance with standard criteria (Radulovacki et al., 1984, Tobler et al., 1997). EEG and EMG signals over 4 second epochs were used to determine whether the mice were awake, in NREM sleep or REM sleep, using a custom-made graphical user interface. NREM sleep had high amplitude EEG (delta activity between 1-5 Hz) and low EMG power (figure 2.6 top), while REM sleep contained low amplitude EEG (theta activity 6-10 Hz) and low EMG power (figure 2.6 bottom). Wakefulness, on the other hand, consisted of low EEG and high EMG amplitudes (Figure 2.7).

P-wave detection

P-wave were detected by filtering the LFP from a single bipolar electrode channel (5-30 Hz bandpass filter) and applying a threshold to detect peaks in the pontine LFP. The threshold was computed by extracting a 1-minute period of LFP signal during the longest NREM sleep episode in the recording and calculating 5 deviations above the mean root mean square (RMS) of the signal during this time. These methods are the same as those described in our recent papers (Tsunematsu et al., 2020, Patel et al., 2020), except only one bipolar electrode channel was used in this study (discussed in Chapter 4, section 4.3.3).

The frequency of P-waves was calculated by dividing the number of P-waves during a single sleep episode by the length of the episode in seconds. Boxplots and histograms were made using the 'boxplot' and 'histogram' MATLAB functions respectively. Coefficients for producing autocorrelograms were calculated by using the 'xcorr' on P-wave timings for each episode and plotting the average across all episodes and recordings.

Electrophysiology data analysis

EEG spectrograms were created using the MATLAB function 'mtspecgramc' (from the Chronux toolbox, http://chronux.org/) with a moving window of 1 second and 0.2 second step size. The time-bandwidth product and tapers were equal to 3 and 5, respectively. EEG spectral analysis for each sleep-wake state was carried out using the MATLAB function 'mtspectrumc' with time-bandwidth product equal to 3 and tapers equal to 5. Spectral size was

averaged across 0.1 Hz bins and collated for each sleep-wake episode. Overall averages and standard error of means across recordings and mice were then calculated to create the plot in figure 3.9a.

NREM sleep

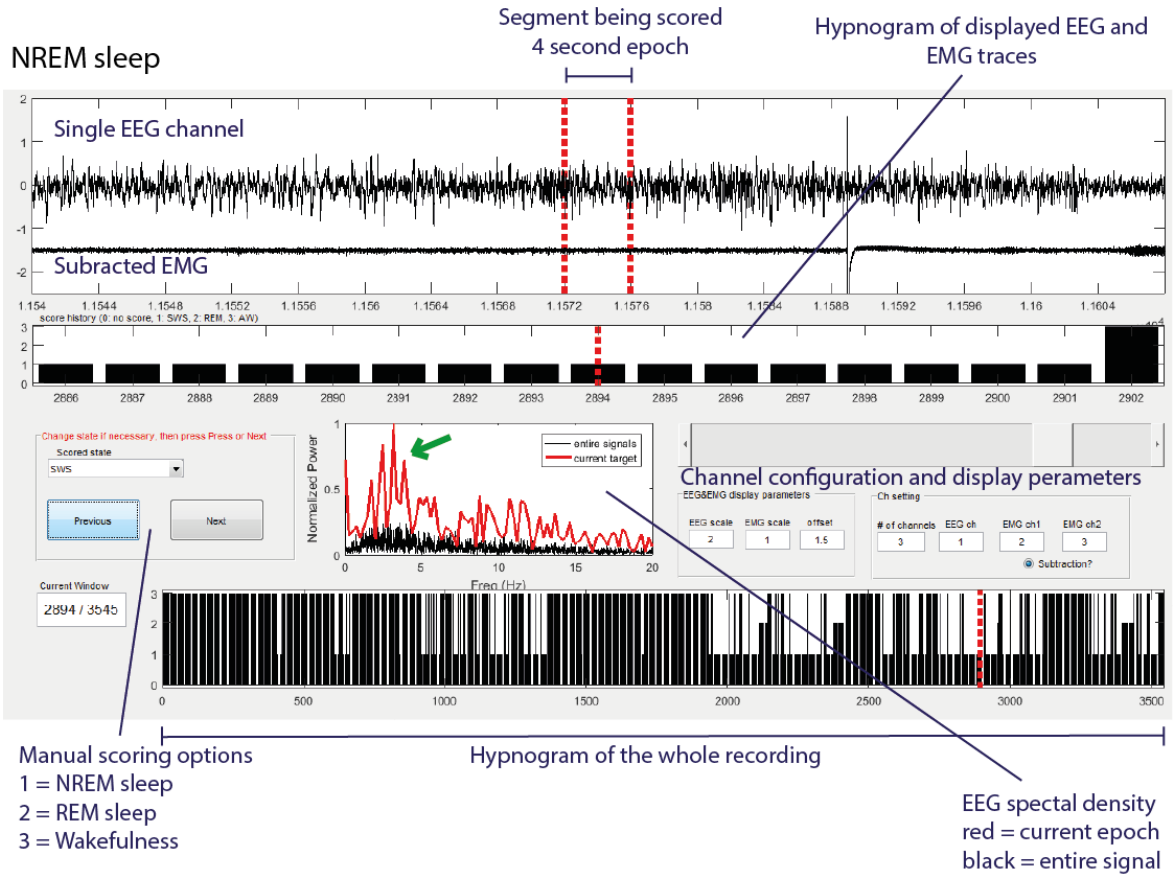

REM sleep

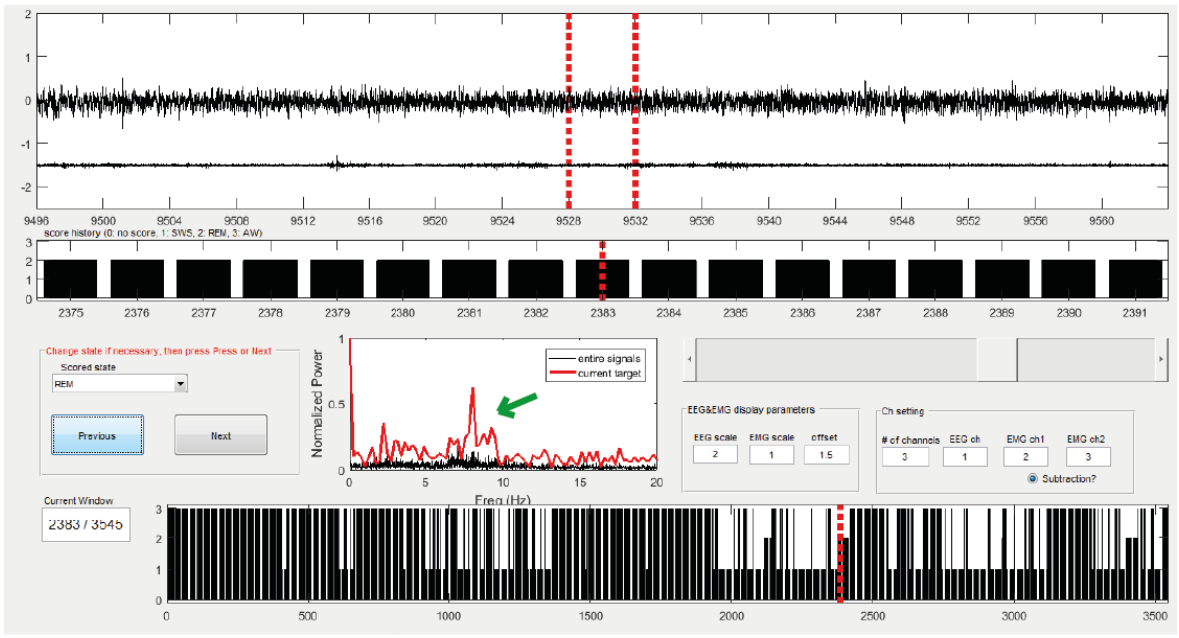

Figure 2.6: Examples of NREM and REM sleep episodes for manual sleep scoring.
Figure shows screenshots of the graphical user interface (GUI) used for sleep scoring. 4 second epochs (marked between red horizontal line, top panel) were scored. EEG spectral density and both EEG and EMG amplitude were taken into consideration when scoring behaviour state. ***(Top)*** *Example of a representative NREM sleep epoch. There is little EMG activity and high amplitude EEG. EEG spectral power is also higher within the delta range (1-5 Hz, green arrow) which is typical for NREM sleep.* ***(Bottom)*** *Example of a REM sleep episode. There is very little EMG activity and EEG amplitude is relatively low. The power spectra also show peaks around the theta range (6-10 Hz, green arrow). REM sleep typically followed NREM sleep in all recordings and also helped differentiate between wakefulness and REM.*

Wakefulness with a lot of movement

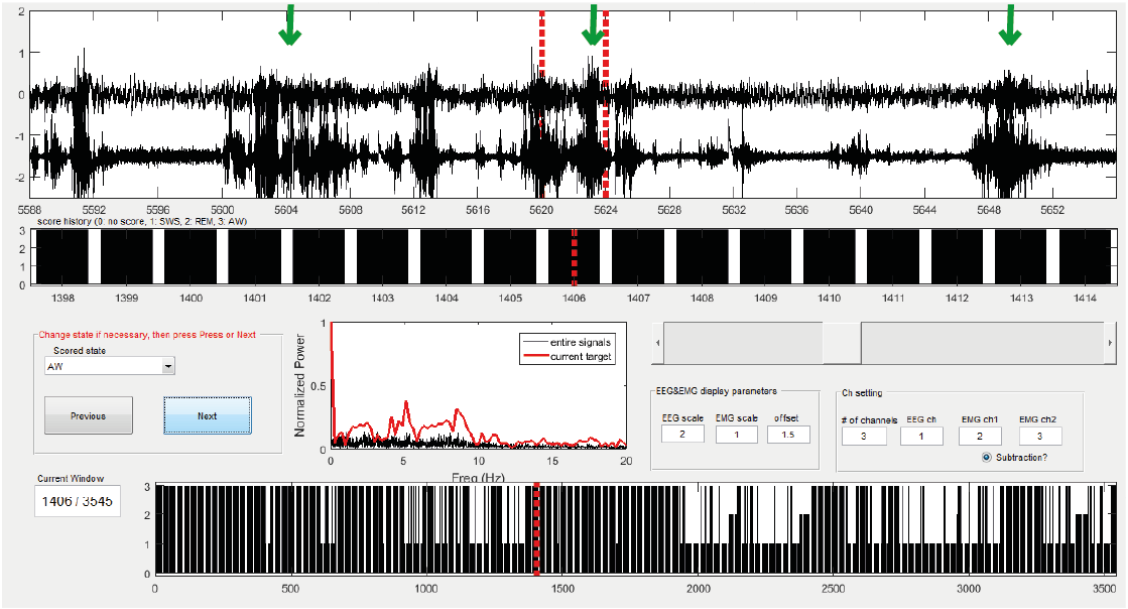

Wakefulness with less of movement

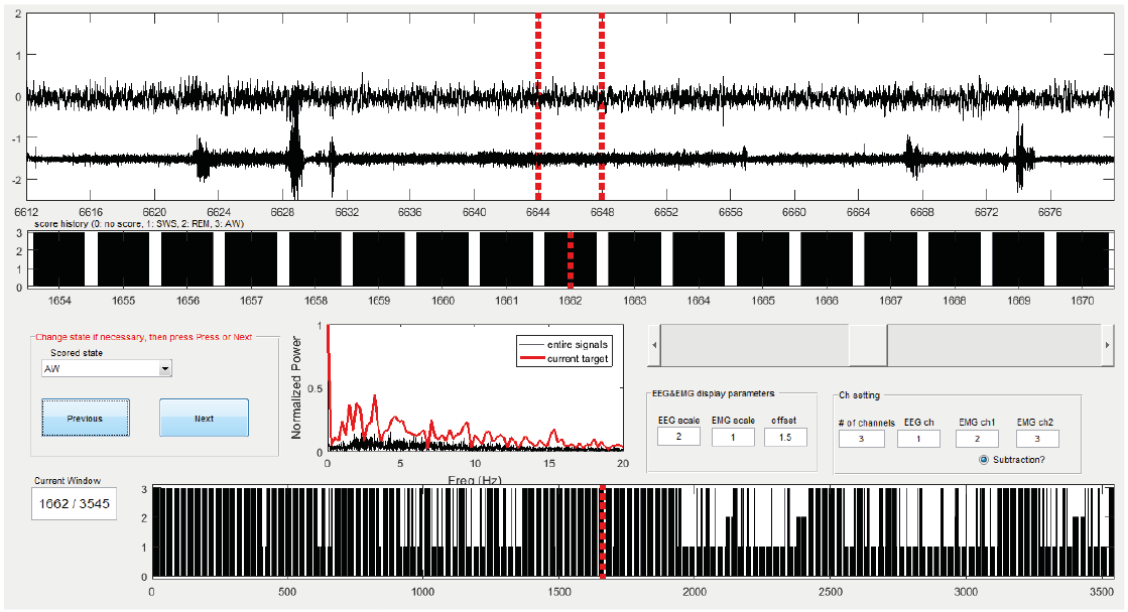

Figure 2.7: Sleep scoring examples of wakefulness.

Two examples of wakefulness. ***(Top)*** *There is lots of EMG activity suggesting that mouse is actively awake. Excessive movement produces artefacts in the EEG trace (green arrows). There is also little delta or theta activity in the power spectra, compared to examples shown in figure 2.6.* ***(Bottom)*** *Example of a period where the mouse is awake but with less movement than the top example. EEG amplitude is low and EMG amplitude during the epoch is considerably larger the those observed during REM sleep (see figure 2.6, bottom, for comparison).*

2.6.2 Fibre photometry

Fluorescence signal extraction

Fluorescence signals (dF) were extracted as described previously (Tsunematsu et al., 2020, Patel et al., 2020). The median fluorescence signal during each illumination period was collated for each LED (405 nm and 470 nm LED). To account for photobleaching, signals from each LED were first fit with an exponential curve and subtracted from the original signal. These signals were then low pass filtered (4 Hz) and the 405nm reference signal was then linearly scaled to fit the 470nm fluorescence signal. The scaled 405nm trace was subtracted from the 470nm trace to provide a motion-corrected 470nm signal (*d*F) (figure 2.8).

GCaMP6s signals data analysis

To calculated sound evoked GCaMP6s responses, fluorescence signals around each sound presentation (-5 to 10 seconds) were extracted and averaged. For sleep/wake recordings, the first 1000 seconds of the recording were excluded from further analysis because photobleaching estimations were difficult to fit. Signals were then normalised across each recording by subtracting the minimum *d*F value from the whole recordings and dividing by the maximum *d*F.

To investigate the changes in GCaMP6s fluorescence activity around REM sleep over normalised time, the start and end times of all REM sleep episodes were extracted and binned into 50 equally spaced time bins. Normalised *d*F and EMG power were averaged across each bin and collated for each episode. The same process was carried out for NREM sleep and wakefulness episodes around REM sleep.

To analyse the underlying rhythmicity in the GCaMP6s signals, a continuous wavelet transform was performed on *d*F signals during individual episodes using the MATLAB function ‘cwt’. The underlying frequency and power of the fluorescence signal was extracted using the function ‘mtspectrumc’. Spectrum power was binned into 0.02 Hz frequencies and collated across recordings and mice for each vigilance state. Episodes shorter than 25 seconds were excluded from this analysis because frequency resolution was poor for short episodes.

For P-wave triggered fluorescence signal analysis, timing of P-waves during each state (REM sleep, all NREM sleep and NREM sleep episodes that directly preceded REM sleep) were extracted. Fluorescence signals were then averaged across events and plotted.

Peaks in GCaMP6s signals were identified by first, lowpass filtering the *d*F signal (0.25 Hz). A threshold was then set for both the first and second half of each recording to account for

photobleaching over time. The mean filtered *d*F signal throughout NREM sleep during each half of the recording was computed and a threshold of 2 standard deviations above these values was set. Timings of the fluorescence peaks were detected using the MATLAB function 'findpeaks'. The occurrences of fluorescence peaks in relation to P-waves were then collated in 0.5 s bins.

2.6.3 Statistical analysis

Statistical analysis was carried out using MATLAB and its Statistics and Machine Learning toolbox (R2016b, Mathworks) and has been described within each figure legend. Analysis typically consisted of exploring state differences for given measurements and required either a one-way ANOVA (with post hoc Tukey's honest significant difference criterion) or a Kruskal-Wallis test (with post hoc Bonferroni). Data are expressed as mean ±SEM, unless otherwise stated.

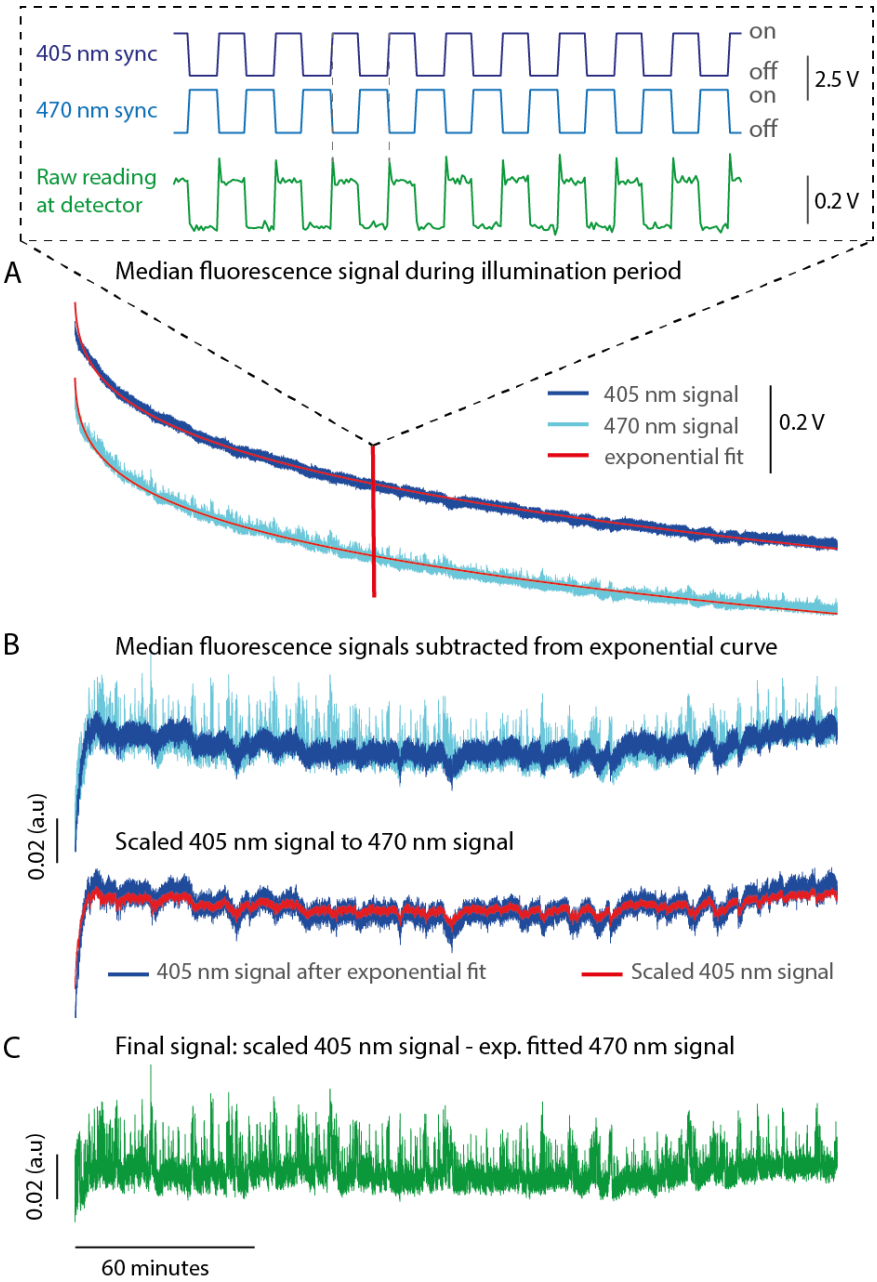

Figure 2.8: Multistep process for fluorescence signal extraction.

(Insert) *The on and off pattern of the LEDs (405 nm LED, dark blue; 470 nm LED, light blue) and reading at detector (green) during a 25 second segment of a sleep-wake recording. LEDs were alternately turned on at 40 Hz.* ***(A)*** *Signals at the detector were averaged (median) during individual illumination periods for each LED. An exponential curve (red) was fitted to account for the gradual decrease in signals due to photobleaching throughout the recording.* ***(B)*** *Averaged signals were then subtracted from their respective exponential curves and low pass filtered at 4 Hz (top; 405 nm, dark blue; 470 nm light blue). The 405 nm signal was then linearly scaled to the 470 nm signal (bottom).* ***(C)*** *Scaled 405 nm signal subtracted from the exponentially fitted 470 nm signal. The first 1000 seconds (16.6 minutes) of the signal were omitted because the photobleaching component of the signal was not accurately fitted to the exponential curve compared to the rest of the recording.*

2.7 Perfusions and histology

Mice were deeply anaesthetised with an intraperitoneal injection of euthatal and lidocaine (1:1 ratio, 0.1ml) and transcardially perfused with 20 ml of 0.1 M saline, followed by 20 ml of 4% paraformaldehyde in 0.1M phosphate buffer solution (PBS). The brain was removed and placed in 4% paraformaldehyde solution overnight (4°C). It was then then placed in 30% sucrose solution and stored in the fridge for at least 2 days.

Post fixation, coronal sections surrounding the PPT/LDT were cut using a freezing microtome (50 µm – 80 µm) and successive sections were placed in 24 plate wells filled with 0.1 M PBS. To verify GCamP6s expression in cholinergic neurons within the brainstem, sections were stained for choline acetyltransferase (ChAT) an acetylcholine synthesising enzyme and Green Fluorescent Protein (GFP) a protein conjugated with GCaMP6s. Brain sections were first washed (10 minute washed, 3 times on a rotating platform at room temperature) with PBS-triton (PBST, 0.1 M PBS and 0.3% triton) and then incubated in a blocking solution for an hour (10% normal donkey serum, Sigma-Aldrich, D9663 in 0.3% PBST). Next, sections were incubated with primary antibodies against GFP and ChAT (mouse anti-GFP 1:2000, Abcam, ab1218; goat anti-ChAT 1:400, Millipore, AB144P) in PBST and 3% goat serum for 12-18 hours (4°C). The primary antibody solution was washed with PBST (10 minutes, 3 times) and incubated in a secondary antibody solution (donkey anti-mouse IgG alexa fluor 488 1:500, Thermo Scientific, SA5-10166; Donkey anti-goat IgG alexa fluor 568 1:500, Invitrogen, A11057) in PBST and 3% normal donkey serum for 2 hours at room temperature. Sections were washed with PBS (20 minutes, 2 times) and then incubated with a 1/5000 solution of DAPI (Thermo Fisher Scientific) in PBS for 5 minutes.

Some sections (pontine area and some section containing the hippocampus) from 5XFAD mice were stained with Thiazine-red to identify amyloid plaques and tau tangles. After cutting coronal sections as describe above, the sections were incubated in 0.05% Thiazine-red in PBS solution (WVR, catalogue number 27419.123) for 15 minutes at room temperature. Sections were then washed in PBS (5 minutes, 3 times) and then incubated with 1/5000 solution of DAPI in PBS.

After washing (30 minutes, PBS at room temperature), sections were mounted on glass slides with gelatine solution. Slides were left to air dry and cover slipped. Sections were observed with an epifluorescent upright microscope (Nikon Eclipse E600, greyscale) and corrected for colour with Image J.

3 State-dependent changes in cholinergic activity

3.1 Brief introduction

3.1.1 Brief overview of the literature

As discussed in chapter 1, the sleep-wake regulating circuitry in the mammalian brain is complex. Networks of neurons are activated or deactivated in a time-locked manner to elicit state transitions or maintain a behavioural state. While brainstem and hypothalamic neurons have been linked to REM sleep generation and initiation, the neuronal mechanisms underlying this brain state are still unknown. Cholinergic PPT/LDT neurons had, in the past, been thought to play a key role in REM sleep regulation, however, it is thought to now play a modulatory role, and research into the exact role of this cluster of neurons is still required to decipher its exact role.

Electrical stimulation of LDT neurons increased the number and duration of REM sleep in cats (Thakkar et al., 1996), while optogenetic stimulation of cholinergic PPT or LDT neurons in mice elicited NREM-to-REM sleep transitions (Van Dort et al., 2015). Chemogenetic stimulation of cholinergic PPT neurons, on the other hand had no effect on REM sleep (Kroeger et al., 2017). Cholinergic PPT/LDT neurons are known to be active during REM sleep (Boucetta et al., 2014, Cox et al., 2016), however the firing rates of these neurons were not monitored during electrical, optogenetic or chemogenetic stimulation studies, thus making it difficult to ascertain how these manipulations may have an underlying effect on REM sleep.

Considering the PPT/LDT nuclei also contain heterogeneous populations of neurons (Wang and Morales, 2009), cell-type specific monitoring of neuronal activity is required to assess the stimulation protocols required to investigate the functional role of PPT/LDT cholinergic neurons in sleep.

3.1.2 Aims and hypothesis

We hypothesised that cholinergic PPT/LDT neuronal activity is correlated with P-wave generation and the initiation of REM sleep. To investigate this, the first aim is to characterise cholinergic PPT/LDT neuronal activity during REM sleep and its transitions.

3.1.3 Overview of this chapter

In this chapter, the success rate of implanted mice will be discussed and results from mice with GCaMP6s fluorescence signals will be presented. Data from mice with a fluorescence

signal and those that transitioned to REM sleep show that cholinergic PPT/LDT activity is highest during REM sleep and contains underlying rhythmic fluctuations.

3.2 Results

3.2.1 Datasets and mice

To monitor cell-type specific population calcium activity during the sleep/wake cycle, a fibre photometry system was used to measure calcium activity from cholinergic PPT/LDT neurons in freely moving mice. Briefly, ChAT-Cre mice were injected with a Cre-dependent viral vector to allow for the expression of GCaMP6s in cholinergic PPT/LDT neurons. During the same surgery, an optic fibre was implanted and targeted to be positioned just above the PPT/LDT. Cortical EEG and EMG screws and wires were also implanted to determine behavioural state during the sleep/wake cycle.

GCaMP6s signals were first verified *in vivo* before recording state-dependent cholinergic activity during sleep-wake states. This section discusses the main technical considerations for successful GCaMP6s fluorescence recordings, surgical optimisations and histological and *in vivo* verifications of fluorescence signals.

Both GCaMP6s injection and optic fibre position need to be on target

Two main factors are required for a successful fluorescence recording, first, in order to express GCaMP6s in cholinergic neurons, the viral injection needs to be on target. Second, the optic fibre needs to be positioned just above the GCaMP6s expressing neurons. If the fibre is far from the area in which neuronal activity is to be recorded, the signal-to-noise ratio will be too low. However, if the fibre is positioned too deep, there is a danger of damaging or even destroying the GCaMP6s expressing neurons. From a total of 37 implanted mice, GCaMP6s fluorescence signals were undetected from a total 30 mice (Figure 3.1). Of these, 11 mice expressed GCaMP6s in PPT/LDT neurons, but the optic fibre was off target. Conversely, the optic fibre was implanted in an appropriate position in 9 mice, but there was no GCaMP6s expression in PPT/LDT neurons. Both viral vector injection and optic fibre implantation were off target in 10 mice and calcium activity was successfully monitored from 7 mice.

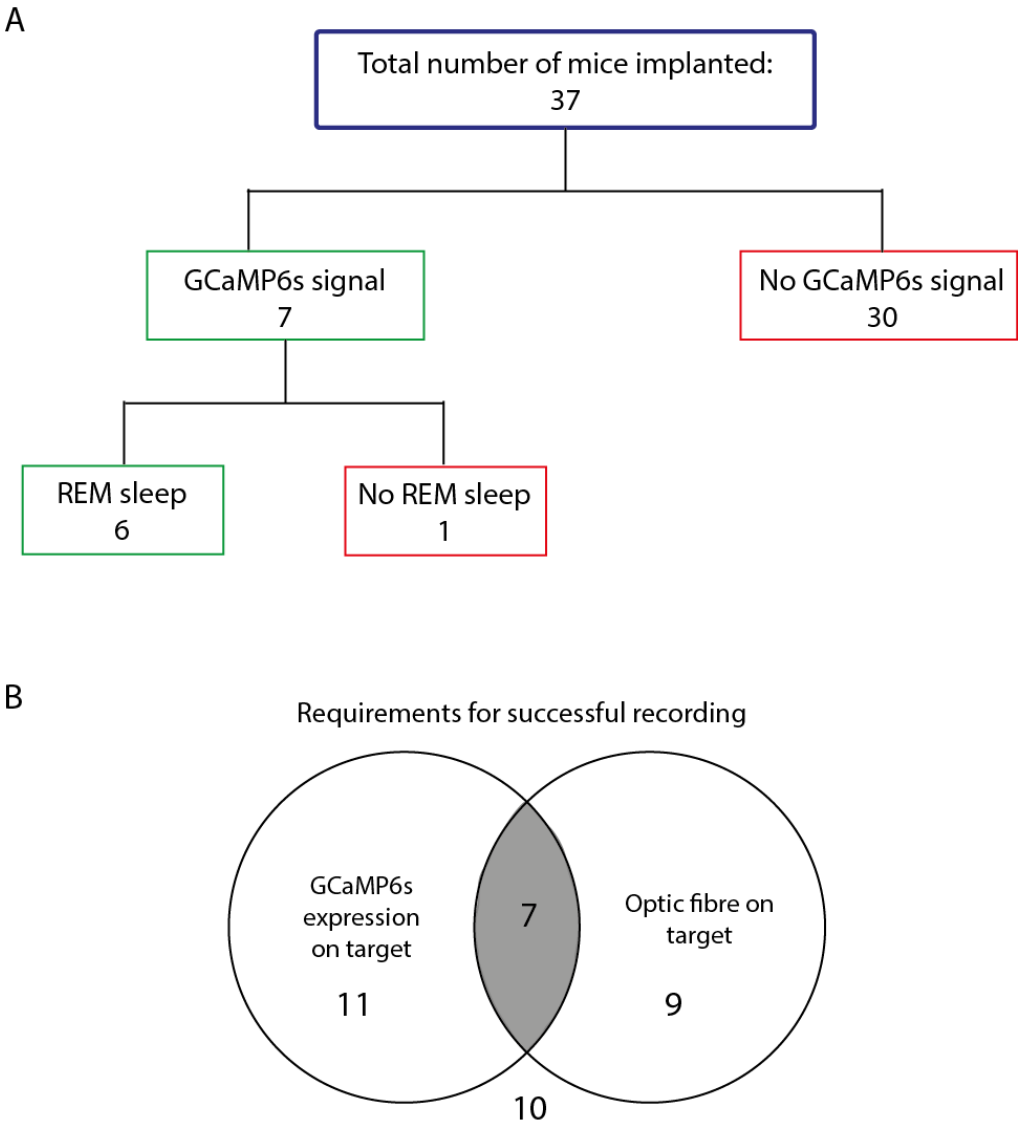

Figure 3.1: Summary of implanted mice.

(A) *Flow chart shows the total number of mice implanted (includes both mice implanted with bare optic fibres and those with optrodes). Of these, 7 mice presented with a GCaMP6s fluorescence signal and 6 mice transitioned to REM sleep during at least one sleep-wake recording.* ***(B)*** *Venn diagram shows the requirements for successful detection of PPT/LDT GCaMP6s neurons. Number denotes the number of mice used during these experiments.*

Optimisation of surgical coordinates

Several rounds of implementation and optimisation were required in order to successfully measure GCaMP6s signals from a small population of neurons deep within the brainstem. This was because the technique was challenging to implement and had not been established within the laboratory. Optimisation steps included adjusting the fibre photometry system itself (discussed in section 2.2.3) and modifying surgical coordinates. Although the PPT/LDT nuclei span quite a distance in the anterior-posterior axis, the shape and depth of the nucleus varies. The initial coordinates (-4.5 mm posterior and 1 mm medial from bregma; 3 mm deep from the surface of the brain) were chosen because it was a midway point in the anterior-posterior axis and avoided the transverse sinus, which can cause severe bleeding if ruptured. While the location of the optic fibre varied across animals, it was routinely implanted too dorsal to the PPT/LDT nucleus (figure 3.2a & b). This was a particular problem when the fibre was positioned -4.35 mm or closer to bregma, where the PPT/LDT nucleus is smaller and deeper, which the surgical coordinates did not account for. To compensate for this and to increase the chances of measuring calcium signals, a second, slightly more posterior coordinate was used (-4.8 mm posterior and 0.75 mm medial from bregma; 2.7 mm deep from the surface of the brain). While fibre locations with the new coordinates were equally varied, 3 out of the 8 mice successfully provided calcium signals (figure 3.2c).

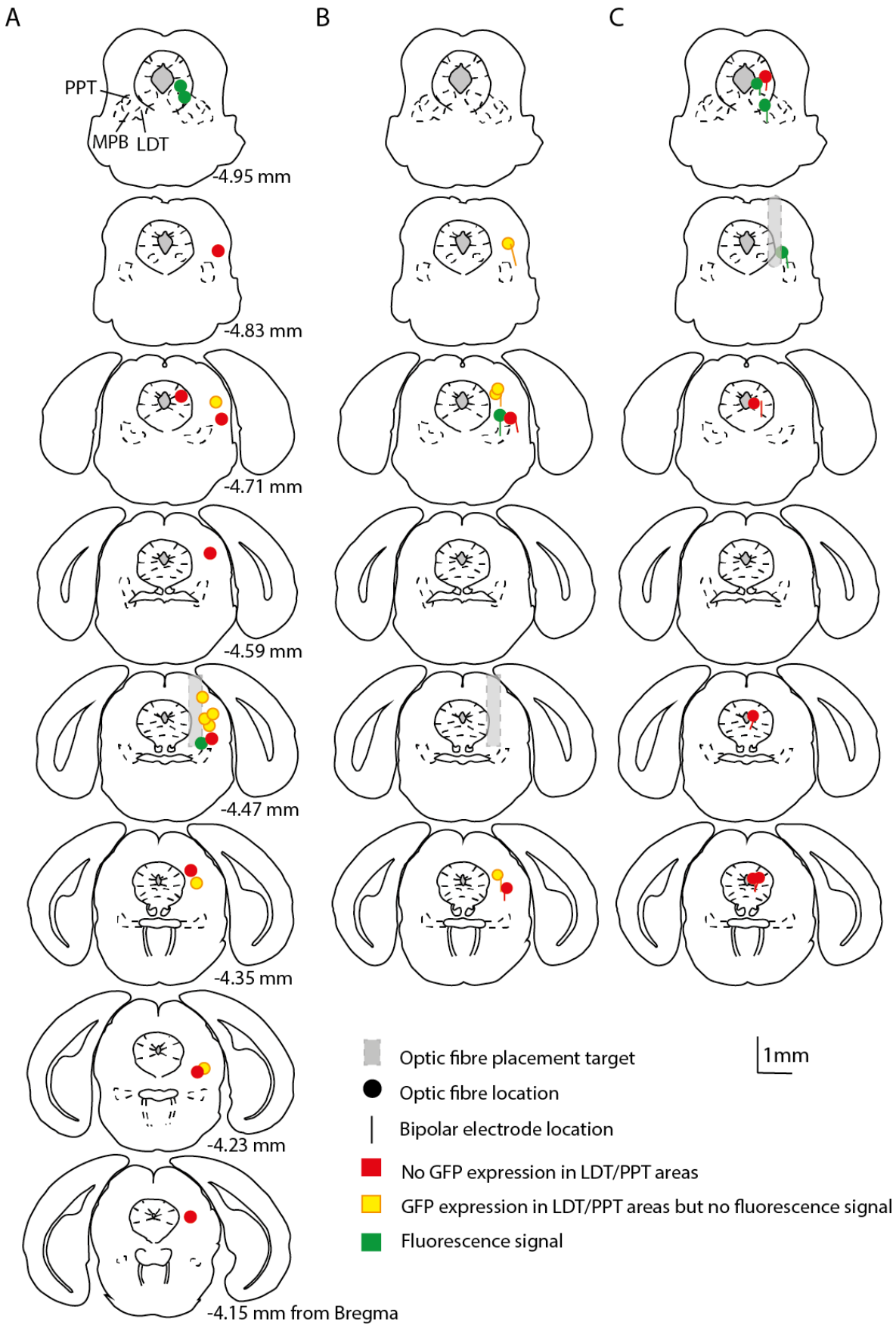
A
B
C
PPT
MPB
LDT
-4.95 mm
-4.83 mm
-4.71 mm
-4.59 mm
-4.47 mm
-4.35 mm
-4.23 mm
-4.15 mm from Bregma
Optic fibre placement target
Optic fibre location
Bipolar electrode location
No GFP expression in LDT/PPT areas
GFP expression in LDT/PPT areas but no fluorescence signal
Fluorescence signal
1mm

Figure 3.2: Summary of optic fibre locations across all mice.

Two sets of stereotactic coordinates were used for implanting the optic fibre. Location of optic fibre tips for each mouse have been depicted according to target coordinates and type of implant (optic fibre or optrode). ***(A)*** *All mice implanted with a bare optic fibre (FP mice) targeting the first coordinate (-4.5 mm posterior, 1 mm medial from bregma and 3 mm deep from the surface of the brain).* ***(B)*** *Mice implanted with an optrode (FPpw mice) targeting the first coordinate.* ***(C)*** *FPpw mice implanted with optrodes targeting the second coordinate (-4.8 mm posterior, 0.75 mm medial from bregma and 2.7 mm deep from the surface of the brain). Coordinates and schematics of brain sections are based on the mouse atlas (Paxinos and Franklin, 2012). Note: 3 mice have been excluded from this figure - 1 did not recover well after surgery and was euthanised, and brains from two other mice were fixed and cut in a strange shape, making it difficult to locate brain areas accurately. This may have been due to poor perfusions and no in vivo GCaMP6s fluorescence signals were observed.*

Confirmation of GCaMP6s expression with immunohistochemistry

To confirm GCaMP6s expression in cholinergic neurons, immunohistochemistry was carried out on all implanted mice brains. The GCaMP6s vector is conjugated with GFP and cholinergic neurons were stained for choline acetyltransferase (ChAT). Histological examination confirmed that GFP co-expressed with ChAT neurons (figure 3.3). However, in all the mice with a successful calcium signal (7 mice), signs of neuronal damage were observed (figure 3.4 & 3.5). Figure 3.5 is an example from mouse FPpw11. While ChAT expression is clearly observed on the contralateral side of the brain, on the ipsilateral side of the same brain, there is little ChAT and GFP expression. In all the mice, fluorescence signals disappeared before they were culled, suggesting that neurons were damaged in some way – either through neurotoxicity, phototoxicity or mechanically through movement of the implant or brain. This is further discussed in section 3.3.

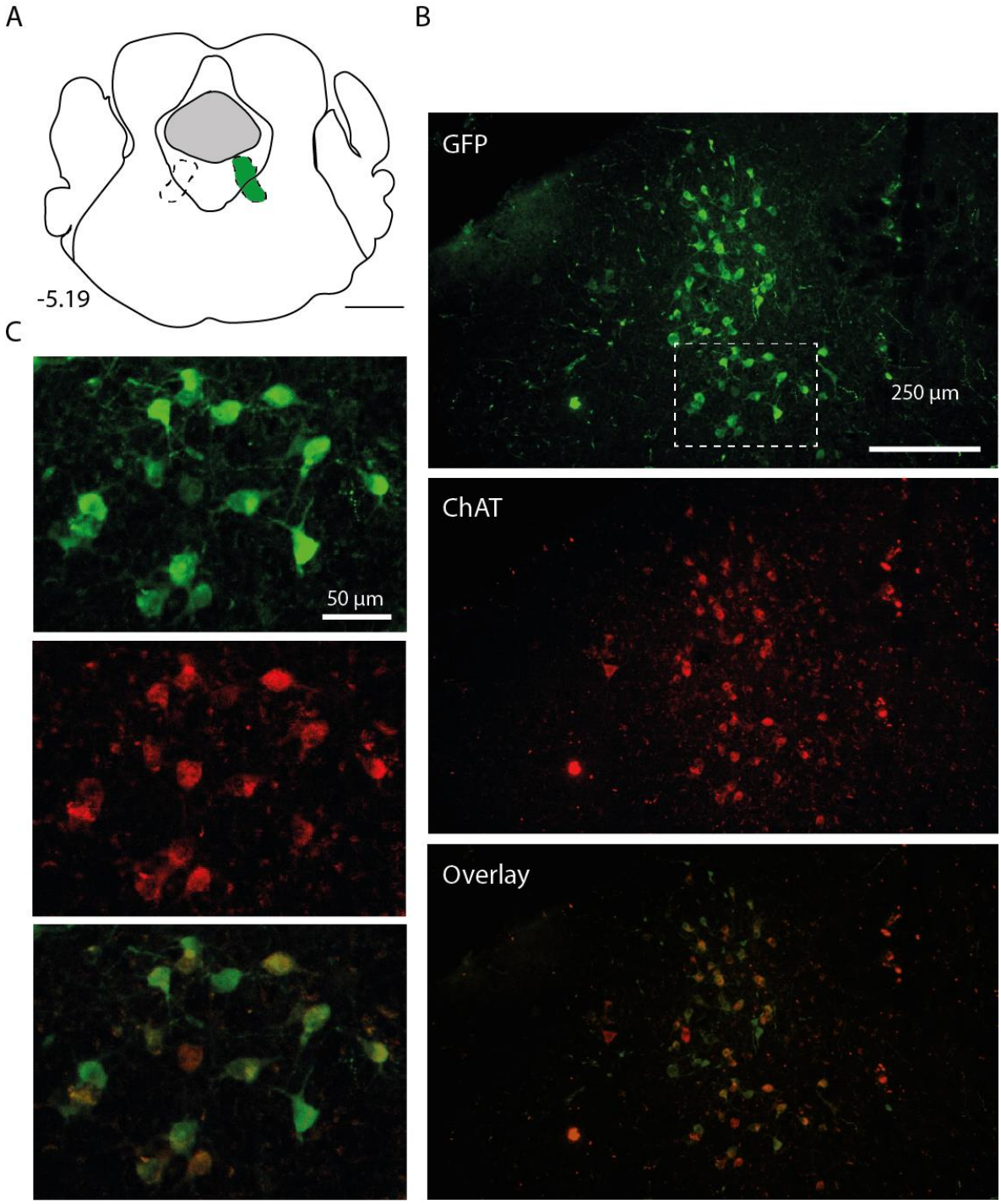

Figure 3.3: Histological example of GCaMP6s expression in cholinergic LDT neurons. ***(A)*** *Schematic of GCaMP6s expressing neurons within the LDT (green).* ***(B)*** *The GCaMP6s viral construct was conjugated with GFP. Therefore, GFP expressing neurons also indicate the expression of GCaMP6s.* ***(C)*** *A magnified view of the selection of neurons co-expressing GFP and ChAT (from B, white box). GCaMP6s fluorescent signals were not obtained from this particular mouse. The optic fibre was not visible in the brain section presented in this figure.*

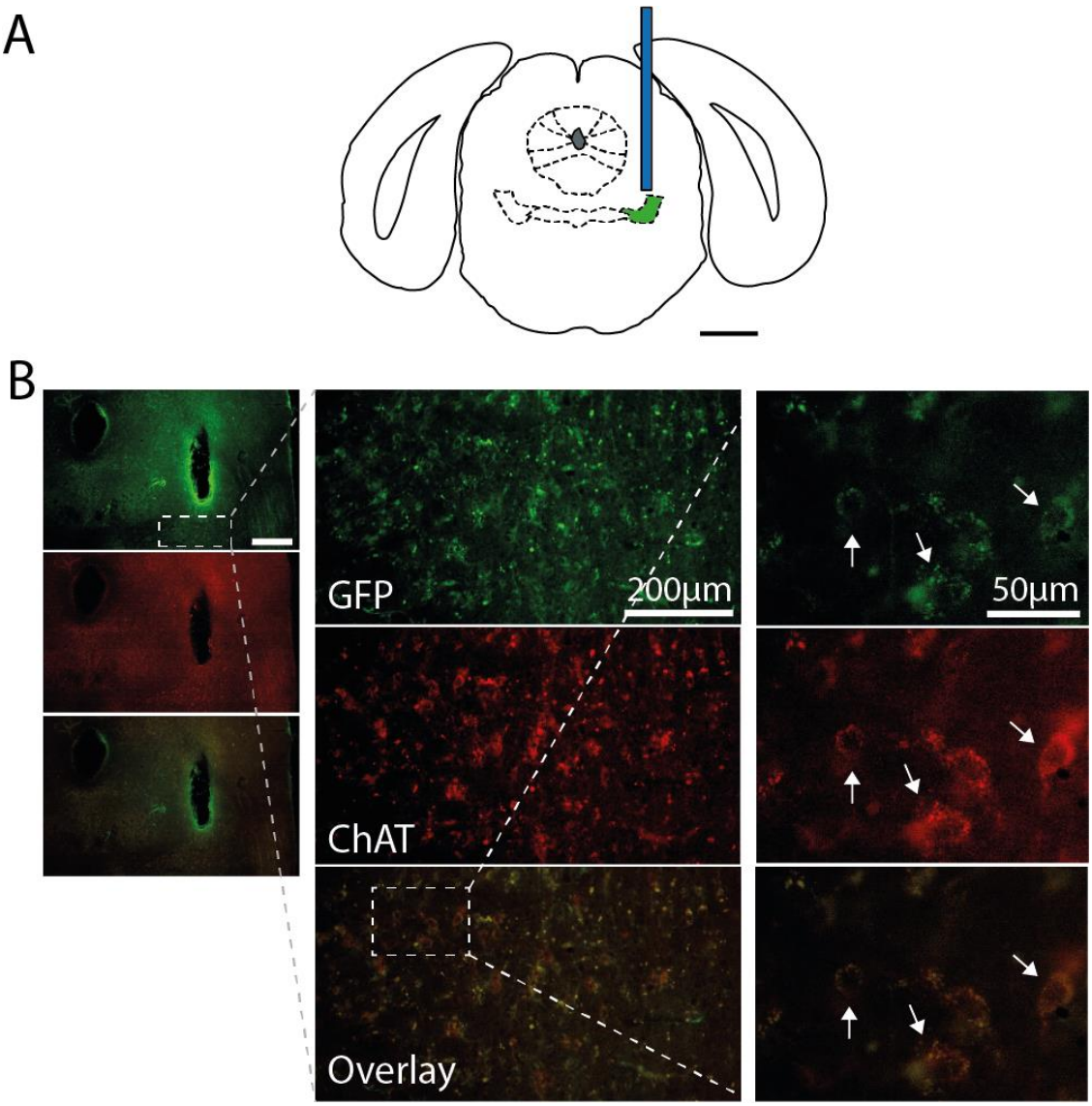

Figure 3.4: Histological example of successful optic fibre implantation but neurons show signs of damage.

(A) *Schematic depicting the location of the optic fibre in mouse FP15 in relation to the PPT (green). Scale bar, 1 mm.* ***(B)*** *Although there are remnants of GCaMP6s (green) expression in PPT cholinergic (red) neurons (arrows), cell bodies are not clearly visible, suggesting cell death.*

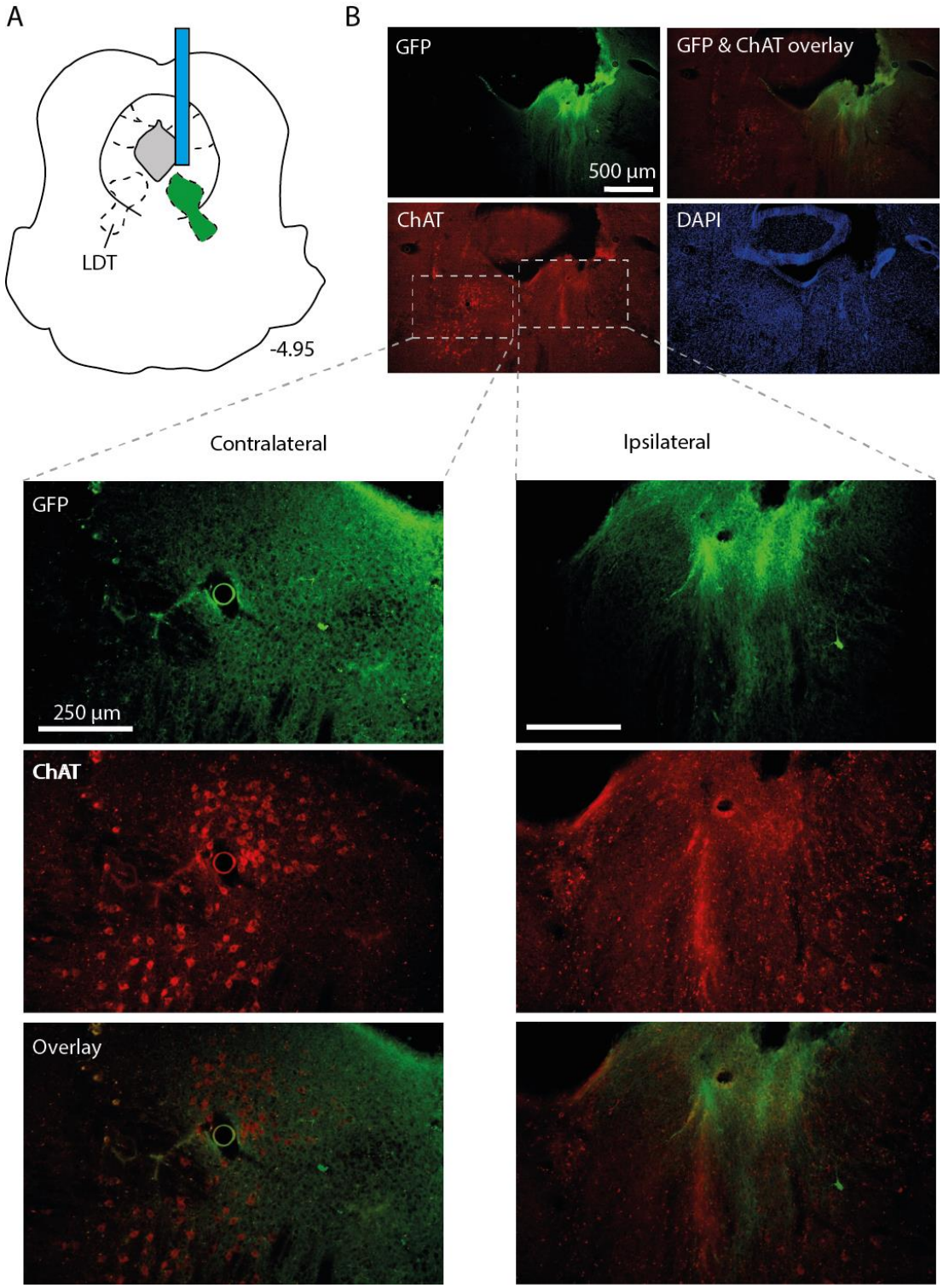

Figure 3.5: Histological example of cell death.

(A) *Schematic depicting the location of the optic fibre in relation to the LDT (green).* ***(B)*** *Epifluorescent images showing GFP, ChAT and DAPI staining from mouse FPpw11, who had a clear GCaMP6s signal. A lesion resulting from the tip of the optic fibre is visible. Inserts show magnifications of the LDT area in the contralateral and ipsilateral sides of the brain. There is clear expression of ChAT neurons on the contralateral side, but little to no ChAT expression in the ipsilateral LDT area.*

Identification of GCaMP6s fluorescence signals in vivo with the startle response

After surgery, mice were allowed to recover for a minimum of 5 days, where their weight and wellbeing was closely monitored. Mice were then slowly habituated to being handled and scruffed (holding the back of the animal's neck to limit head movement). Once mice were comfortable with being handled, they were familiarised to being connected to the tethers, approximately 2 weeks after surgery and fluorescence signals were recorded over a short period of time (20-30minutes) to assess whether calcium signals were being successfully measured. Since the activation of PPT/LDT neurons have been implicated in the startle response (Koyama et al., 1994, Fendt et al., 2001, Azzopardi et al., 2018), mice were presented with random bursts of loud sound (60 dB, 100 ms). It was hypothesised that if the viral injection and optic fibre location are on target, PPT/LDT neuronal activity will increase in response to an unexpected sound. Indeed, there are fluctuations in GCaMP6s fluorescence signals (figure 3.6a) and there were clear fluorescence signals, EEG and EMG event related potentials (ERPs) in relation to sound presentation (figure 3.6b). There was a general increase in fluorescence ERP peaks with increased illumination (chi-square(4, 61) = 14.75, p = 0.0052, Kruskal-Wallis; $p < 0.05$ for 0.8 V vs 2.5 V illumination and 1.5 V vs 2.5 V illumination with Bonferroni multiple comparisons test) (Figure 3.6c, left), however, trial-to-trial variability and low trial numbers make it difficult to assess the true amplitude of these fluorescence peaks. Increased illumination intensities did not affect the size of EMG ERP peaks (figure 3.6c, right) (chi-square(3,42) = 0.21, p = 0.99, Kruskal-Wallis), suggesting that the increases in fluorescence signal peaks were not due to movement but a true GCaMP6s signal.

Comparing this to mice that did not have a clear fluorescence signal, example traces from two mice show no calcium fluctuations or sound evoked calcium ERPs (figure 3.7). It should be noted that examples from two mice have been presented because, sound presentation in mouse FPpw7 (figure 3.7 a-c) shows a clear startle response, suggesting that the mouse can hear the sound, but the illumination intensities were not as high as presented in figure 3.6. The second example (figure 3.7 d-f) on the other, had a more comparative illumination range but EEG and EMG signals were not measured. Fluorescence ERPs in response to loud sounds were observed in 7 mice and indicated that GCaMP6s fluorescence signals were being successfully detected.

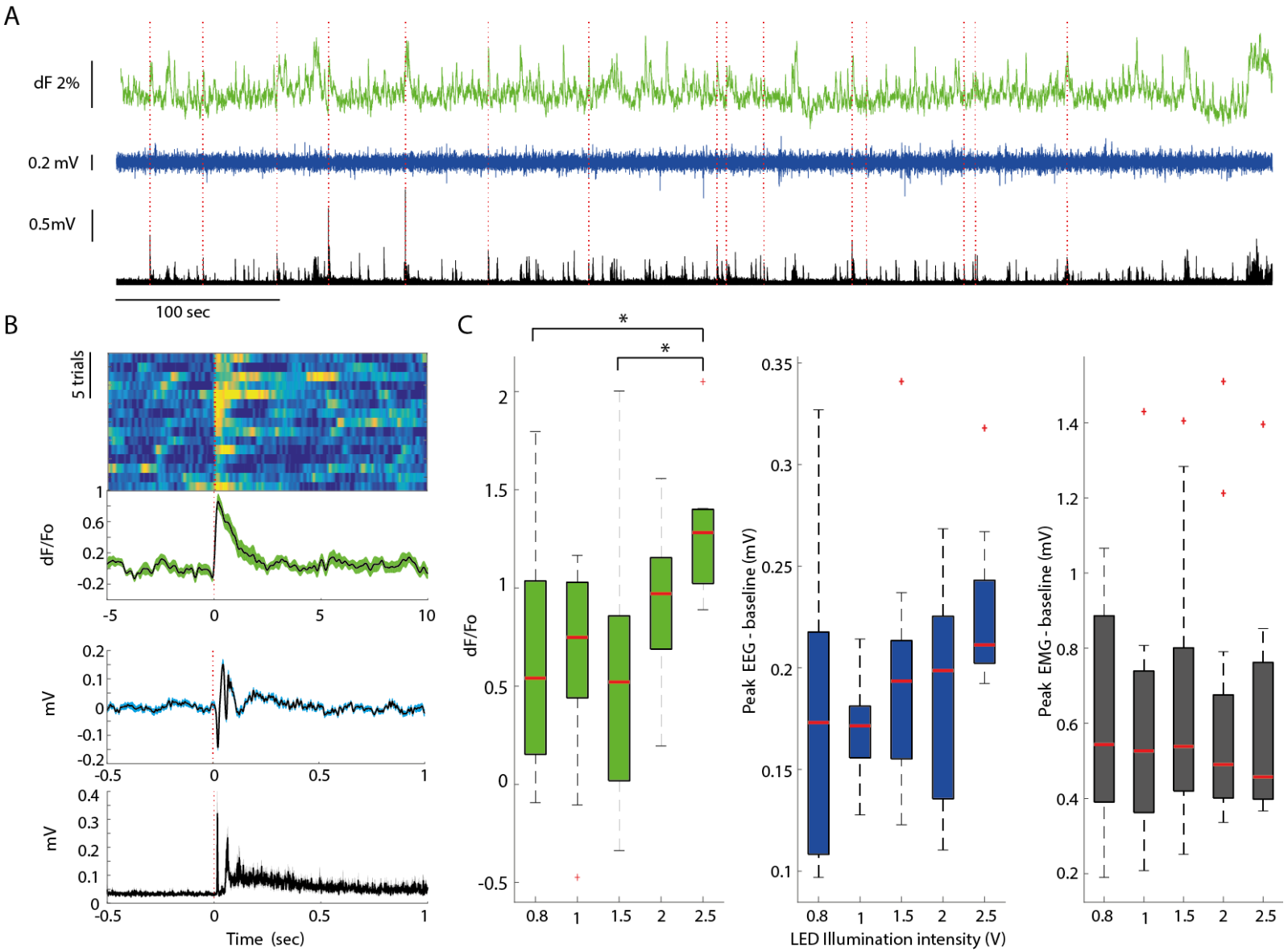
A
dF 2%
0.2 mV
0.5mV
100 sec
B
5 trials
dF/Fo
mV
mV
Time (sec)
C
dF/Fo
Peak EEG - baseline (mV)
Peak EMG - baseline (mV)
LED Illumination intensity (V)

Figure 3.6: Startle response elicits GCaMP6s, EEG and EMG event related potentials.
Traces are from an individual mouse (FPpw14) during a single recording session. ***(A)*** *Example GCaMP6s (green), EEG (blue) and EMG power (black) traces during the random presentation of loud sound (red dotted lines). Illumination intensity is 2 V* ***(B)*** *ERPs corresponding to (A). Time zero indicates onset of sound presentation. Colour map show changes in GCaMP6s signal during individual trials. Fluorescence signals were subtracted from the baseline (-5 to 0 sec) and then divided by baseline. Solid lines denote mean and shaded area indicates ±SEM.* ***(C)*** *Boxplots showing the median maximum fluorescence (green), EEG (blue) and EMG power (grey) peaks following sound presentation during different LED illumination intensities. Peaks were subtracted from baseline (-5 to 0 sec, for GCaMP6s signal; -0.5 to 0 sec, for EEG and EMG signals). Red crosses depict outliers. Kruskal-Wallis tests were carried out to assess if there was a difference in peak amplitude across illumination intensities (for GCaMP6s fluorescence peaks: chi-square(4,61) = 14.75, p = 0.005; for EEG peaks: chi-square = 7.97, p = 0.10; for EMG peaks, chi-square = 0.21, p = 1.0). *, p < 0.05 with Bonferroni multiple comparisons test.*

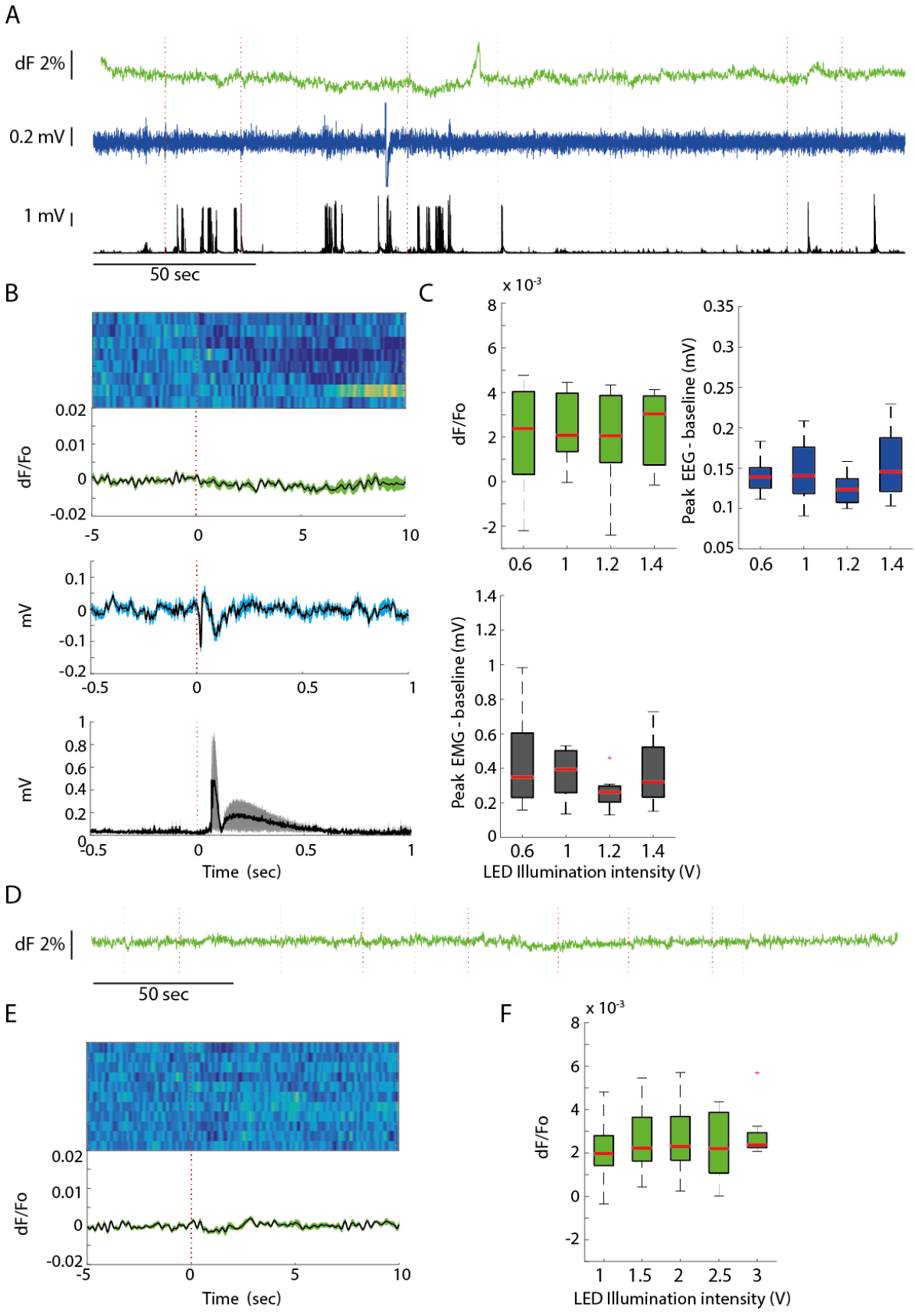
A
dF 2%
0.2 mV
1 mV
50 sec
B
dF/Fo
mV
mV
Time (sec)
C
x 10-3
dF/Fo
Peak EEG - baseline (mV)
Peak EMG - baseline (mV)
LED Illumination intensity (V)
D
dF 2%
50 sec
E
dF/Fo
Time (sec)
F
x 10-3
dF/Fo
LED Illumination intensity (V)

Figure 3.7: Loud sound presentation elicits EEG and EMG ERPs but not GCaMP6s ERPs in mice with no fluorescence signal.

(A) *Example GCaMP6s (green), EEG (blue) and EMG power (black) traces during presentation of loud sound and 1 V illumination intensity.* ***(B)*** *ERPs corresponding to (A).* ***(C)*** *Boxplots showing median peaks in GCaMP6s (green), EEG (blue) and EMG (grey) ERP peaks. Peaks across illumination intensity were not significantly different (for fluorescence peaks, chi-square = 0.21, p = 0.98; for EEG peaks, chi-square (3,42) = 5.84, p = 0.12; for EMG power peaks, chi-square = 3.07, p = 0.38, with Kruskal-Wallis).* ***(D)*** *GCaMP6s trace during sound presentation recording. Illumination intensity is 2V* ***(E)*** *ERP corresponding to (D).* ***(F)*** *ERP peaks with varying illumination intensities were not significantly different (chi-square (4,62) = 2.12, p = 0.71, with Kruskal-Wallis test). For D-F, EEG and EMG signals were not recorded.*

3.2.2 Sleep/wake architecture in freely moving mice

In addition to detecting calcium signals from the mice, in order to investigate the state-dependent activity – specifically during REM sleep – mice needed to transition into REM sleep during the recordings. From the 7 mice where calcium activity was monitored, 1 mouse did not transition into REM sleep. Table 3.1 summarises the data sets obtained and used for analysis in this chapter (total of 17 datasets and 81 REM sleep transitions).

Table 3.1: List of successful monitoring of GCaMP6s activity during the sleep/wake cycle.

Mouse ID	Sex	Age at surgery (weeks)	Total no. of recordings	No. of recordings with REM sleep
FP15	F	17	3	3
FP16	F	21	2	0
FP22	M	12	4	3
FPpw3	M	18	3	3
FPpw11	F	36	6	6
FPpw12	F	8	2	1
FPpw14	F	28	2	1

To assess the population activity profile of cholinergic PPT/LDT neurons during sleep/wake states, long recordings were carried out (3-5 hr). Mice were connected to the electrophysiology and fibre photometry systems via tethers and placed in a perspex box lined with absorbent paper and bedding and allowed to settle and transition through the sleep-wake cycle over several hours. Figure 3.8 is a representative example of a typical sleep/wake recording. During NREM sleep, EEG power spectra is high at low frequencies and there is little EMG activity. During wakefulness, there is a lot of EMG activity and EEG has low amplitude, high frequency fluctuations. While the EEG trace looks similar during REM sleep, EEG power is high in the theta range (6-10 Hz) and there is little EMG activity. Looking at the sleep/wake architecture of this single recording, there were several periods of wakefulness and NREM sleep and a few REM sleep transitions (4 episodes in this case). These observations appeared to be true of all the recordings. EEG spectral analysis showed high power in the delta (1-5 Hz) and theta (6-10 Hz) ranges for NREM and REM sleep, respectively (figure 3.9a). Mice spent the most amount of time awake (55.7% ± 2.7%) and the least amount of time in REM sleep (2.3% ± 0.4%) (figure 3.9b). While there were more transitions to NREM sleep and wakeful episodes compared to REM sleep ($F = 180.9$, $p = 4.45 \times 10^{-23}$, One-way ANOVA; $p < 0.001$ for NREM vs REM and REM vs AW with Tukey's post hoc test), the average duration of episodes between behavioural states were not significantly different (61 seconds ± 5.8, 62.7 sec ± 8.5 and 81 sec ± 6.6, for NREM, REM and AW respectively; $F = 2.45$, $p = 0.097$, One-way ANOVA) (figure 3.9c & d).

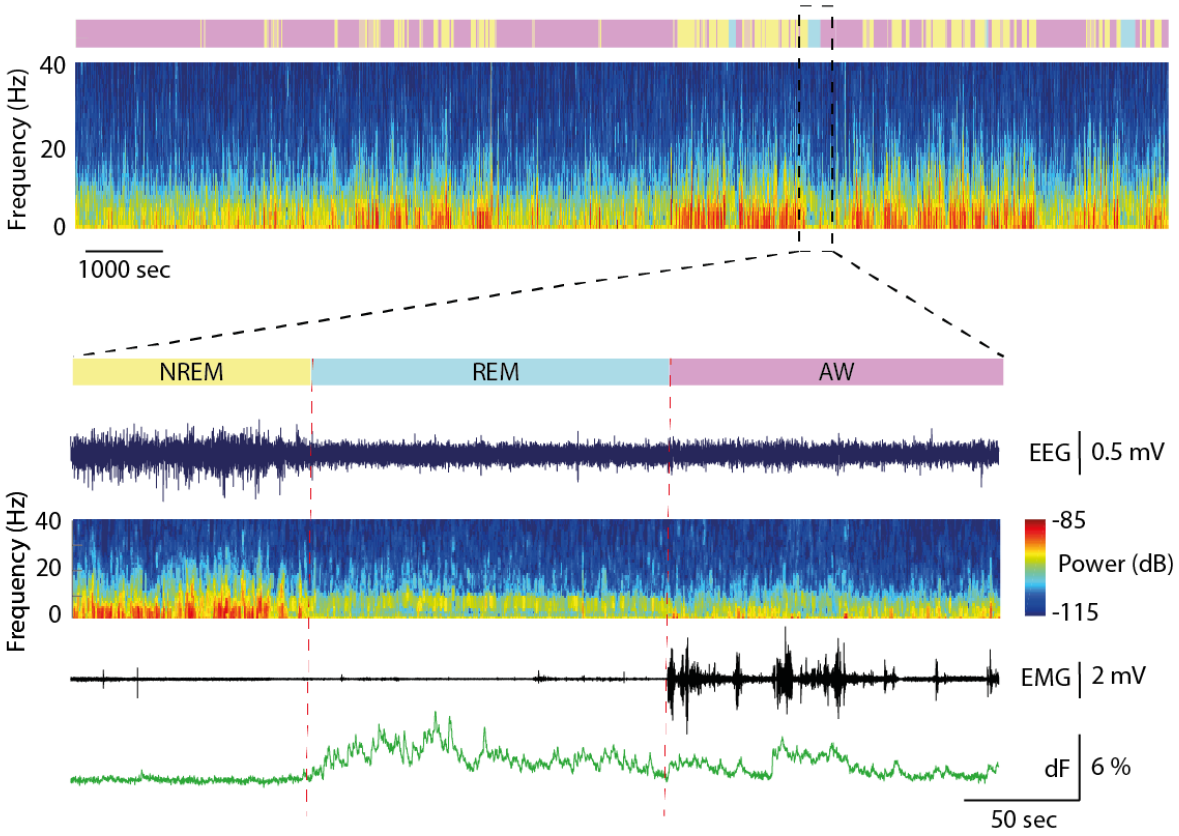

Figure 3.8: Example EEG, EMG and GCaMP6s traces from a sleep/wake recording. *Hypnogram indicating the behavioural state of the mouse during each 4 second epoch and EEG power spectrogram during a single sleep/wake recording. (NREM sleep, yellow; REM sleep, blue; wakefulness, purple). Insert shows an example EEG (blue), EMG (black), GCaMP6s (green) traces and EEG power spectrogram during a series of transitions from NREM sleep to REM sleep to wakefulness*

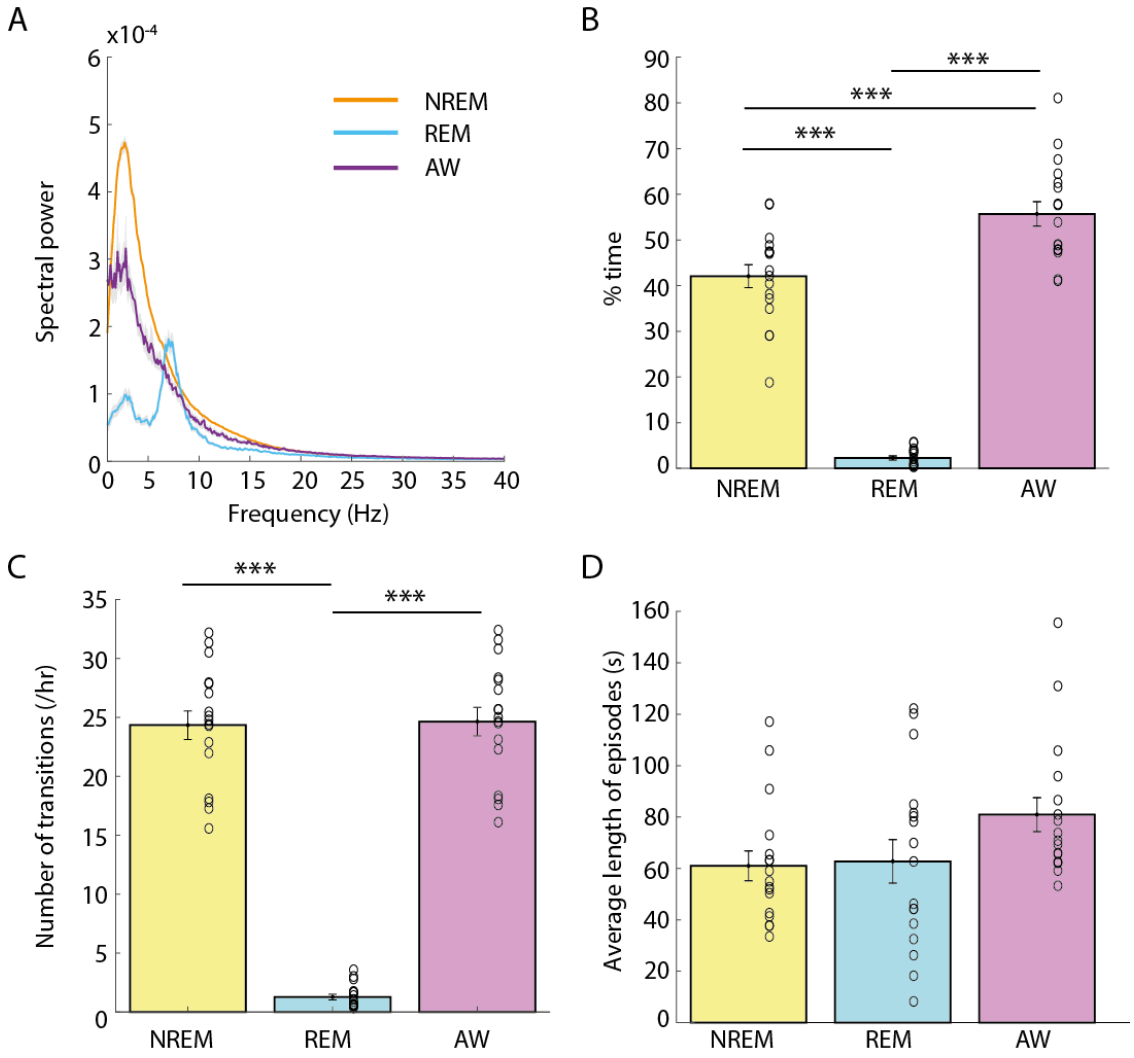

Figure 3.9: General sleep/wake architecture of recordings where successful GCaMP6s signals were detected.

(A) *Averaged EEG power spectral traces during each sleep/wake state (6 mice, 17 recordings). Shaded area represents ± SEM. Bar graphs show* ***(B)*** *mean percentage of time spent in each behavioural state,* ***(C)*** *the number of transitions into each state and* ***(D)*** *the average length of each behavioural state. Open circles depict values from individual recordings. Error bars show ±SEM. A one-way ANOVA was used to test whether values were statistically different across behavioural states (for (B), F = 169.6, p = 1.73x10^{-22}; for (C), F = 180.9, p = 4.45x10^{-23}; for (D), F = 2.45, p = 0.097) ***, p < 0.001, with Tukey's honestly significant difference test (HSD).*

3.2.3 Cholinergic PPT/LDT neuronal activity is highest during REM sleep

Single trial observations of GCaMP6s signals showed that calcium transients were low during NREM sleep and higher during REM sleep and wakefulness (figure 3.8). To confirm this observation, summary analysis showed that mean fluorescence signals were higher during REM sleep and wakefulness compared to NREM sleep, although only signals during REM

sleep was significantly higher than NREM sleep (F = 5.82, p = 0.0054, one-way ANOVA; p = 0.0041 NREM vs REM with Tukey's post hoc test) (figure 3.10).

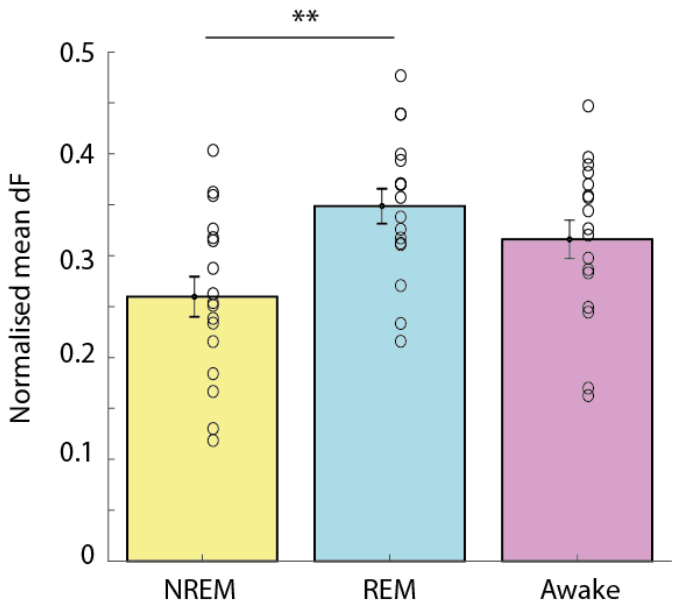

Figure 3.10: Normalised mean GCaMP6s fluorescence signals are highest during REM sleep .

*Fluorescence signals were normalised for each recording and the mean dF across each behavioural state calculated. Data from 6 mice and 17 recordings. Error bars depict ± SEM. Data point show mean dF signal for each recording. Statistical test includes a one-way ANOVA (F = 5.83, p = 0.0054) **, p < 0.01 with Tukey's HSD post hoc test.*

3.2.4 Cholinergic activity profiles vary around different state transitions

To assess how PPT/LDT cholinergic neurons become active during the initiation of REM sleep, signals (GCaMP6s, EEG and EMG) were extracted around state transitions. A gradual increase in cholinergic activity tone was observed during the end of NREM sleep as mice transition into REM sleep, which subsequently peaks during REM sleep (figure 3.11). In contrast, during NREM-to-AW transitions, cholinergic PPT/LDT activity increases drastically and peaks at the onset of wakefulness. Thus, although an increase in cholinergic tone is observed during both NREM-to-REM and NREM-to-AW transitions, the activity profiles vary between states. Delta power (1-5 Hz) during NREM sleep in NREM-to-REM transitions also appear to be higher than that during NREM-to-AW transitions, suggesting that mice are in deeper NREM state during the former transitions. During REM-to-AW transitions, cholinergic activity decreases while EMG power increases.

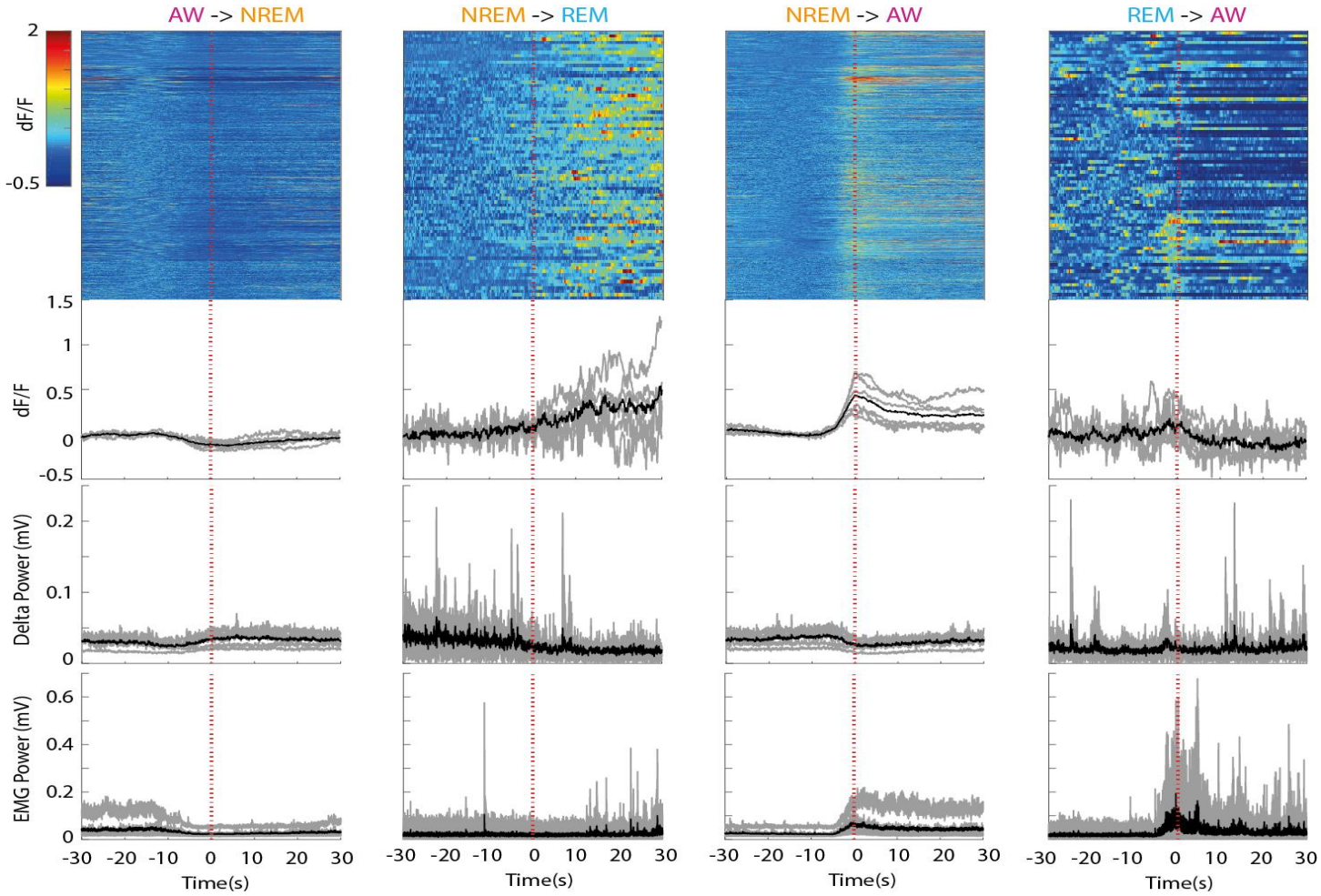

Figure 3.11: Changes in cholinergic PPT/LDT activity, EEG and EMG during state transitions.

Colour matrix shows changes in cholinergic activity around individual transitions. dF signals were calculated by subtracting fluorescence signals from baseline (average between -20 and -10 seconds) and subsequently divided by the baseline. Traces show grand averaged dF/F signals, EEG delta power (1-5 HZ) and EMG power (black). Grey lines indicate average values for each mouse.

3.2.5 GCaMP6s activity peaks at the end of REM sleep and contains rhythmic fluctuations

To investigate the population cholinergic activity during REM sleep further, GCaMP6s and EMG power transients during NREM-to-REM-to-AW transitions were extracted and normalised across time. As shown in previous figures, cholinergic PPT/LDT neuronal activity is lowest during NREM sleep. The activity profile gradually increases just before REM sleep onset to near the end of REM sleep, where cholinergic activity is at its peak. There is a reduction in cholinergic activity during wakefulness, but it is higher than that during NREM sleep (figure 3.12). While these insights are valuable, normalising the GCaMP6s signals over time does not preserve the temporal dynamics and the length of REM sleep can skew the shape of this figure. Therefore, the activity profile of cholinergic neurons in real time were investigated. Figure 3.13 shows examples of GCaMP6s fluorescence and the corresponding spectrograms during each behavioural state. During REM sleep, large, low frequency fluctuations in GCaMP6s signals are observed (figure 3.13). While these fluctuations can also be seen during wakefulness, they are not as consistent. To summarise these observations, power spectral analysis during all state episodes longer than 25 seconds was carried out. Shorter episodes had inadequate spectral resolution so were excluded. Indeed, spectral power between approximately 0.1 and 0.9 Hz is highest during REM sleep compared to both wakefulness and NREM sleep (figure 3.14a). Autocorrelation of the GCaMP6s fluorescence signal also shows small peaks at approximately 10, 15 and 20 seconds during REM sleep but there are no fluctuations during NREM sleep and wakefulness (figure 3.14b). This suggests that there are underlying rhythmic fluctuations in cholinergic activity during REM sleep, which is further explored in chapter 4 where GCaMP6s signals are correlated with LFP data.

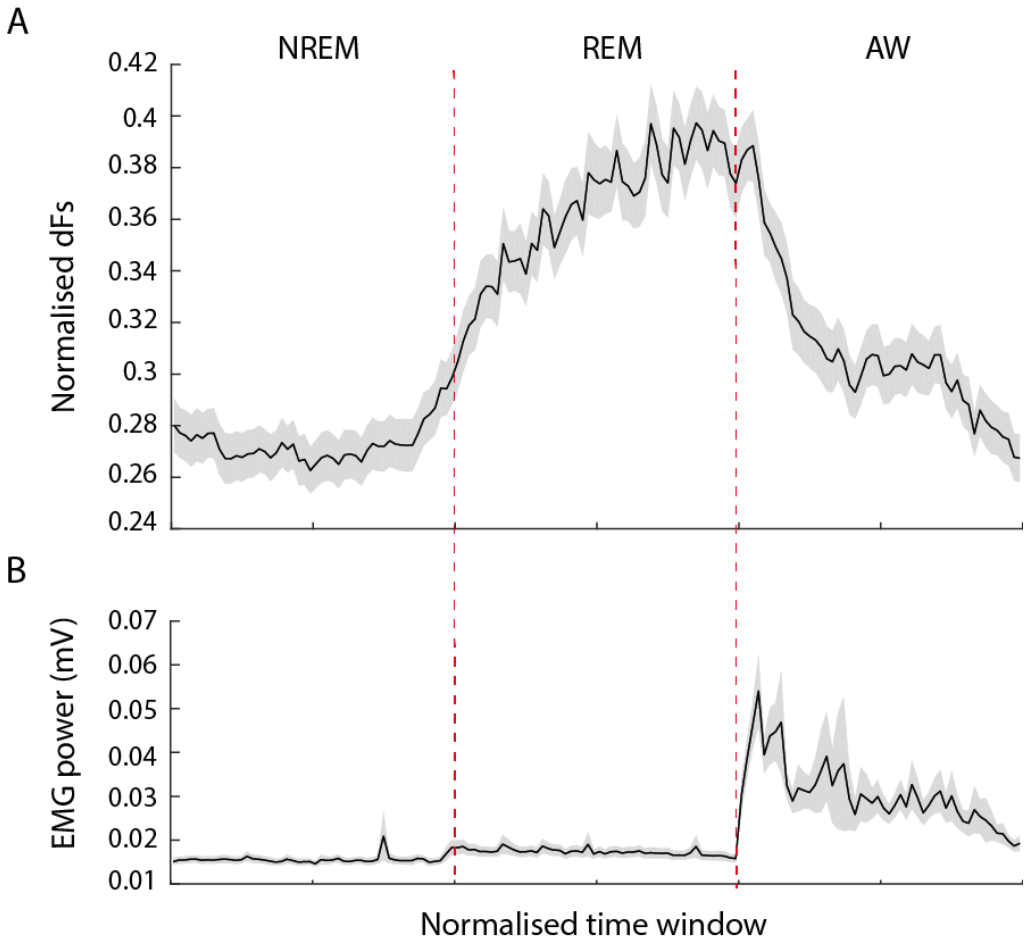

Figure 3.12: PPT/LDT GCaMP6s activity during REM sleep and its surrounding behavioural transition states.

*Averaged GCaMP6s **(A)** signals and EMG power **(B)** during subsequent NREM sleep, REM sleep and wakefulness state transitions. Time during each state was normalised and segmented into 50 bins. Signals (fluorescence and EMG) were then averaged across each bin. Shaded areas indicate ±SEM.*

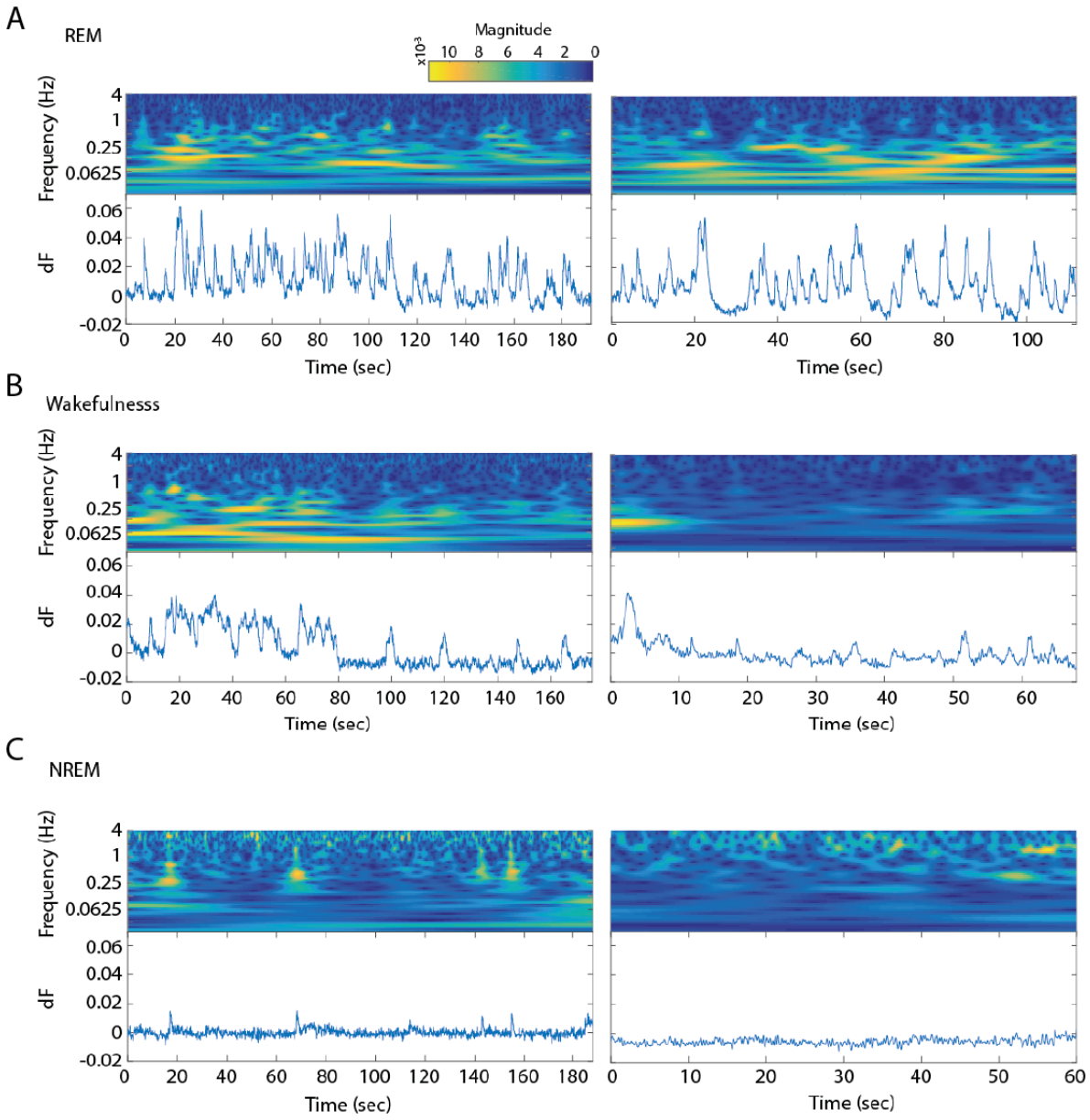

Figure 3.13: Example GCaMP6s power spectral traces during each sleep/wake state.
All traces are from a single sleep/wake recording (FPpw11). Representative GCaMP6s power spectrograms and traces during REM sleep ***(A)****, wakefulness* ***(B)*** *and NREM sleep* ***(C)****.*

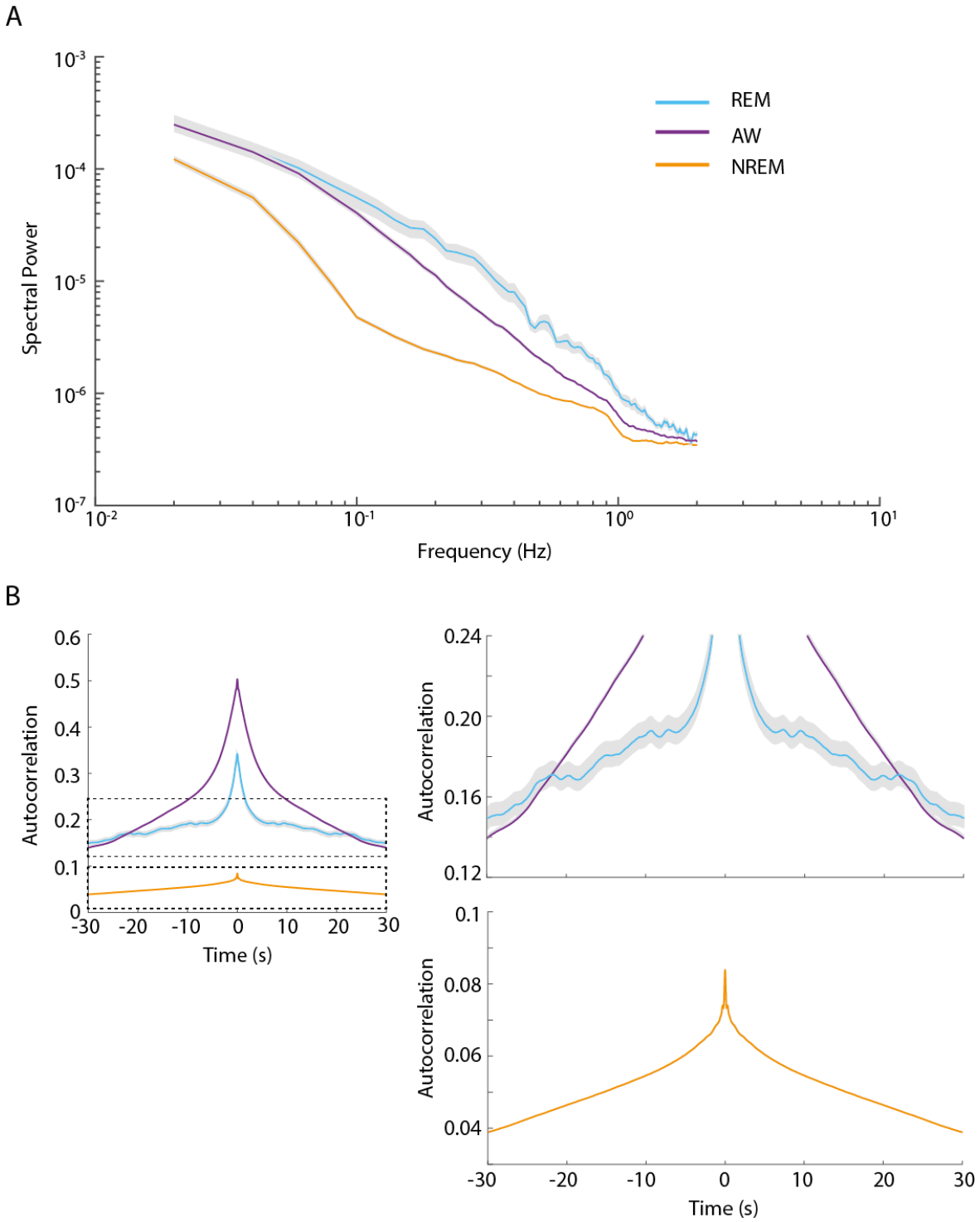

Figure 3.14: Average GCaMP6s power spectral analysis.

(A) *Spectral fluorescence power during REM sleep, NREM sleep and wakefulness.* ***(B)*** *Autocorrelogram of fluorescence signals during sleep-wake states. Inserts (right) show magnified traces during REM and awake (top) and NREM sleep (bottom). Episodes shorter than 25 seconds were excluded. Shaded areas depict ±SEM*

3.3 Discussion

3.3.1 Summary of findings

Results from this chapter shows that the fibre photometry system is sensitive enough to monitor calcium transients from a small population of neurons. Observations show that there was little cholinergic PPT/LDT GCaMP6s activity during NREM sleep and maximal activity during REM sleep, which is consistent with previous activity monitoring studies (Maloney et al., 1999, Boucetta et al., 2014, Cox et al., 2016, Cisse et al., 2018). Fluorescence signals observed in this study are unlikely to be due to movement artefacts because signals are highest during REM sleep, when EMG power is lowest.

Cholinergic tone also started to increase before the onset of REM sleep, suggesting that cholinergic PPT/LDT neurons may contribute to the initiation of REM sleep. The role of PPT/LDT neurons in the initiation of REM sleep have also been implicated in an optogenetic stimulation study by Van Dort and colleagues (2015). The authors carried out bilateral optogenetic stimulation of cholinergic PPT or LDT neurons during NREM sleep, REM sleep and wakefulness. While the probability of REM sleep increased when neurons were stimulated during NREM sleep, the duration of REM sleep episodes did not change. Equally, stimulation during REM sleep had no effect on REM sleep duration, suggesting that there may be different mechanisms regulating REM sleep initiation and REM sleep maintenance.

3.3.2 Implications of PPT/LDT activity on REM sleep

While this study does not provide a causal role for PPT/LDT neuronal regulation of REM sleep, it does support many studies that provide evidence for its role in REM sleep. It should, however, be noted that cholinergic PPT/LDT neurons most probably do not act alone in controlling REM sleep. First, as well as cholinergic neurons, both glutamatergic and GABAergic PPT/LDT neurons have been found to be REM-on (Maloney et al., 1999, Boucetta et al., 2014, Cox et al., 2016). Cox et al (2016) monitor calcium activity from glutamatergic and GABAergic PPT/LDT neurons in mice and found that although GABAergic neurons were maximally active during wakefulness, there was some activity during REM sleep too. Glutamatergic neurons, on the other hand were maximally active during REM sleep and their activity pattern also changed before state transitions to REM sleep. They did not, however assess changes in cholinergic activity with state transitions but results from this study and that from Cox and colleagues, suggest that changes in both cholinergic and glutamatergic PPT/LDT neurons may be important for the initiation of REM sleep.

Second, the PPT/LDT is the largest source of brainstem acetylcholine but the number of cholinergic PPT/LDT neurons are outnumbered by GABA and glutamatergic cell types (Wang and Morales, 2009, Mena-Segovia et al., 2009). Given that the activation of such a small number of neurons has a robust effect on REM sleep initiation (Van Dort et al., 2015), adds to the evidence that these neurons are important for REM sleep regulation, but could equally suggest that they are not so important. It has been suggested that the fast transmission of GABAergic and glutamatergic neurons are the driving forces of sleep-wake regulation while the slower transmission of cholinergic neurons have a modulatory effect on sleep-wake states (Luppi et al., 2006, Saper and Fuller, 2017).

Given that the PPT/LDT has both outputs and inputs to and from other sleep/wake regulating areas, suggest that it has some role in sleep/wake regulation (Martinez-Gonzalez et al., 2011). For example, the thalamus not only receives inputs from cholinergic PPT/LDT neurons (Woolf and Butcher, 1986, Pare et al., 1988, Kroeger et al., 2017), but concentrations of acetylcholine increased during REM sleep and wake within the thalamus as observed in a microdialysis study in rats (Williams et al., 1994), suggesting that cholinergic PPT/LDT neurons have a direct impact on thalamic nuclei, a relay hub for sensory motor signals and thalamocortical circuits. Williams and colleagues (1994) also carried out a retrograde tracing from the thalamus and reported that although the thalamus also receives inputs from cholinergic basal forebrain neurons, most cholinergic inputs were from the PPT/LDT. Cholinergic PPT/LDT neurons also have extensive projections to the reticular formation (Jones, 1990, Semba et al., 1990), which in turn regulate sleep-wake states. However, it should be noted that glutamatergic and cholinergic neurons have both shared and distinct projections to basal ganglia, thalamic, brainstem and forebrain structures (Martinez-Gonzalez et al., 2011, Kroeger et al., 2017), which makes deciphering the roles of each cell type on REM sleep regulation difficult. Additional functional studies are therefore required to tease apart the role of each PPT/LDT cell type on REM sleep. To do this, retrograde and/or anterograde viral tracing techniques could be used to selectively express opsins in specific neurons and projections to assess their effects on sleep-wake states (Kim et al., 2017).

3.3.3 Implications of cholinergic PPT/LDT neurons in arousal

Auditory evoked responses

To assess whether the optic fibre and viral injections were on target, loud sounds were randomly presented to mice during the habituation phase of the experiments. This study showed time locked increases in GCaMP6s signals to the sound presentation in mice with GCaMP6s fluorescence signals, which is in line with previous experiments in rats where

putative cholinergic LDT neurons increased firing in response to loud auditory pure tones (90 dB) (Koyama et al., 1994). Koyama and colleagues also applied other sensorimotor stimuli, such as lightly touching the tail, air puffs to the face and flashes of light, which also elicited increases in neuronal firing rate. Lightly touching the mice in the present study, also elicited an increase in GCaMP6s signals online, however, this was not systematically tested, and precise sync pulses were difficult to generate to analyse offline. Therefore, sound was the only sensory modality presented in this study and provided an adequate test for checking whether mice had a successful GCaMP6s signal.

Anatomically, cholinergic PPT/LDT neurons receive inputs from and send projections to auditory areas such as the primary auditory cortex and inferior colliculus (Mena-Segovia et al., 2008, Schofield and Motts, 2009, Motts and Schofield, 2009), suggesting a role for PPT/LDT neurons in gating acoustic stimuli. PPT/LDT neurons have also been implicated in mediating the startle response and/or prepulse inhibition (PPI) (Fendt et al., 2001, Jones and Shannon, 2004, Azzopardi et al., 2018, Garcia-Rill et al., 2019). These neurons may, therefore, play a role in arousal by alerting the brain when salient, potentially dangerous sounds have been perceived.

Activity differences between REM and AW states

This study also shows that activity patterns of cholinergic PPT/LDT neurons vary between REM sleep and wakefulness. Not only did activity profiles differ between NREM-to-REM sleep and NREM-to-AW transitions, but the overall tone was higher during REM sleep and there appeared to be underlying rhythmic activity during REM sleep, which wasn't as prevalent during wakefulness. Juxtacellular recordings report denser firing during REM sleep and sparser firing during wakefulness in individual cholinergic PPT and LDT neurons in head-fixed unanaesthetised mice (Boucetta et al., 2014, Cisse et al., 2018), suggesting that the neurons behave differently during sleep-wake states. Changes in firing patterns of cholinergic PPT/LDT neurons may explain the behavioural discrepancies between optogenetic and chemogenetic stimulation of cholinergic PPT/LDT neurons. Like Van Dort and colleagues (2015), Cisse et al (2018) also optogenetically stimulated cholinergic PPT/LDT neurons and observed that mice preferentially transitioned from NREM sleep to REM sleep and not wakefulness. Chemogenetic activation, on the other hand, resulted in increased time in light NREM in mice (Kroeger et al., 2017). While Cisse and colleagues monitored activity from a small population of cholinergic neurons with juxtacellular recordings, neither studies by Van Dort nor Kroeger monitored changes in neuronal activity. It is possible that the differences in stimulation patterns between these manipulation techniques can change neuronal activity patterns differently and thus result in different behavioural changes.

3.3.4 Experimental considerations

One of the main experimental limitations to take into consideration when interpreting the results from this study is that it includes data from several methodical optimisation steps. As this fibre photometry technique and associated surgical procedures where not a standard practice in the laboratory, I adjusted both the fibre photometry system and surgical coordinates targeting the PPT/LDT nuclei. Success rates were low because I had difficulty getting both the GCaMP6s vector and optic fibre on target. One reason for this could have been because both the micropipette for the viral vector and the optic fibre are different diameters and shapes so have different effects on the brain upon insertion. The craniotomy over the PPT/LDT was made as small as possible, but this restricted the view to the brain. Although the surface of the brains could be seen and the optic fibre was seen entering the brain, it is possible that the dura didn't break completely and thus restricted the depth of the implant. Initial implantations resulted in some GFP expression in PPT/LDT neurons, but the optic fibre was positioned too dorsal to capture fluorescence signals. Another reason for variable results in terms of PPT/LDT targeting could have been due to my initial inexperience with surgical technique. Surgical technique would have improved over time and subtle changes would have been made but they are difficult to quantify and document. Another difficulty in targeting the PPT/LDT is that it is quite long in the anterior-posterior axis, but the depth, shape, size and mediolateral positions vary throughout. As a result, placement of the injection site and optic fibre tip must be accurate.

Another important factor is that in mice where a fluorescent signal was detected, the signals suddenly disappeared after a few recordings. Upon histological examination, ChAT neuron looked damaged suggesting that GCaMP6s could have been neurotoxic to neurons. In fact the neurotoxic effect of GCaMP6 has been reported, where dissected cortical neurons infected with AAV-*Syn*-GCaMP6f had a significantly greater amount of apoptosis compared to those infected with AAV-*Syn*-EGFP (Yang et al., 2018). Overtime, GCaMP6s has been reported to accumulate in the nucleus of neurons and has been linked to causing neuronal damage or death (Chen et al., 2013, Yang et al., 2018). An optimisation step for finding the ideal dilution of the GCaMP6s viral vector was not carried out for this study as recommended by Resendez and colleagues (2016), and may be beneficial for future experiments. Another possible reason for losing fluorescence signals could be due to a neuroinflammatory response to damage caused by the implant itself, as gliosis has been reported to be a barrier to signal detection (Salatino et al., 2017). However, it is difficult to ascertain the cause of neuronal damage in this study as immunostaining for glia and astrocytes was not carried out.

Overall, this chapter shows that cholinergic PPT/LDT neuronal activity is consistent with that of the literature, however, further functional studies are required to elucidate their role in REM sleep regulation.

4 P-wave dependent cholinergic activity

The previous chapter showed brainstem cholinergic activity during sleep-wake states and transitions, on the seconds to minutes timescale. This chapter will explore cholinergic PPT/LDT population activity in relation to sub second electrophysiological waves, P-waves. First a brief overview of P-waves and the role of cholinergic PPT/LDT neurons in their generation will be provided. The results sections will then assess the occurrence of P-waves during REM and NREM sleep and compare them with cholinergic PPT/LDT calcium transients.

4.1 Introduction

4.1.1 Brief overview of the literature

P-waves have been observed in many mammalian species, with cats and rats being the most common animal model used for researching their neurobiological mechanisms (Callaway et al., 1987, Datta, 1997). PGO-waves are a result of synchronous neuronal firing that originate in the pons and propagate to the lateral geniculate body (LGB) and then to the occipital cortex in cats. While they are not present in the rat LGB, the pontine components are thought to be analogous between rats and cat. They are therefore, referred to as PGO waves in cat and P-waves in rat. The functions of P-waves are unknown, but they have been proposed to play a potential role in regulating REM sleep, learning and dreaming (Gott et al., 2017). Research into the mechanism underlying P-waves was very active between the 1960s and early 2000s, but due to their neurobiological complexity and limitations in technological tools, exploration into the cause and function of P-waves ceased. As a result, many questions have remained unanswered.

Early activity mapping and functional studies in cats found that the brainstem was crucial for the generation of P-waves (Sakai and Jouvet, 1980, Webster and Jones, 1988, Datta and Hobson, 1995). While neurons active during P-waves are not confined to specific brainstem nuclei, cholinergic neurons, of which the PPT/LDT nuclei are the largest brainstem acetylcholine source, were proposed to be one of the subsets of neurons that play a part in P-wave generation (Callaway et al., 1987, Datta, 1997). PPT lesions reduced PGO-wave density and the total duration of REM sleep (Shouse and Siegel, 1992) and microinjections of carbachol or neostigmine in the pons increased both the total percentage of REM sleep and PGO waves in cats (Baghdoyan et al., 1984b, Baghdoyan et al., 1984a, Datta et al., 1992). In rats, carbachol microinjections into the pons increased P-wave density during REM sleep and resulted in better performances in an active avoidance learning task compared to the group of mice treated with saline injections (Mavanji and Datta, 2003), suggesting that P-waves may

play some role in the regulation of REM sleep and memory consolidation. Added to this, P-waves have been reported to occur most frequently during REM sleep in both cats and rats (Thomas and Benoit, 1967, Marks et al., 1980), which mirrors the activity of cholinergic PPT/LDT neurons (Boucetta et al., 2014, Cisse et al., 2018).

Although lesion and pharmacology studies have been valuable in understanding the general nature of P-waves, the spatial resolution of these manipulations were too course to unpick the underlying neurobiology of P-waves. One limitation of previous P-wave studies is that they lacked cell-type specific monitoring of neurons and as a result it is unknown how certain cells within the brainstem contribute to the generation of P-waves. For example, neurons with different discharge patterns were identified within the PPT/LDT by Steriade and colleagues (1990b). These included neurons that were active (PGO-on) or inactive (PGO-off) during P-waves, but the cell types of these neurons are unknown.

As discussed in chapter 1, mice have become increasingly popular for basic research, in part due to the creation of an expanding library for genetic modifications through transgenics and viral vectors. As these modifications allow for cell-type specific manipulation and monitoring of neurons, the mouse model has become a powerful tool for investigating the neurobiology of the brain in health and disease. With regards to P-waves, they were previously undiscovered in mice, until our recent study reported them to present (Tsunematsu et al., 2020) . The current study, for the first time, aims to build on our previous findings and monitor cholinergic PPT/LDT population calcium transients in relation to P-waves in mice.

4.1.2 Aims and hypothesis

Considering carbachol or neostigmine administration to the pons have resulted in enhanced REM sleep and P-waves (Baghdoyan et al., 1984a, Baghdoyan et al., 1984b, Mavanji and Datta, 2003), it is hypothesised that P-waves and cholinergic PPT/LDT activity are correlated. To address whether the activity of cholinergic PPT/LDT neurons are correlated with P-waves, activity dynamics during the sub-second to second timescale were investigated. Cholinergic PPT/LDT calcium transients and extracellular electrophysiological activity from neurons surrounding the area were simultaneously measured using a hybrid implant, which consisted of a bipolar electrode attached to the optic fibre.

.

4.2 Results

This chapter will first provide an overview of the number of mice and datasets used to carry out analysis on the co-occurrence of P-waves and GCaMP6s signals. I will then characterise the frequency and occurrences of P-waves during NREM and REM sleep states and then assess P-wave triggered GCaMP6s signals during these states. Finally, GCaMP6s activity peaks were identified and correlated with P-waves. Results show that P-waves during REM sleep coincide with cholinergic PPT/LDT fluorescence signals and their peaks.

4.2.1 Data sets and mice

As discussed in section 3.2.1, a total of 17 mice were implanted with hybrid optic fibres and 4 of these mice successfully provided calcium signals. P-waves were detected from 3 of the 4 mice (figure 4.1, table 4.1) and a total of 6 recordings were used for analysis in this chapter.

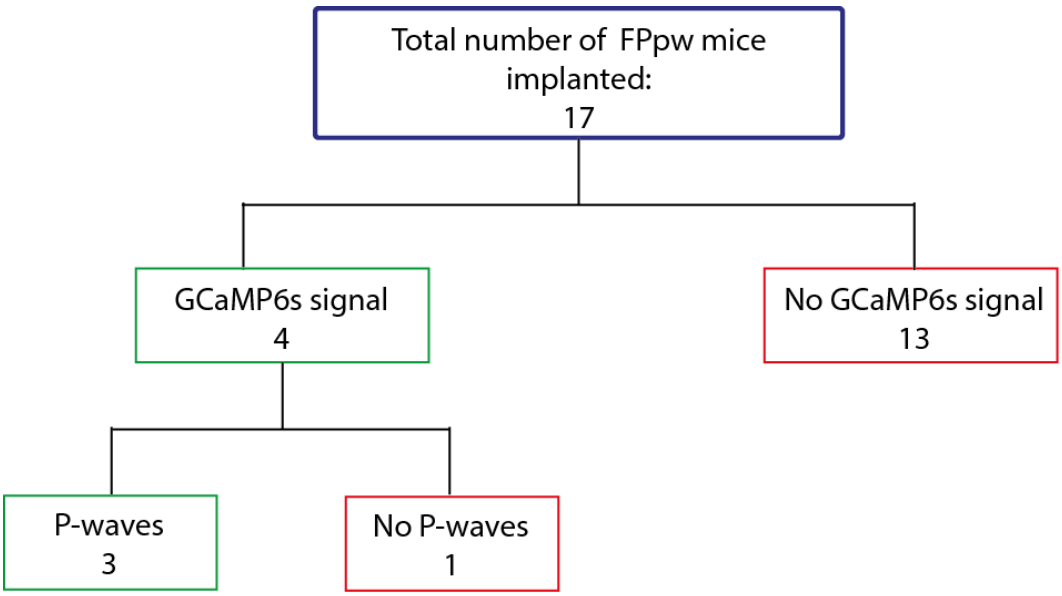

Figure 4.1: Summary of implanted P-wave mice.

Flow chart shows the total number of mice implanted with optrodes to allow for the simultaneous recording of cholinergic PPT/LDT GCaMP6s fluorescence activity and pontine LFP to detect P-waves. A total of 3 mice had both a fluorescence signal and P-waves. FPpw, fibre photometry P-wave.

Table 4.1: List of datasets with successful simultaneous P-wave and GCaMP6s fluorescence signals.

Mouse ID	Recording	NREM sleep transitions		REM sleep transitions	
		Total	Per hour	Total	Per hour
FPpw11	#1	110	24.7	6	1.3
	#2	107	24.2	2	0.5
	#3	134	31.3	7	1.6
	#4	108	30.5	6	1.7
FPpw12	#1	143	32.1	2	0.4
FPpw14	#1	76	18.0	2	0.5

4.2.2 P-waves occur during NREM and REM sleep

P-waves were identified by detecting peaks in pontine LFP above a threshold set for each recording. The threshold was defined to be 5 standard deviations about the root mean square pEEG signal during the longest NREM episode. The timings of these P-waves were collected during both NREM and REM sleep, but not during wakefulness because pEEG traces could be contaminated with movement artefacts and were difficult to filter out. As P-waves have been known to occur just before and during REM sleep, NREM sleep episodes were split into to two groups. The first group included all NREM sleep transitions while the second only included a subset of NREM episodes that transitioned into REM sleep. Figure 4.2 shows a representative example of all recorded signals during these states. Upon initial observation, both electrophysiological and fluorescence signals look similar during NREM sleep, irrespective of whether the episode transitions to wakefulness or REM sleep (figure 4.2). Cortical EEG consists of high amplitude, low frequency oscillations, with little EMG and GCaMP6s activity, which is consistent with data shown in chapter 3. P-waves occur sporadically, and with no clear pattern during both types of NREM sleep. Electrophysiology and GCaMP6s signals during REM sleep, on the other hand appear to differ in comparison with NREM sleep. Apart from differences in cortical EEG and GCaMP6s signals (as explored in chapter 3), P-waves seem to occur in a burst fashion and align with periods when GCaMP6s activity is high (figure 4.2b & bottom insert).

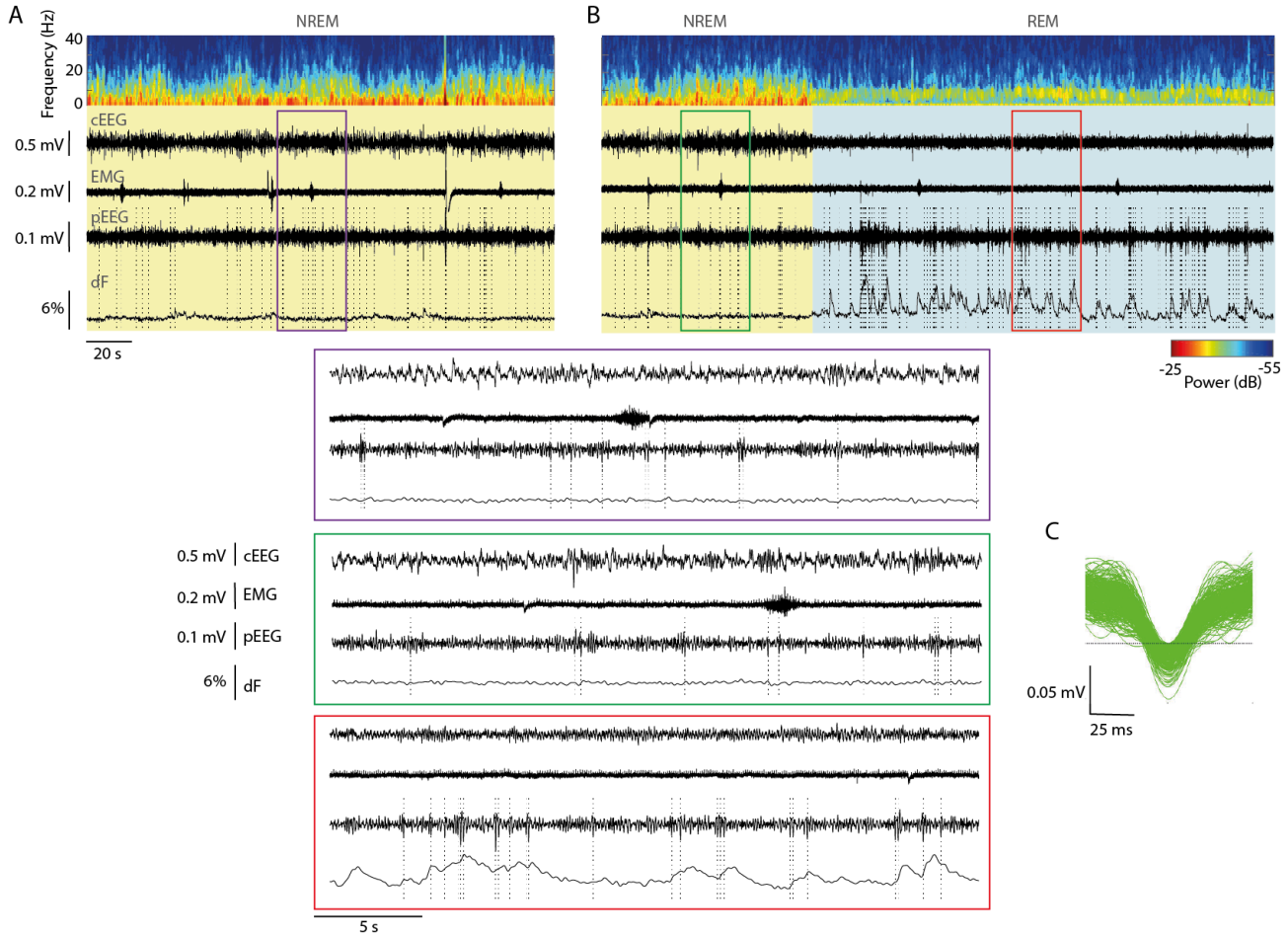

Figure 4.2: Representative electrophysiology and GCaMP6s traces during NREM and REM sleep.

(top to bottom) EEG power spectrogram, cortical EEG, EMG, pontine EEG and GCaMP6s signals during an example NREM sleep episode that transitions to wakefulness ***(A)*** *and during consecutive NREM and REM sleep episodes* ***(B)****. Dotted lines represent P-wave occurrences. Inserts show signals over a 30s period over the corresponding coloured boxes in* ***(A)*** *and* ***(B)****.* ***(C)*** *Waveforms of all P-waves during REM sleep in this recording (304 P-waves). Dotted line represents threshold for this recording.*

4.2.3 P-waves occur more frequently during REM sleep compared to NREM sleep

To quantify and explore these initial observations further, the frequency of P-waves and time between consecutive P-waves (interpeak intervals) were calculated for each state. Indeed, P-waves occur more frequently during REM sleep compared to those that occur during all NREM sleep episodes (figure 4.3a) (chi-square = 21.16, $p = 2.55 \times 10^{-5}$, Kruskal-Wallis; $p < 0.01$ all NREM vs REM & all NREM vs NREM preceding REM, with post hoc Bonferroni) and with the least time in between consecutive P-waves compared to both NREM sleep groups (figure 4.3b) (chi-square = 238.28, $p = 1.81 \times 10^{-52}$, Kruskal-Wallis; $p < 0.001$, all NREM vs REM; $p < 0.05$ NREM preceding REM vs REM, with multiple comparisons Bonferroni). Whilst it is difficult to observe a clear pattern in the autocorrelation lag during REM sleep, many P-waves occur within 2 seconds of each other. The highest and first P-wave autocorrelation peak during REM sleep occurs at a 110 ms lag (0.035 ± 0.012 normalised autocorrelation), while the second largest peak occurs at 1430 ms lag (0.018 ± 0.014 normalised autocorrelation) (figure 4.3c).

Similarities and differences in P-waves between NREM sleep groups

As mentioned above, P-waves have been reported to occur during REM and NREM sleep in cats and rats (Brooks and Bizzi, 1963, Marks et al., 1980, Farber et al., 1980). The characteristics of P-waves during NREM sleep preceding REM sleep and all NREM sleep episodes were, therefore, compared to identify whether there are differences in P-wave activity between both state groups. Although the times between consecutive P-wave are not significantly different during all NREM sleep episodes and those that transition to REM sleep (figure 4.3b), the median frequency of P-waves during NREM sleep episodes preceding REM sleep is higher (figure 4.3a) (0.21 Hz and 0.30 Hz, median frequency of P-waves during all NREM sleep episodes and NREM sleep preceding REM sleep, respectively). Both groups of NREM sleep show relatively weak P-wave autocorrelations (compared to REM sleep). However, clear differences during both NREM sleep groups can also be observed in the P-wave autocorrelograms. P-waves appear to be more rhythmic during NREM sleep episodes that transition to REM sleep compared to all NREM sleep episodes. Additionally, the first and largest peak during all NREM sleep episodes is slightly slower and less correlated compared to P-waves occurring during NREM sleep episodes that transition to REM sleep (140 ms, 0.009 ± 0.0013 normalised autocorrelation during all NREM sleep episodes; 120 ms, 0.011 ± 0.0036 normalised autocorrelation during NREM sleep that transitions to REM sleep). This suggests that P-waves preceding REM sleep occur more frequently and dynamically compared to those that occur during all NREM sleep episodes. P-waves during and before

REM sleep also have similar autocorrelation profiles but with lower correlation values during the preceding NREM sleep episodes.

4.2.4 Cholinergic PPT/LDT activity is correlated with P-wave occurrence, especially during REM sleep

To assess whether P-waves coincide with changes in cholinergic PPT/LDT activity, the GCaMP6s signal around P-waves was extracted and compared across sleep states. There was a moderate, average increase in cholinergic activity during all NREM sleep episodes, and a slightly larger increase during P-waves occurring during NREM sleep before REM sleep. In contrast, larger P-wave triggered increases in GCaMP6s signals were consistently observed during REM sleep (figure 4.4).

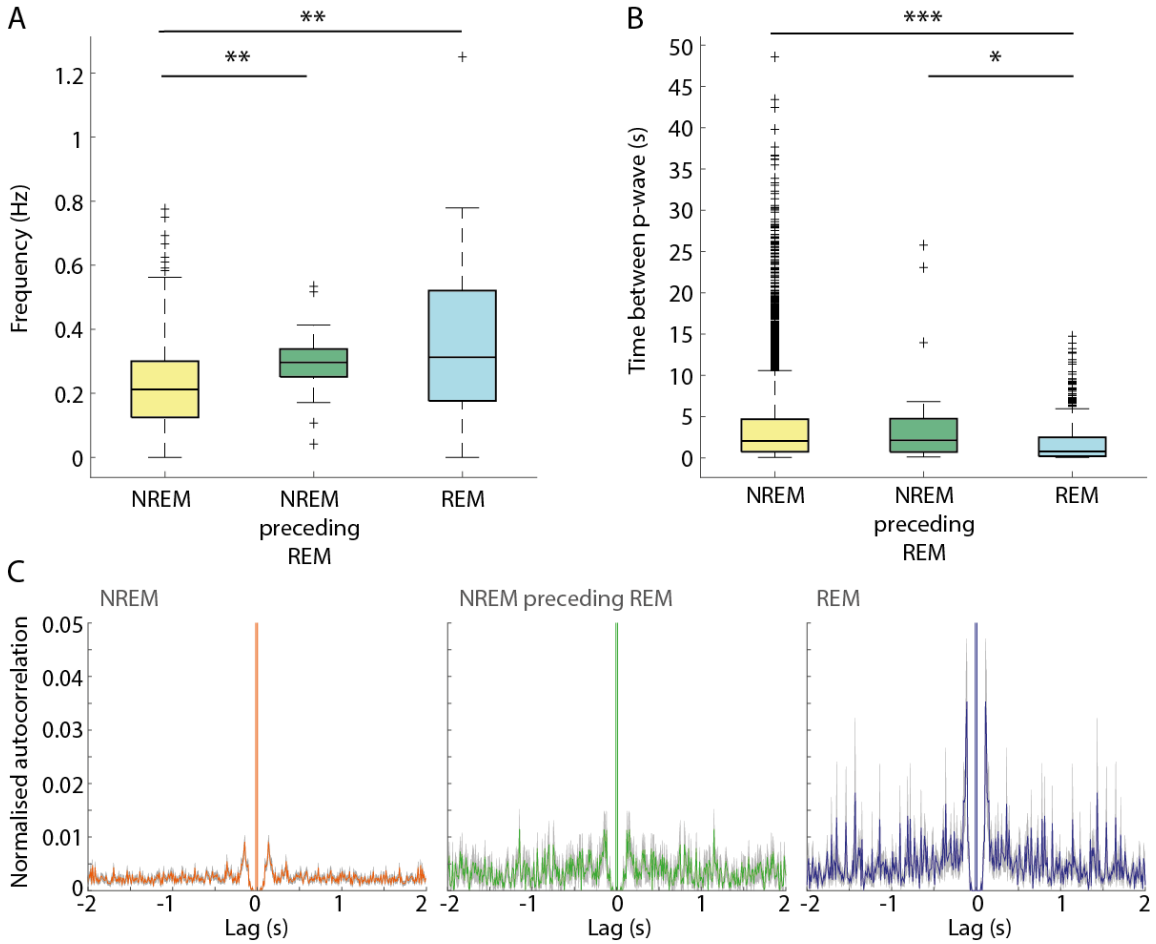

Figure 4.3: Summary of P-wave occurrences during NREM and REM sleep.

Frequency of P-waves (chi-square = 21.16, p = 2.55x10^{-5}, Kruskal-Wallis) ***(A),*** *time between consecutive P-waves (chi-square = 238.28, p = 1.81x10^{-52}, Kruskal-Wallis)* ***(B)*** *and averaged autocorrelation of P-waves* ***(C)*** *during all NREM sleep episodes, NREM sleep episodes that precede REM sleep and REM sleep. Data collated from 6 recordings and 3 mice (25 REM sleep and 656 NREM episodes). *, p < 0.05; **, p < 0.01; ***, p < 0.001, with Bonferroni multiple comparisons test. Boxplots show median, lower and upper quartiles and outliers (crosses) for each state. Shaded area represents ±SEM.*

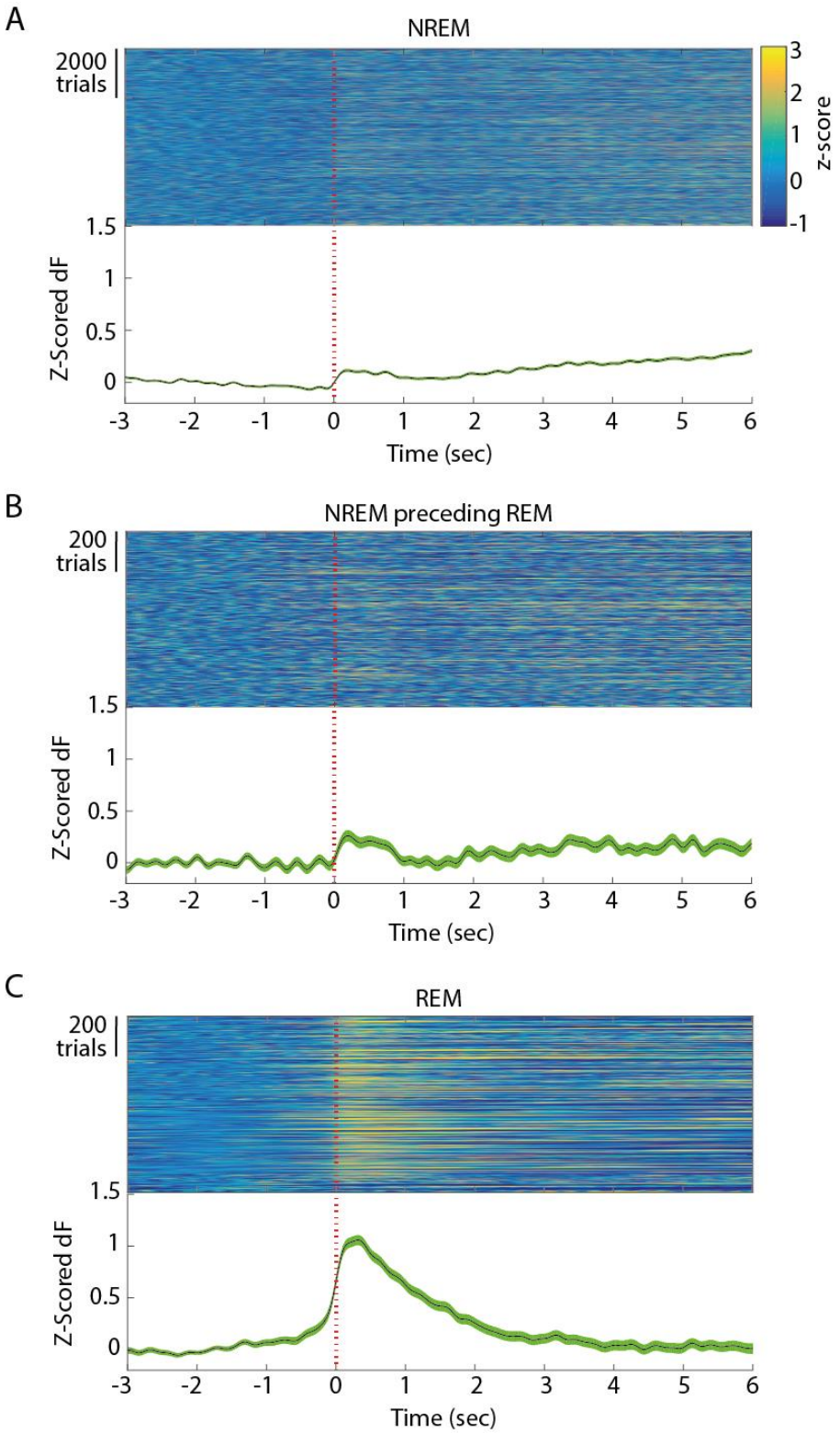

Figure 4.4: P-wave triggered GCaMP6s signals during NREM and REM sleep.

Z-scored GCaMP6s signals around P-waves during all NREM sleep episodes ***(A)****, NREM sleep episodes occurring just before REM sleep* ***(B)*** *and REM sleep episodes* ***(C)*** *from 6 recordings (3 mice). The baseline was taken across -3 and -1 seconds before P-wave trough (time zero). Colour maps show individual trials while traces depict mean and ±SEM z-scored fluorescence.*

4.2.5 Peaks in cholinergic PPT/LDT activity occur more prominently during REM sleep compared to NREM sleep

As discussed previously in chapter 3 (section 3.2.5), rhythmic fluctuations in GCaMP6s activity during REM sleep were observed. It was hypothesised that these fluctuations during REM sleep may coincide with P-waves. Considering P-waves were detected during both NREM sleep and REM sleep, peaks in fluorescence signal were first detected and compared between both sleep states. Example REM and NREM sleep traces show that many more fluorescence peaks were detected during REM sleep compared to NREM sleep (figure 4.5). This observation is further validated with summary analysis. The frequency of GCaMP6s fluorescence peaks are significantly higher during REM sleep compared to both all NREM sleep episodes and those that precede REM sleep (figure 4.6a) (chi-square = 102.9, $p = 4.63 \times 10^{-23}$, Kruskal-Wallis; $p < 0.001$, both NREM groups vs REM, with Bonferroni multiple comparisons). Fluorescence peaks were not detected in 91.2% of all NREM sleep episodes and 28% of REM sleep episodes (figure 4.6b). Of the episodes where multiple peaks were detected, the time between consecutive fluorescence peaks (interpeak interval) during REM sleep were also shorter compared to both NREM sleep groups (figure 4.6c). Most calcium activity peaks during REM sleep also occurred within 20 seconds after the previous peak (figure 4.6d) and had the highest autocorrelation at 4, 7, and 11 seconds lag, which corresponds to 0.09 - 0.25 Hz. This is consistent with fluorescence spectral analysis data presented in chapter 3 (figure 4.6e & figure 3.14). A very small number of peaks occurred with a 5 second lag (0.2Hz) during all NREM sleep episodes. As there were only 3 interpeak intervals for NREM sleep episodes that precede REM sleep, the autocorrelation peaks occurring for this condition are difficult to interpret. Few interpeak intervals suggest that more than one fluorescence peak was rarely detected and there is little rhythmicity in cholinergic calcium activity during NREM sleep before REM.

4.2.6 P-waves and cholinergic fluorescence peaks occur together during REM sleep

While data presented in this chapter show that both P-waves and GCaMP6s fluorescence peaks are present during REM sleep, the correlation between the occurrences of both events have not been assessed. To evaluate whether P-wave and fluorescence peaks coincide, the number of P-waves occurring around fluorescence peaks (and vice versa) were evaluated. Figure 4.7a shows that P-waves consistently occur around 1 second before fluorescence peaks during REM sleep but are randomly observed during NREM sleep. Equally, while there were few fluorescence peaks observed around P-waves during both NREM sleep groups, GCaMP6s peaks appear just after P-waves during REM sleep (figure 4.7b).

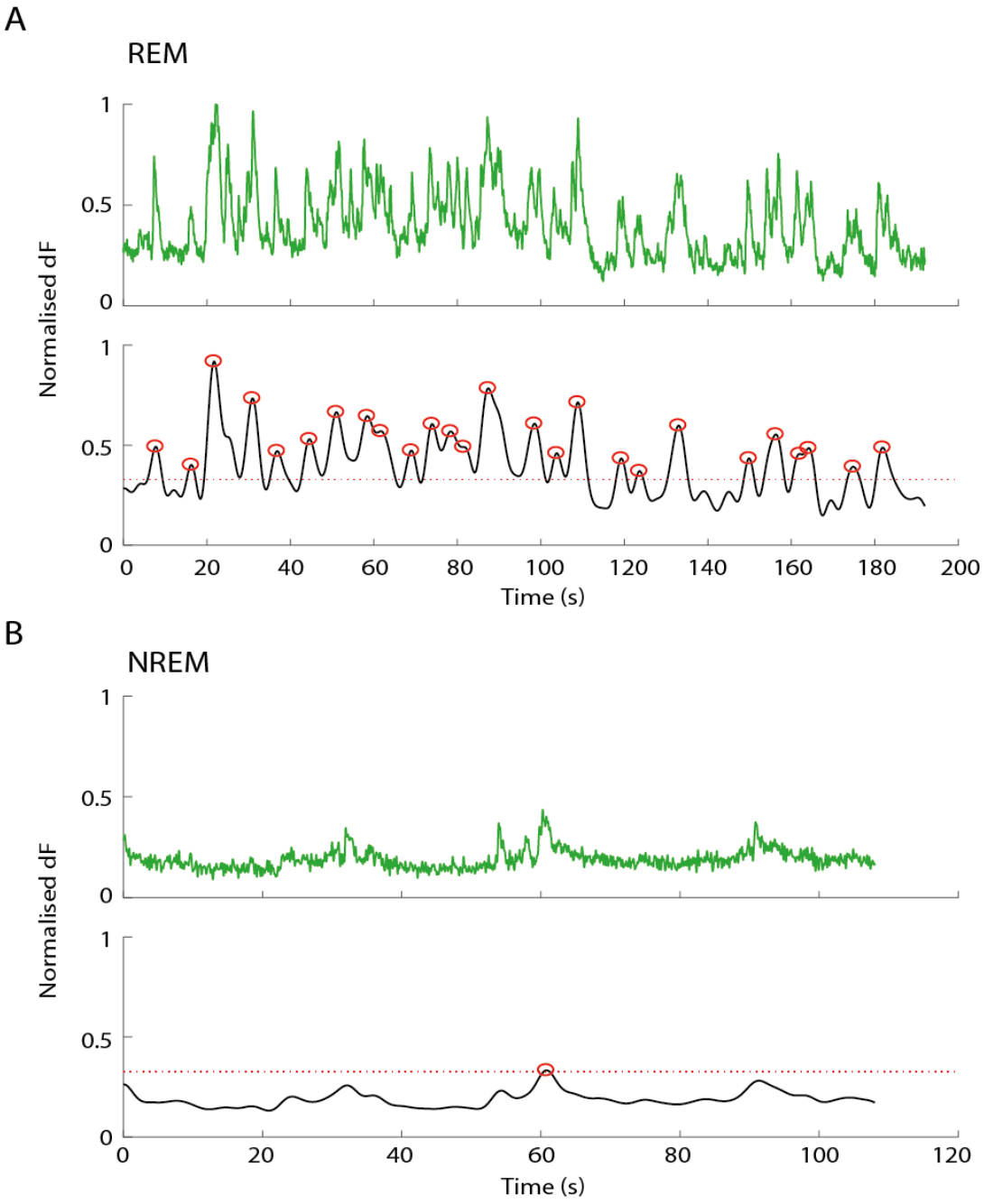

Figure 4.5: Identification of GCaMP6s activity peaks.

*Raw GCaMP6s traces (green trace) during an example REM **(A)** and NREM sleep **(B)** episode. Fluorescence signals were lowpass filtered at 0.25Hz (black trace) and peaks (red circle) above the threshold (red dotted line) were identified. To account for photobleaching, recordings were split in half and thresholds for each half were calculated by computing 2 standard deviations above the mean raw fluorescence during NREM sleep.*

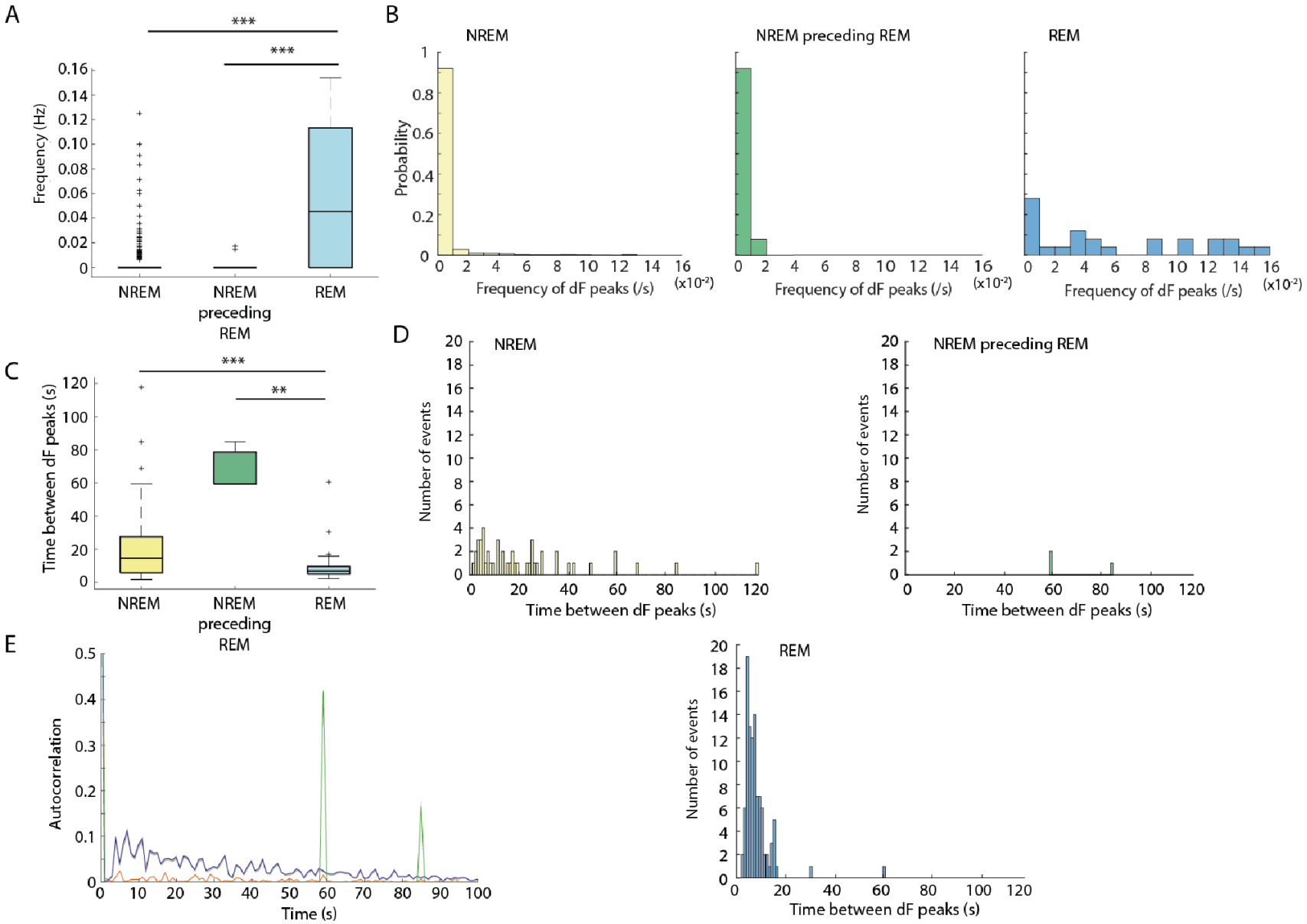
A
***
***
Frequency (Hz)
0.16
0.14
0.12
0.10
0.08
0.06
0.04
0.02
0
NREM
NREM preceding REM
REM
B
NREM
NREM preceding REM
REM
Probability
1
0.8
0.6
0.4
0.2
0
0 2 4 6 8 10 12 14 16
(x10-2)
Frequency of dF peaks (/s)
C
***
**
Time between dF peaks (s)
120
100
80
60
40
20
0
NREM
NREM preceding REM
REM
D
NREM
NREM preceding REM
REM
Number of events
20
18
16
14
12
10
8
6
4
2
0
0 20 40 60 80 100 120
Time between dF peaks (s)
E
Autocorrelation
0.5
0.4
0.3
0.2
0.1
0
0 10 20 30 40 50 60 70 80 90 100
Time (s)

Figure 4.6: Summary of fluorescence peak occurrences during NREM and REM sleep.

(A & B) *Frequency of GCaMP6s peaks and histogram showing the proportion of peaks during all NREM sleep episodes (yellow), NREM sleep episodes preceding REM sleep (green) and REM sleep (blue). (Chi-square = 102.9, p = 4.63x10^{-23}, Kruskal-Wallis)* ***(C & D)*** *Boxplot and histogram showing the time between consecutive fluorescence peaks for each sleep condition. Note, only 3 interpeak intervals were detected during NREM preceding REM sleep. (Chi-square = 24.2, p = 5.56x10^{-6}, Kruskal-Wallis) **, p < 0.01; ***, p < 0.001, with Bonferroni post hoc test.* ***(E)*** *Averaged autocorrelogram of GCaMP6s peaks. Shaded area represents ±SEM.*

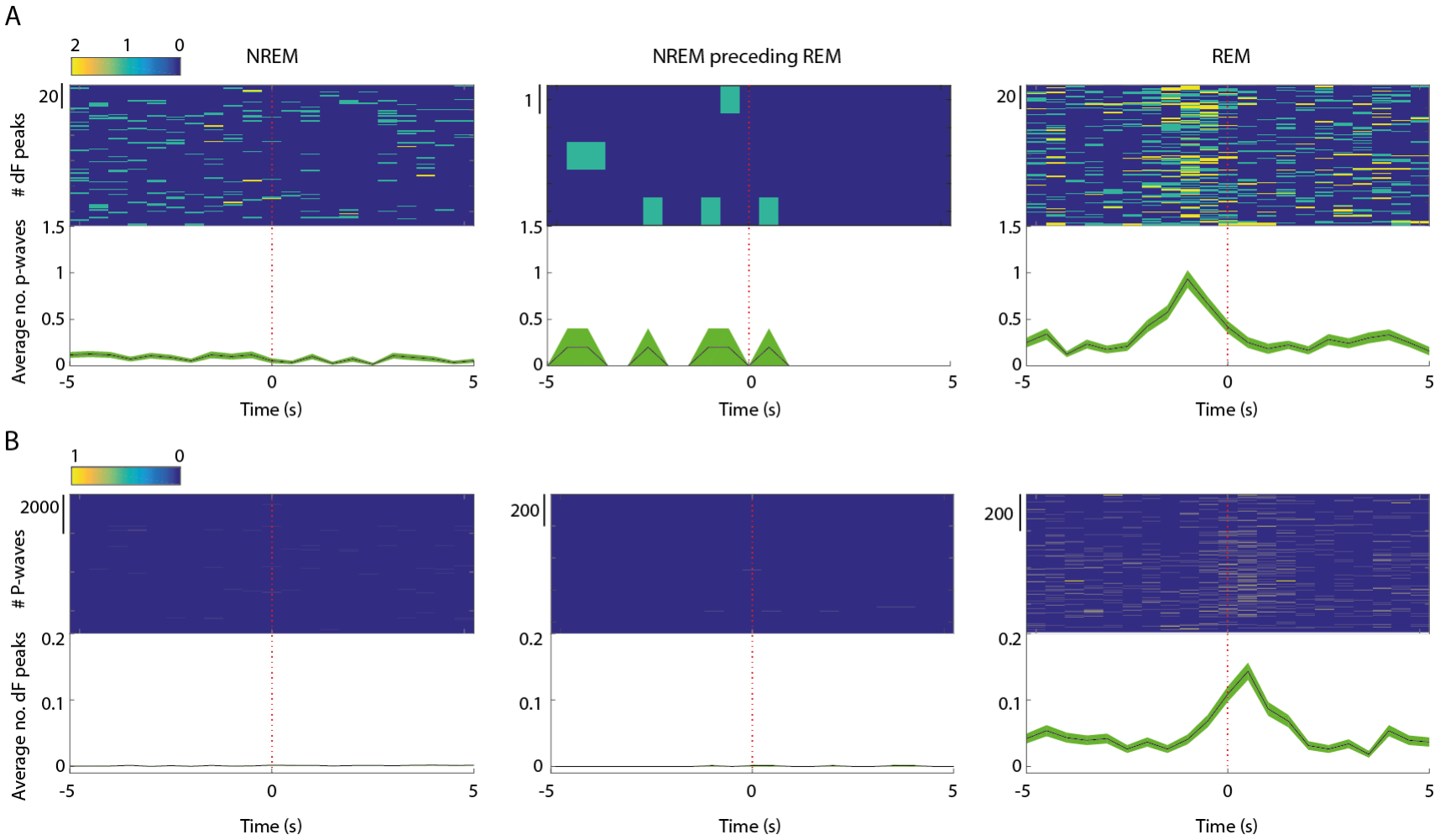

Figure 4.7: Co-occurrence of P-waves and GCaMP6s signal peaks.

(A) *Number of P-waves that occur around fluorescence peak during all NREM sleep episodes (left), NREM sleep episodes that transition into REM sleep (middle) and REM sleep (right).* ***(B)*** *Number of fluorescence peaks in relation to P-waves. Traces below colour maps show average number of P-waves (A) or fluorescence peaks (B). Shaded area indicate ± SEM. Time bin is 0.5 s.*

4.3 Discussion

4.3.1 Summary of findings

This study is the first to investigate the correlation between cholinergic PPT/LDT activity and P-waves in mice. The mice were implanted with optrodes to simultaneously monitor cell-type specific calcium transients from cholinergic PPT/LDT neurons and LFP in the pontine area. P-waves and fluorescent signals were successfully recorded from 3 mice and 6 recordings. P-waves were more frequent during REM sleep compared to NREM sleep, which is consistent with observations in cats and rats (Brooks and Bizzi, 1963, Thomas and Benoit, 1967, Marks et al., 1980, Farber et al., 1980, Datta and Hobson, 1994). P-waves during REM sleep also coincided with the greatest increases in cholinergic calcium transients during REM sleep. The larger summation of calcium transients during REM sleep compared to NREM sleep suggest that a larger population of cholinergic neurons were synchronously activated. While a causal relationship between cholinergic PPT/LDT neurons and P-waves cannot be ascertained from this study, these results are in line with previous studies suggesting that these neurons play some role in the generation of P-waves in cats and rat (Baghdoyan et al., 1984a, Baghdoyan et al., 1984b, Shouse and Siegel, 1992, Mavanji and Datta, 2003).

Given that cholinergic neurons during NREM sleep are virtually silent, as seen in this study and within the literature (Cox et al., 2016), it is possible that P-wave generating mechanisms differ between NREM and REM sleep. Neurons in the dorsal subcoeruleus of rats (caudo-lateral peribrachial area in cats) have also been implicated in the generation of P-waves (Datta and Hobson, 1994, Datta et al., 1998, Mavanji et al., 2004). Considering the close proximity of the dorsal subcoeruleus, PPT/LDT and other sleep-wake regulating structures and propagating nature of P-waves, it is difficult to pinpoint the generating mechanisms with traditional techniques such as lesions, pharmacology and electrophysiology used in previous studies. Further studies are required to tease apart the temporal and cell-type specific neural activity in relation to P-waves. This may be possible through investigating the effects of cell type specific optogenetic stimulation on P-wave occurrences.

4.3.2 Differences in P-wave observations

Although P-waves in this study occurred at a higher frequency during REM compared to NREM sleep, many P-waves were also detected during NREM sleep. While this pattern is consistent with reports in the literature, there appear to be some differences between species. P-waves in cats during REM sleep have been reported to occur four times more often than rats, with an average of 60 waves/min in cats (Jouvet, 1972) and 15.5 wave/min in rats (Marks

et al., 1980). In the present study, we found that P-waves during REM sleep occurred at similar frequencies to rats with a median of 18.6 waves/min.

Only one other study has investigated P-waves in mice (Tsunematsu et al., 2020) , however, differences in experimental setup, electrode location and data analysis make comparing results difficult. Mice were head-fixed in the previous study, which may have affected sleep/wake architecture and depth of both NREM and REM sleep. A combination of these factors may also explain why P-waves observed in our previous paper were more frequent (~60 waves/min during REM sleep) than those detected in this study.

In summary, although the present study is the first of its kind, further studies investigating the neuronal underpinnings of P-waves in mice are required to gain a better understanding of the generation and propagation of P-waves.

4.3.3 Limitations

Single channel analysis

It should be noted that P-waves in this study were detected using a single channel on the implanted bipolar electrode. This is because a fewer number of P-waves were detected when the signal from two channels were subtracted in recordings from FPpw11. It is difficult to ascertain the reason for detecting fewer P-waves with this mouse but one reason for this could be due to the position of the two electrodes in the brain. The higher electrode was designed to serve as a reference channel and would ideally be positioned just above the PPT/LDT area. The lower electrode would preferably be positioned within the PPT/LDT nuclei and the subsequent subtracting of the channels would result in the LFP of the neurons in the area. However, if the tips of the electrodes are positioned too close together or both implanted within the same population of neurons, subtracting the signals would cancel out. The resulting deflections in pontine LFP, used to detected P-waves, would not be as prominent and difficult to identify. For consistency, P-waves in the other two mice were also detected using a single channel. Consequently, results presented in this study should be interpreted with care.

One limitation with using a single channel for detecting P-waves is that without a reference channel to compare with, we are more likely to detect movement related artefacts (false positives). This is not a problem during REM sleep, where mice experience muscle atonia, however, artefacts may be present during NREM sleep where moderate amounts of movement is expected. Second, without a local reference channel, it is difficult to isolate where the signals are coming from. LFP recorded from a single channel could, and most likely is, a

result of volume conduction where neuronal activity from several brain regions contribute the LFP signal.

Data limitations

P-waves were detected in 3 of the 4 mice that had a successful fluorescent signal. It is unclear as to why P-waves were not detected in FPpw3, however, a combination of the location and impedance of the bipolar electrodes may have affected the success. While the bipolar electrodes appeared to be positioned within the PPT (-4.71 mm from bregma) and impedances were within an appropriate range, it is possible that the electrodes were damaged, or the tips were obstructed with tissue if the skull or dura were not removed sufficiently during surgical implantation. For future studies it may be appropriate to develop a protocol to check the impedance of implanted electrodes.

Data presented here, is also dominated by one mouse, FPpw11, who contributed 4 of the 6 recordings analysed in this chapter. Refining the location of bipolar electrodes and repeating experiments with more mice in the future could help correlate the location of electrodes with P-wave properties.

Temporal differences between GCaMP6s and electrophysiology signals

The temporal resolution of GCaMP6s signals is drastically slower than extracellular electrophysiological signals. This is due to a combination of intrinsically slow calcium transients and the time constants associated with the fluorescent indicator - GCaMP6s has a rise time (τ_{peak}) of 179 ms and a decay time ($\tau_{1/2}$) of 550 ms, which makes comparing fluorescence and electrophysiological signals difficult. Results presented here, suggest that P-waves and the increase in cholinergic calcium activity coincide, but determining which one precedes the other is difficult to ascertain. One way to solve this would be to extrapolate neuronal activity from GCaMP6s signals through deconvolution or other computational approaches such as template matching and Bayesian inference (Yaksi and Friedrich, 2006, Grewe et al., 2010, Theis et al., 2016, Pnevmatikakis et al., 2016, Friedrich et al., 2017). Optogenetically tagging neurons to monitor cell-type specific neuronal activity in relation to P-waves could also be insightful (Mendrela et al., 2018, Cisse et al., 2018). Another way to overcome this problem would be to use genetically encoded voltage indicators (GEVIs), which have faster kinetics, but photobleaching is still a problem and therefore not compatible with long recordings required for sleep-wake studies (Adam et al., 2019, Piatkevich et al., 2019). Studies with GEVIs are therefore dependent on future technological developments.

4.3.4 Future work

Considering glutamatergic neurons have also been implicated in playing a role in both REM sleep and P-waves (Datta, 1997, Datta, 2002, Luppi et al., 2006, Saper and Fuller, 2017), it would be beneficial to repeat this study on PPT/LDT glutamatergic neurons. Activity mapping studies observed heterogenous populations of neurons that were active or inactive during P-waves (Steriade et al., 1990b, Datta and Siwek, 2002), which could indicate cell-type specific neural activity. It would also be interesting to unpick the interactions of both cholinergic and glutamatergic neuronal activity in relation to P-waves. To do this, simultaneous recordings of both cell-types with spectrally distinct reporters would be ideal.

While this study has been valuable in confirming and identifying P-waves and cholinergic PPT/LDT activity, it does not provide any clues on the key neurons needed for P-wave generation. To do this, gain/loss of function studies with the use of optogenetics and chemogenetic will need to be carried out in the future. Although both optogenetic and chemogenetics have their own limitations, they have not been used to study P-waves before. Additionally, to monitor single cells activity, optogenetic tagging studies can also be carried out. In optogenetic tagging experiments, neurons selectively express an opsin such as channel rhodopsin (ChR2), which are briefly stimulated with an optical protocol. ChR2-tagged neurons are then identified electrophysiological, allowing for cell-type specific monitoring of neuronal activity (Cisse et al., 2018).

5 A pilot study on pontine cholinergic activity in an Alzheimer's Disease mouse model

5.1 Introduction

In chapters 3 and 4, an increase in cholinergic PPT/LDT tone during REM sleep and P-waves was shown. Sleep disruptions in neurogenerative diseases, such as Alzheimer's Disease (AD) have been documented in both humans and animal models (Wulff et al., 2010, Rothman and Mattson, 2012). As a result, a pilot study was carried out to investigate PPT/LDT cholinergic activity in a mouse model of AD.

In this chapter, a brief introduction into Alzheimer's Disease and its implications on REM sleep will be discussed. Preliminary data, comparing sleep/wake architecture between a mouse model of AD and non-AD mice will then be shown and cholinergic PPT/LDT fluorescence signals from a single mouse will be presented. Implications of this study and future investigations will then be discussed.

5.1.1 Overview of Alzheimer's Disease

Dementia is an age-related neurodegenerative disease affecting approximately 50 million people around the world (World Health Organization, 2019a) and the global cost of dementia was estimated to equal $818 billion USD in 2015 (Wimo et al., 2017). Considering aging is a major risk factor for developing dementia, with a growing aging population worldwide, dementia, not only has a devastating impact on patients' lives and their families, but also increases the economic, healthcare and social care burden on wider society (Sloane et al., 2002, Knapp et al., 2007, Bond et al., 2012).

Alzheimer's Disease (AD) is the most prevalent form of dementia, comprising of between 60-70% of patients diagnosed with dementia (Ott et al., 1995, World Health Organization, 2019b). AD is a progressive disease that results in gradual loss of memory, cognition, sleep regulation and other neuropsychiatric deficits, which can eventually lead to the institutionalisation of patients (Knapp et al., 2007, Belger et al., 2019). Neurophysiological hallmarks of AD include the presence of neuropathological amyloid beta (Aβ) plaques (specifically from $A\beta_{42}$) and neurofibrillary tangles (NFT) from the build-up of tau proteins, which leads to neuroinflammation and cell death (Cummings et al., 1996, Mattson, 2004).

Approximately 2.2% of dementia patients develop early onset AD (before the age of 65), which is also known as familial AD (FAD) and has been linked to mutations in genes encoding one

of three proteins - amyloid precursor protein (APP), presenilin 1 (PS1) or presenilin 2 (PS2) (Knapp et al., 2007, Cruts et al., 2012). The vast majority of AD patients, on the other hand, develop late onset, or sporadic AD, which has been attributed to a combination of genetic and environmental factors. NFT and Aβ plaques deposition have been associated with the ε4 allele of a polymorphic protein apolipoprotein E (ApoE) and individuals who carry this polymorphism have an increased risk of developing AD (Saunders et al., 1993, Nalbantoglu et al., 1994, Liu et al., 2013). The aetiology of AD is uncertain, but aging is thought to be one of the major risk factors for developing the disease (Matthews and Brayne, 2005).

No cure is currently available for AD, but four pharmacological interventions are available to ease symptoms in the UK and US. Three of these (donepezil, rivastigmine and galantamine) are acetylcholinesterase inhibitors (AChEIs), which restrict the breakdown of acetylcholine and the fourth drug (memantine) is a NMDA receptor antagonist. These drugs have been reported to have moderate benefits to cognitive function, but many patients did not experience the therapeutic effects of the drugs and side effects included nausea, vomiting and diarrhoea (Birks et al., 2000a, Birks et al., 2000b, Raskind et al., 2000, Bond et al., 2012).

There is a clear need for a better understanding the progression of the AD and its impact on normal physiological brain functions. This could, in turn, provide potential for discovering better treatments and diagnosis tools.

5.1.2 Mouse models of AD

Technology for detecting and imaging neural correlated of AD in humans is improving, however, invasive techniques are still required to carry out basic research and for discovering potential treatments. Animal models of the AD are essential for this. While several species of animals have been used to investigate various aspects of AD, such as the fruit fly (Drosophila melanogaster), *C.* elegans, and zebra fish (Van Dam and De Deyn, 2011), mouse models of AD have been increasingly used over the past few decades. This is because animal husbandry for mice is relatively simple and transgenic manipulations are common practice.

Transgenic mouse models of AD have been developed since the 1990s and involve the knock-out or insertion of single AD-related genes or manipulating a combination of these genes, such as human APP, presenilin 1 and 2; and tau proteins (See reviews (Van Dam and De Deyn, 2011, Lee and Han, 2013, Gotz et al., 2018)). Commonly used APP models include the Tg2576 and APP23 mouse models, which express the Swedish familial mutation of human APP (Hsiao et al., 1996, Sturchler-Pierrat et al., 1997, Hsiao, 1998). In both models, mice

developed Aβ plaque deposition at 9 and 6 months of age, respectively, but no neurofibrillary tangles. PS1 and PS2 models increase the $A\beta_{1-42}/A\beta_{1-40}$ ratio, however, Aβ plaque deposition was only observed in some models (Lee and Han, 2013). PS1-transgenic mice did not form Aβ plaques but did show signs of neurodegeneration (Chui et al., 1999). When PS1 mutant mice were crossed with APP lines, plaque deposition was accelerated (Flood et al., 2002). This led to the development of mice models with mutations in both the APP and PS1 genes, one of which includes the 5xFAD (or Tg6799) mouse model. These mice express 5 familial associated mutations on the APP and PS1 proteins, develop Aβ plaques at 2 months and have memory impairments (Oakley et al., 2006).

5.1.3 Alzheimer's disease, sleep disruption and pontine cholinergic pathology

Patients typically experience drastic changes to their circadian rhythms, including daytime sleepiness and disruptions to night-time sleep patterns. These disturbances have been reported to cause stress on both the patients and their caregivers and is one of the reasons for institutionalising patients (McCurry et al., 2000). Sleep disturbances are observed in 14-59% of patients with mild cognitive impairments and occur before signs of cognitive decline (Hatfield et al., 2004, Beaulieu-Bonneau and Hudon, 2009, Ju et al., 2013). Poor sleep quality has also been linked to memory dysfunction and Aβ peptide regulation, suggesting that both AD pathology and sleep have a bidirectional effect on each other (Westerberg et al., 2010, Ju et al., 2014, Musiek et al., 2015, Vanderheyden et al., 2018). Sleep disturbances may even play a causal role in accelerating AD as well as other neurodegenerative diseases (Mander et al., 2016, Vanderheyden et al., 2018).

Disturbances in REM sleep

Not only is REM sleep an elusive behavioural state but disruptions in REM sleep appear to have consequences on neurodegenerative diseases. REM sleep behavioural disorder (RBD), where people lack muscle atonia during REM sleep, often leads to people enacting frightening or unpleasant dreams and can be dangerous for both patients and their bed partners, with 32% of patients in a study having injured themselves and 64% harming their sleeping partners (Olson et al., 2000). RBD has also been strongly linked to the development of Parkinson's disease and other α-synucleinopathies such as Dementia with Lewy Bodies and Multiple systems atrophy, where approximately 33-43% of PD patients have this sleep disorder (Gagnon et al., 2002, Galbiati et al., 2019). In a meta-analysis of RBD studies, Galbiati and colleagues (2019) reported approximately 3% of patients with RBD also had AD. Most interestingly, RBD diagnosis occurred before the development neurodegenerative diseases. In one particular longitudinal study, 81% of the patients diagnosed with RBD were reported to

develop a neurodegenerative disease after 14 years of the RBD diagnosis (Schenck et al., 2013). Although RBD is most prevalent in diseases with α-synucleinopathies, 4 out of 15 patients diagnosed with AD also presented with REM sleep without atonia (RSWA) in a polysomnography study, suggesting that disturbances to REM sleep may not be exclusive to α-synucleinopathies (Gagnon et al., 2006). RSWA is characterised by an increase in muscle activity during REM sleep and coupled with dream enactment results in the diagnosis of RBD (AASM, 2005).

In addition to this, the administration of donepezil, an acetylcholinesterase inhibitor, for 6 months increased the total amount of REM sleep in patients with AD compared to the placebo group (Moraes Wdos et al., 2006). Cognitive improvements were also associated with the group receiving donepezil treatment suggesting that improvements in both REM sleep and the enhancement of cholinergic transmission may be beneficial for AD patients (Moraes Wdos et al., 2006). Reductions in acetylcholinesterase activity in PPT/LDT areas were also observed in AD patients, and there were more profound reductions in those with sleep disturbances in an MRI study (Eggers et al., 2007).

Sleep disruptions in mouse models of AD

Transgenic mouse models of AD, in part, mimic the bidirectional effects of sleep disturbances and Aβ deposition observed in humans. Concentrations of Aβ in the interstitial fluid (ISF) surrounding neurons fluctuate with the sleep-wake cycle and sleep deprivation increased both Aβ ISF concentrations and Aβ plaque load in Tg2576 mice (Kang et al., 2009). Equally, both sleep-wake cycles and the diurnal Aβ ISF fluctuations were disrupted after Aβ plaque formation in female APP/PS1 mice (Roh et al., 2012). Additionally, although exercise appeared to have a protective effect on plaque depositions, mice with the same amount of exercise and sleep deprivation had an increase in Aβ plaque load (Minakawa et al., 2017). This suggests that sleep disturbances may have an accelerating effect on the progression of AD.

Studies also report a reduction in time spent in sleep in APP/PS1, Tg2576 and 5xFAD mouse models (Wisor et al., 2005, Jyoti et al., 2010, Schneider et al., 2014). However, in a study investigating sleep in Tg2576, APP/PS1 and 3xTgAD strains of mice, the amount of time spent in wake, NREM and REM sleep for each group of mice were not statistically different from their control litter mates, but there were differences in EEG spectral power (Kent et al., 2018). These discrepancies could be due to differences in experimental protocols and the way in which sleep-wake cycles are reported. For example, Kent and colleagues only report the

percentage of time the mice spent in each state, but do not investigate whether the sleep-wake cycle was more fragmented.

Cholinergic degeneration in AD

Cholinergic basal forebrain neurons are one of the first groups of neurons that atrophy during the progression of AD (Grothe et al., 2012). Although degeneration of basal forebrain cholinergic neurons also occurs as a process of aging, the decline in cholinergic neurons are greater in patients with AD, which in turn reduces connectivity to cortical areas of the brain and may explain some of the cognitive impairments observed in AD patients (Schliebs and Arendt, 2006, Grothe et al., 2012). Cholinergic neuronal degeneration has also been reported to occur before the deposition of Aβ plaques in a mouse model with the overexpression of human APP (PDAPP) (German 2003). These mice also exhibited a loss of cholinergic nerve terminals in the cortex.

Although basal forebrain cholinergic neurons are more susceptible to degeneration than those in the brainstem, brainstem cholinergic neurons have also been reported to have an impact on AD neurobiology. Not only were 17 month old Tg2576 mice more active during the light phase compare to control mice, but Aβ immunisation restored the total percentage of REM sleep in 22-month old Tg2576 mice to those of control mice of the same age (Wisor et al., 2005). Higher doses of donepezil were also reported to have a lower efficacy on sleep latency on Tg2576 mice than controls (Wisor et al., 2005), suggesting that the disruptions in sleep are, in part, due to aberrant cholinergic signalling. In line with this, both a reduction in total REM sleep and the number of cholinergic PPT neurons have been reported in 6 and 12 month old Tg2576 mice (Zhang et al., 2005).

5.1.4 Objectives

Since sleep-wake cycles are disrupted early in the progression of AD in both humans and mice models, it would be advantageous to investigate the neural correlates disrupting sleep. This could help diagnose patients earlier or provide a target for early intervention, especially if sleep and the progression of AD are bidirectional. As presented in chapters 3 and 4, cholinergic PPT/LDT neurons are most active during REM sleep and GCaMP6s activity is correlated with P-waves. The loss of cholinergic neurons is correlated with disease progression and increased sleep disturbances. It is therefore, hypothesised that 5xFAD mice will have disturbances in their sleep/wake cycle and reduced PPT/LDT cholinergic activity during REM sleep. Lower cholinergic tone is also predicted to influence P-wave occurrences.

To investigate this, cholinergic PPT/LDT calcium transients, cortical EEG, EMG and pontine LFP (as with chapter 4) were monitored in 5xFAD mice expressing Cre-recombinase in ChAT neurons.

5.2 Results

5.2.1 Data sets and mice

GCaMP6s fluorescence signals were measured from one 5xFAD mouse

To examine whether pontine cholinergic activity and REM sleep is affected by AD, a total of 10 mice were implanted with optrodes and EEG/EMG headcaps (same as in chapter 4) (figure 5.1). All mice expressed Cre-recombinase in ChAT neurons; 7 of these were FAD-positive, while 3 were FAD-negative and served as a control. One FAD-positive mouse had a successful GCaMP6s fluorescence signal. A control mouse also had a successful fluorescence signal, however, the signal disappeared after a single recording. This could have been due to slight movement of the optic fibre implant, which could have in turn damaged or pulled the tip of the fibre away from GCaMP6s expressing neurons.

Optic fibre placement and GCaMP6s injection targeting

Figure 5.2 shows the optic fibre locations of all implanted mice and indicates whether GCaMP6s expression was observed in PPT/LDT neurons. While optic fibre locations were close to the PPT/LDT areas in 8 out of the 10 mice, GCaMP6s expression was not observed in 6 mice (figure 5.2). This suggests that although surgical techniques were becoming more consistent, viral injection targeting needed more optimisation.

Sleep/wake recordings

Even though GCaMP6s fluorescence signals were only observed in one mouse, sleep/wake recordings were carried out on most of the mice to assess differences in sleep/wake architecture between FAD-positive and FAD-negative mice. Of the 7 FAD-positive mice, sleep/wake recordings were obtained from 5 mice (figure 5.1 & table 5.1). One mouse was excluded because the electrophysiology tether would not attach to the headcap, which meant that EEG and EMG signals could not be obtained for sleep scoring. A second mouse was excluded because he learnt to jump out of the recording box and needed to be disconnected from the recording system over several recording attempts. Of the control litter mates, 2 mice were excluded because one did not recover well after surgery and the other had a very noisy electrophysiology signal. This was most likely due to poor grounding where either the ground

screw over the cerebellum did not have contact with the top of the brain or there was a disconnection between the wire connecting the screw to the connector.

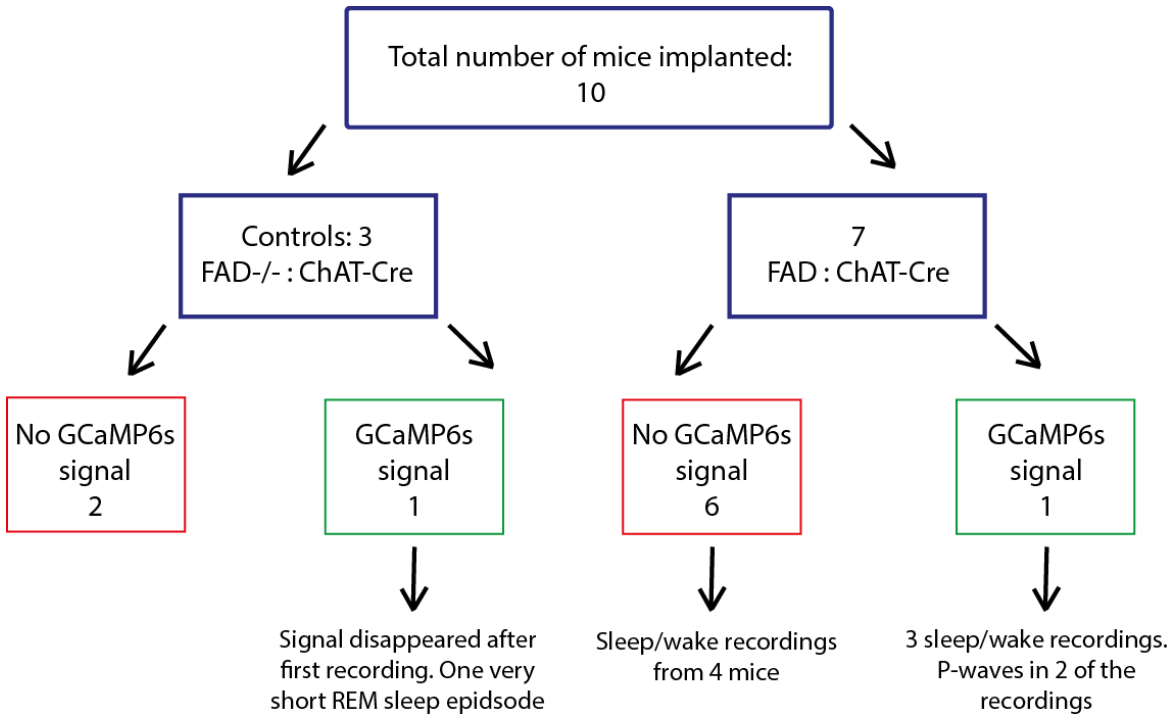

Figure 5.1: Summary of implanted FAD mice.

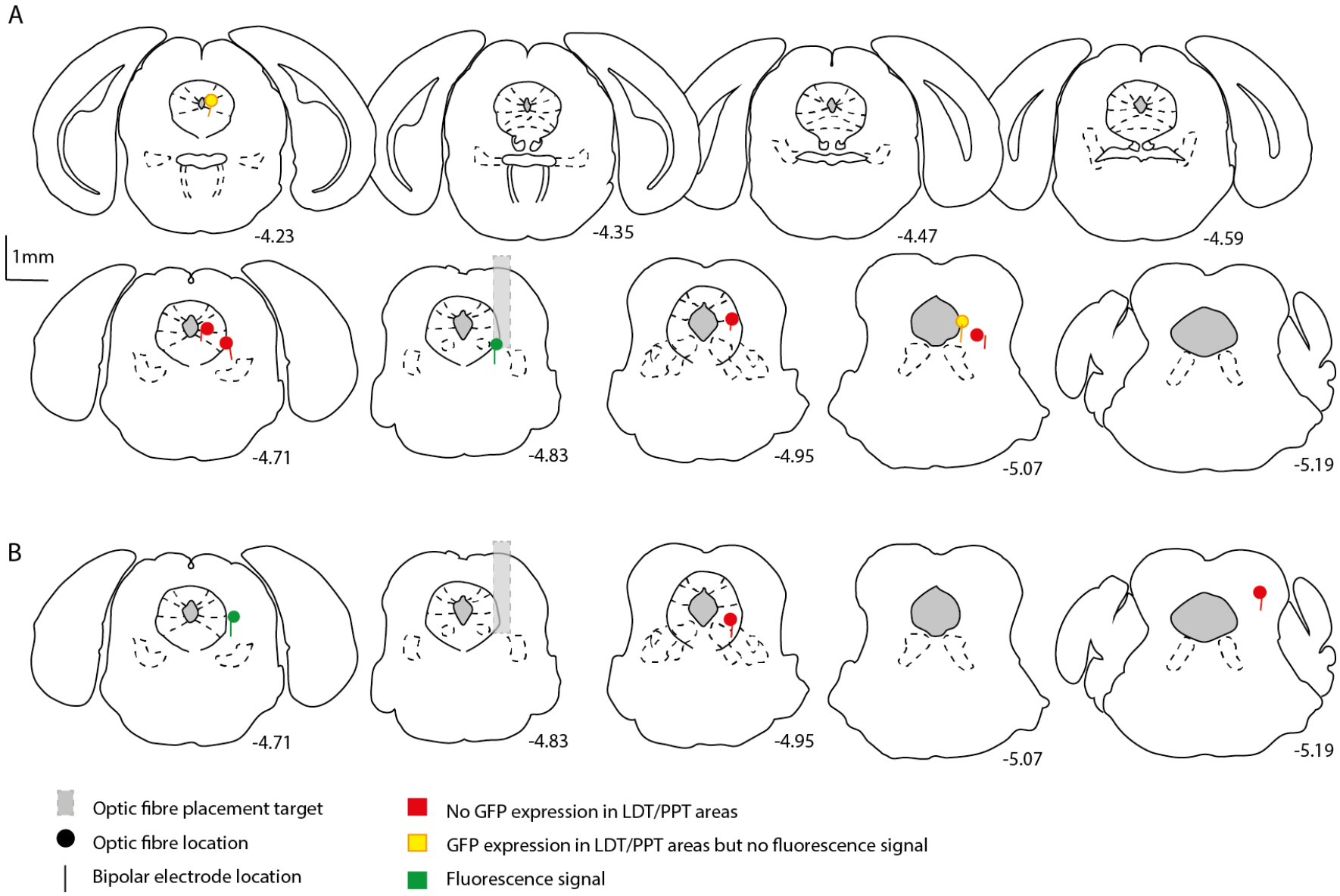
A
-4.23
-4.35
-4.47
-4.59
1mm
-4.71
-4.83
-4.95
-5.07
-5.19
B
-4.71
-4.83
-4.95
-5.07
-5.19
Optic fibre placement target
Optic fibre location
Bipolar electrode location
No GFP expression in LDT/PPT areas
GFP expression in LDT/PPT areas but no fluorescence signal
Fluorescence signal

Figure 5.2: Optic fibre locations for 5XFAD mice and control litter mates.

(A) *Optic fibre locations for the 7 implanted 5xFAD positive mice. GFP expression was not observed in 4 of the mice (red), suggesting that the viral injection was off target. GFP expression was observed in 2 mice however, optic fibres were positioned too far away from GFP expressing cells to successfully measure GCaMP6s fluorescence signals (yellow). One mouse did have a GCaMP6s fluorescence signal (green).* ***(B)*** *Optic fibre locations from 3 implanted FAD-negative litter mates. GCaMP6s fluorescence signals were observed from one mouse but disappeared after a single sleep/wake recording. Numbers indicate distance from bregma (mm) (Paxinos and Franklin, 2012).*

Table 5.1: List of sleep/wake recordings from FAD-positive mice.

Mouse ID	Age (weeks)	GCaMP6s signal?	Rec #	REM sleep?	P-waves?
FPpw_FAD1	26.3	no	1	no	-
			2	no	-
			3	no	-
FPpw_FAD2	22.7	no	1	no	-
FPpw_FAD3	22.7	no	1	no	-
			2	no	-
			3	no	-
FPpw_FAD5	21.6	no	1	no	-
			2	1	yes
			3	1	yes
FPpw_FAD7	15.4	yes	1	3	-
			2	7	yes
			3	1	yes

5.2.2 Sleep/wake cycle is disrupted over time in FAD-positive mice

Sleep/wake recordings were carried out from a total of 5 FAD-positive mice aged between 15.4 and 26.3 weeks (table 5.1). To assess whether sleep is disrupted in FAD-positive mice, sleep/wake architecture was compared with non-FAD mice. This included recordings from 14 ChAT-Cre mice (mixture of FP and FPpw mice) and a FAD-negative ChAT-Cre mouse. Mice without GCaMP6s fluorescence signals were included in this analysis. FAD mice spent significantly more time awake and less time in NREM sleep compared to non-FAD mice (figure 5.3a) (NREM, $T = 3.0$, $p = 0.008$ & AW, $T = 2.84$, $p = 0.01$, unbalanced unpaired t-test). In

general, the number of transitions to each state were not statistically different between FAD and non-FAD mice (figure 5.3b) (NREM, $T = 1.05$, $p = 0.31$; REM, $T = 1.11$, $p = 0.28$; AW, $T = 1.02$, $p = 0.32$, unpaired t-test). The average length of NREM and REM sleep episodes were shorter in FAD mice compared to non-FAD mice, however, only differences in NREM sleep being significantly different (figure 5.3c) (24.2 ± 2.3 s vs 50.5 ± 1.1 s, NREM; 28.3 ± 7.8 vs 39.7 ± 2.3, REM; mean ± SEM, FAD vs non-FAD). Although average lengths of awake episodes were not significantly different between FAD and non-FAD mice ($T = 2.05$, $p = 0.06$, unpaired t-test), one FAD mouse appears to have very long wake episodes (figure 5.3c).

To assess whether the variability in sleep/wake measurements in FAD-positive mice was correlated with aging and the progressive build-up of Aβ plaques, data was plotted as a function of the mouse's age (figure 5.3d-f). Indeed, the FAD-positive mouse that spent the most amount of time awake (97.4%) was the eldest (figure 5.3a). Equally, this mouse also had the longest wakeful episode and the fewest transitions into NREM sleep and wakefulness (figure 5.3b & c). The older FAD-positive mice tended to spend more time awake and less time in NREM sleep compared to their younger phenotypes. They did not transition to REM sleep after approximately 22 weeks of age.

To assess whether the disruption in the sleep/wake cycle of FAD-positive mice was due to general aging or the accumulation of Aβ plaques, the linear regression between both groups was compared. General aging in non-FAD mice does not appear to have such a drastic effect on the time spent in each state or the number of transitions compared to FAD-positive mice (figure 5.3 d,e,g&h) (NREM: slope = -2.41 vs 0.51; REM: slope = -0.35 vs -0.04, percent/week FAD vs non-FAD). Ageing also appears to be correlated with a reduction in the length of wakefulness in non-FAD mice at a rate of -1.8 s/week but increases at a rate of 142.6 s/week in FAD-positive mice.

Overall, data suggests that non-FAD ageing mice spend a similar amount of time in each sleep/wake state but have more fragmented sleep compared to their younger phenotypes. Ageing in FAD-positive mice, on the other hand, has a more drastic effect on the reduction of sleep in general.

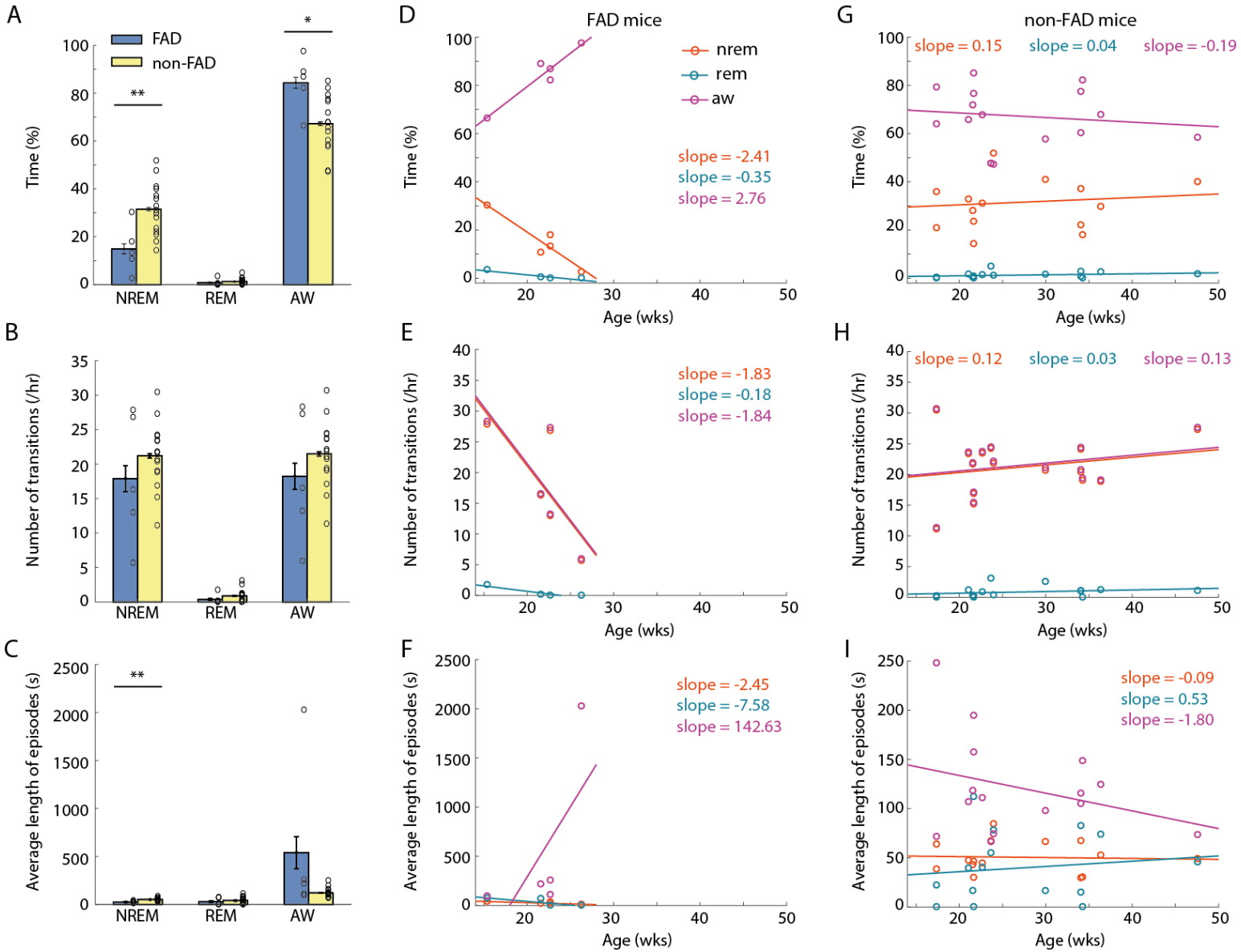
A
FAD
non-FAD
**
*
Time (%)
NREM
REM
AW
B
Number of transitions (/hr)
C
Average length of episodes (s)
D
FAD mice
nrem
rem
aw
slope = -2.41
slope = -0.35
slope = 2.76
Age (wks)
E
slope = -1.83
slope = -0.18
slope = -1.84
F
slope = -2.45
slope = -7.58
slope = 142.63
G
non-FAD mice
slope = 0.15
slope = 0.04
slope = -0.19
H
slope = 0.12
slope = 0.03
slope = 0.13
I
slope = -0.09
slope = 0.53
slope = -1.80

Figure 5.3: Sleep/wake architecture for 5XFAD mice and non-FAD mice.

(A) *Mean percentage of time spent in each sleep/wake state for each FAD-mouse (blue; n=5 mice) and non-FAD-mouse (yellow; n=15 mice). Circles represent individual mice. Error bars indicate ±SEM. Unpaired t-tests were carried out for each sleep/wake state to assess whether values between FAD and non-FAD populations were different. (NREM sleep, T value = 3.0, p = 0.008; REM, T = 0.733, p = 0.47; AW, T = 2.84, p = 0.011).* ***(B)*** *Number of NREM, REM and wake transitions per hour for both groups of mice (NREM, T = 1.05, p = 0.31; REM, T = 1.11, p = 0.28; AW, T = 1.02, p = 0.32, unpaired t-test).* ***(C)*** *Average length of episodes for both groups of mice (NREM, T = 3.33, p = 0.004; REM, T = 0.62, p = 0.54; AW, T = 2.05, p = 0.06, unpaired t-test).* ***(D-I)*** *Percentage of time (D & G), number of transitions (E & H) and length of episodes (F & I) for each state as a function of age (at perfusion) for FAD mice (D, E & F) and non-FAD mice (G, H & I). Linear regression analysis denotes the relationship between mouse age and sleep measurements. Note: y-axis scales differ between F and I.*

5.2.2 Cholinergic PPT/LDT activity is highest during REM sleep and coincide with P-waves in a FAD-positive mouse

From the single FAD-positive mouse with a successful GCaMP6s fluorescence signal, the average fluorescence signal was consistently highest during REM sleep compared to NREM sleep and wakefulness (0.26 ± 0.01, 0.36 ± 0.01, 0.31 ± 0.01, NREM sleep, REM sleep and wakefulness, respectively) (figure 5.4). This is in line with data presented in non-FAD mice in chapter 3 (section 3.2.3). Data is from a single mouse, who happened to also be the youngest FAD-positive mouse (15.4 weeks), which make is difficult to ascertain whether cholinergic PPT/LDT GCaMP6s signals differ in FAD-positive mice compared with non-FAD mice.

In chapter 4, P-waves and GCaMP6s fluorescence signals were simultaneously measured and compared. Increases in cholinergic PPT/LDT signals occurred with P-waves (figure 4.4). To assess whether similar responses occurred in the FAD-positive mouse recorded here, the same analysis was carried out. Indeed, P-wave triggered calcium transients were highest during REM sleep compared to NREM sleep (0.34 ± 0.03, 0.41 ± 0.06 and 0.54± 0.05 z-scored dF for all NREM, NREM preceding REM and REM sleep episodes, respectively) (figure 5.5), which is consistent with previous results in non-FAD mice.

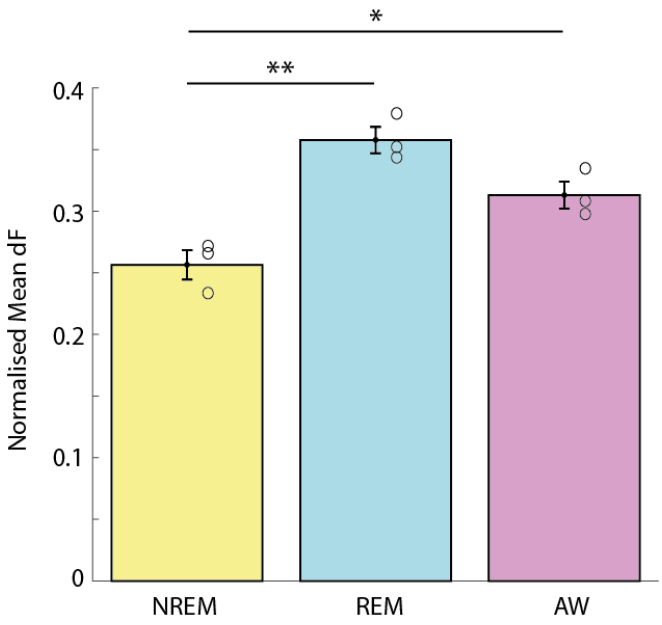

Figure 5.4: Mean GCaMP6s fluorescence signal during NREM, REM and wakefulness in a FAD-positive mouse.

*Normalised fluorescence signals averaged for each state across 3 recordings (circles) from a single FAD mouse. ($F = 20.47$, $p = 0.0021$, one-way ANOVA). *, $p < 0.05$; **, $p < 0.01$, with post hoc Tukey's honest significant difference test*

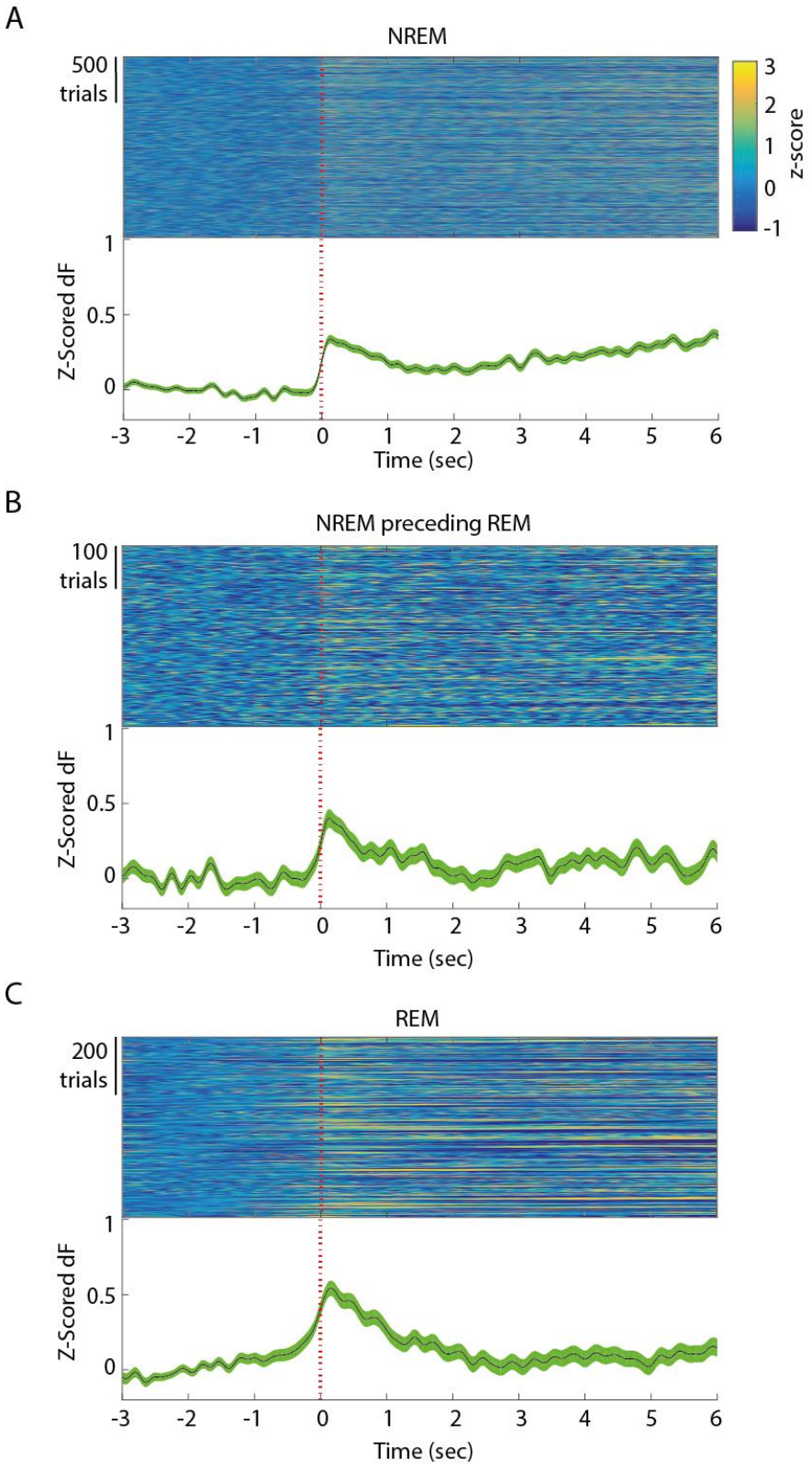

Figure 5.5: P-wave triggered GCaMP6s signals in a FAD mouse.

*Z-scored changes in fluorescence activity around each p-wave (colour maps) and averaged across p-waves (line graph) during NREM sleep **(A)**, NREM sleep episodes that occur directly before REM sleep **(B)** and REM sleep **(C)**. Shaded area indicate ± SEM.*

5.3 Discussion

5.3.1 Summary of results

This preliminary study shows that sleep-wake cycles are disrupted in FAD-positive mice as they age. This is in line with human data, where alterations in sleep have been reported in both elderly people and patients with AD (Moser et al., 2009, Peter-Derex et al., 2015, Mander et al., 2017). Reductions in NREM and REM sleep have also been reported both aging mice and mouse models of AD (Ingram et al., 1982, Wisor et al., 2005, Jyoti et al., 2010, Hasan et al., 2012, Schneider et al., 2014). However, differences in experimental protocols, mouse models and reporting also make comparing sleep-wake architecture between different studies difficult. One particular study carried out a range of tests, including assessing sleep on 5XFAD mice at 3, 6, and 9 months of age (Schneider et al., 2014). They reported that 9-month old 5XFAD mice spent less time in REM sleep than their wild-type litter mates, when REM sleep as a proportion of total sleep was calculated but there were no significant changes in the percentage of time spent in NREM sleep and wakefulness between transgenic and wildtype groups. Schneider and collages, did not assess sleep in younger mice, making it difficult to compare the results with the present study. Another study investigated differences in sleep architecture in three different mouse models of AD (Tg5276, APP/PS1, 3XTgAD), but did not include 5XFAD mice, or investigate the effects of aging on sleep (Kent et al., 2018).

The aim of this study was to investigate cholinergic PPT/LDT GCaMP6s activity in 5xFAD mice compared to their control littermates, however, data from both FAD-positive and FAD-negative pairs were not obtained. This means that fluorescence data presented from the single FAD-positive mouse is difficult to interpret and put into context of AD.

5.3.2 Experimental limitations

One key limitation to this study is the lack of data. Fluorescence GCaMP6s data was only obtained from a single mouse, so data should be interpreted with caution. When comparing sleep/wake architectures, the sex of the mice was not taken into consideration. Female 5xFAD mice were reported have greater disruptions to the sleep-wake cycle compared to males (Sethi et al., 2015). Sethi and colleagues used a piezoelectric system to score the sleep-wake state of the mice and without EEG/EMG measurements could not separate sleep into REM and NREM. In future, a systematic exploration between the progression of AD and sleep between male and female mice would be valuable. Another consideration to take when interpreting these results is that fact that sleep-wake measurements from non-FAD mice were not taken from littermates. This adds several confounding factors to the study as sleep patterns can vary between different mouse lines (Hasan et al., 2012, Panagiotou et al., 2017) and there are

differences in EEG power between young and old mice (Panagiotou et al., 2017, Soltani et al., 2019), suggesting that sleep-wake architecture may not be the only differences in aging. In future, it may, therefore, be beneficial to investigate the effects of aging on sleep architecture and EEG power in AD mice, whilst taking genotypes and sex into consideration. While Kent and colleagues did investigate the effects of AD on EEG spectral power, they did not compare findings with younger mice (2018).

Another limitation of this study is that fact that the 5xFAD mouse model is based on familial AD, which represents only a small fraction of patients. It should, however, be noted that there are no animal models that recapitulate human AD and studies have provided useful insights into AD-related aberrations on neuronal circuitry and disease progression.

Finally, due to the nature of the experimental set up, sleep/wake architecture is difficult to accurately assess. Recordings were taken over approximately 4 hours and cannot give an accurate representation of a 24hr cycle. Connecting the mice to the recording system could also add additional confounding factors through handling and stress. Developing a wireless system that allows for 24-hour recordings would be valuable for mitigating this limitation.

Mice implanted for this pilot study also had a low success rate. As discussed in chapter 3 (section 3.3), this is because implementation of the fibre photometry technique is challenging. Although optic fibre placement was fairly consistent across these mice and positioned close to PPT/LDT areas, few mice (4/10) had GCaMP6s expression in those areas. This suggests that further optimisation of viral vector injection is required. It may therefore, be beneficial to carry out an optimisation study in future to consistently get optic fibre and injection sites on target.

5.3.3 Future work

5xFAD models of AD develop Aβ deposits at 2 months (Oakley et al., 2006), and considering the youngest FAD mouse in this study is 15 weeks old, it would be interesting to carry out a long-term study of sleep architecture and PPT/LDT cholinergic activity on individual mice.

Since cholinergic basal forebrain neurons have been reported to degenerate during the early stages of AD in humans, it would be interesting to monitor basal cholinergic calcium transients just before the onset Aβ plaque accumulation in mice. This may provide new biomarkers on the disease, which could be useful in the identification and treatment of the disease.

As discussed, AD is a complex, multifactorial disease that has largescale and widespread detrimental effects on brain circuitry and human behaviour. Sleep is highly conserved and important for physiological function and as a result, there are several systems in place to regulate sleep-wake states. When one system is disrupted, other systems likely compensate. However, several neuronal systems fail in AD and influence sleep, indicating the severity of the disease.

6 General discussion and conclusions

6.2 Summary of results

The overall aim of this study was to investigate brainstem cholinergic activity in relation to sleep-wake states and P-waves in freely behaving mice. To do this, a fibre photometry system was designed and assembled to monitor population calcium transients from cholinergic PPT/LDT neurons in a cell-type specific manor. The first set of mice were implanted with optic fibres and EEG/EMG electrodes to monitor GCaMP6s fluorescence signals and sleep-wake states. Next, a group of mice were implanted with an additional custom-made optrode to simultaneously monitor fluorescence signals and pontine LFP. Simultaneous P-wave and cholinergic PPT/LDT activity has not been carried out before. This study, therefore, provides novel insights into the potential generation mechanisms of P-waves.

Finally, a pilot study was carried out on 5XFAD mice, a mouse model for Alzheimer's Disease to investigate changes in cholinergic PPT/LDT activity in disease. Although results and their implications have been discussed in their respective chapters, the main findings are described below.

- Cholinergic PPT/LDT neurons are active during REM sleep and wakefulness, with GCaMP6s signals being greatest during REM sleep, which is consistent with other activity mapping studies (Maloney et al., 1999, Boucetta et al., 2014, Cox et al., 2016, Cisse et al., 2018).
- GCaMP6s fluorescence activity during REM sleep contained consistent high amplitude undulations. While these fluctuations were also present during wakefulness, they were not as consistent. In fact, spectral analysis and autocorrelation analysis suggests that fluorescence signals during REM sleep contain underlying rhythmic fluctuations, which are not present during wakefulness. This is in line with juxtacellular recordings from cholinergic PPT/LDT neurons, where neurons fired at a greater frequency during REM sleep compared to wakefulness (Boucetta et al., 2014, Cisse et al., 2018). The activity profile during NREM sleep, on the other hand, has flat, with very little signal, suggesting that cholinergic neurons are silent during this state.
- In mice where P-waves were detected, this study for the first time, showed that increases PPT/LDT cholinergic activity corelate with P-waves in mice. P-waves were more frequent during REM sleep compared to NREM sleep, which is in line with observations in cats and rats (Brooks and Bizzi, 1963, Thomas and Benoit, 1967, Farber et al., 1980, Marks et al., 1980, Datta and Hobson, 1994).

- P-waves during REM sleep coincided with larger increases in cholinergic PPT/LDT calcium transients compared to all NREM sleep episodes and NREM sleep episodes preceding REM sleep, showing that cholinergic neurons are more active during P-waves in REM sleep.
- As sleep disruptions and cholinergic neuronal degeneration is linked to AD in humans and animal models (Zhang et al., 2005, Wulff et al., 2010, Rothman and Mattson, 2012), a pilot study was carried out to investigate the effect of disease on sleep-wake architecture, cholinergic PPT/LDT calcium transients and P-waves. Although data is sparse, data shows that sleep architecture is more fragmented in 5XFAD mice. As they age, FAD-positive mice generally spent less time sleeping (both NREM and REM sleep), whereas FAD-negative mice do not show such dramatic changes in their sleep-wake architecture during aging. Changes in cholinergic activity between FAD-positive and FAD-negative mice were not assessed, as only one FAD mouse had a successful GCaMP6s fluorescence signal.

In conclusion, this study shows that cholinergic PPT/LDT neuronal activity coincide with REM sleep initiation and P-waves. While this study cannot provide a causal relationship between PPT/LDT cholinergic activity and REM sleep or P-waves, it does provide results that are consistent with the literature (as discussed above). Considering the generation mechanisms of P-waves have not been assessed in mice before, this study shows that cholinergic PPT/LDT neurons play some role in P-wave regulatory mechanisms. As mice have become an increasingly popular animal models for sleep research (Herice et al., 2019), the recent observations of P-waves in mice (Tsunematsu et al., 2020, Patel et al., 2020) provides a foundation for interrogating the mechanism underlying P-waves.

6.3 Experimental difficulties and limitations

One of the main limitations of this study is that few animals have been included. This is because the experimental protocol was challenging to implement and required several factors to be in alignment for successful GCaMP6s signals from cholinergic PPT/LDT neurons to be captured. As discussed in chapter 3 (section 3.3.4), both viral vector injection and optic fibre targeting was required to be accurate. Microinjection of the vector and implantation of the optic fibre was carried out in a single surgery in this study, which is what many other fibre photometry studies also do (Gunaydin et al., 2014, Eban-Rothschild et al., 2016, Kim et al., 2016, Cho et al., 2017, Inoue et al., 2019, Sych et al., 2019, Pisano et al., 2019). Some studies, however, carry out two surgeries where the vector in injected in one surgery and allowed time

to express in desired cells. In the second surgery, the optic fibre or cranial window is implanted (Chen et al., 2013, Marshall et al., 2016, Meng et al., 2018, Piatkevich et al., 2019). The two-stage surgeries may be more useful for studies aiming to image calcium or voltage dynamics at single cell resolution as it can provide clear field of views and reduce the build-up of scar tissue (Salatino et al., 2017). In future, it may also be useful to develop a protocol for carrying out the two-step surgery for this study, as checking fluorescence signals during implantation of the optic fibre would mean that adjustments to depth could be made and reduce the number of mice required for implantation. This was not carried out in this study because the surgery room was too small to contain the fibre photometry system and the connecting desktop computer without breaking aseptic technique.

Another limitation of this study is the fact that calcium transients and electrophysiology signals have different temporal resolutions. While GCaMP6s fluorescence signals have been valuable for assessing cell-type specific neuronal activity, they are difficult to directly compare with electrophysiological signals. In this study, P-waves are shown to coincide with GCaMP6s signals and, fluorescence signal peaks during REM sleep. While results suggest that fluorescence peaks occur just after P-waves, it is difficult to assess the precise time lag. Optogenetically tagging neurons and monitoring cholinergic PPT/LDT neurons with extracellular electrophysiology in relation to P-waves may be beneficial to alleviate the limitations of GCaMPs6 (Mendrela et al., 2018, Cisse et al., 2018).

In future, methodological adjustments can be made to improve the success rate of experiments. This includes carrying out a pilot study to find optimised concentrations of the GCaMP6s viral vector to reduce the toxic effects of GCaMP6 (Resendez et al., 2016, Yang et al., 2018). This would be especially valuable for monitoring cell-type specific neuronal activity over several months, for example, for investigating the progression of AD on cholinergic neuronal pathology in individual 5XFAD mice over time. Second, recently developed tapered fibre may be useful to integrate into the fibre photometry system developed here as they allow for light delivery and collection to be adjusted over a 2 mm length of tissue (Pisano et al., 2019). This could mitigate the problem of optic fibre targeting faced in this study and may even do less damage to tissue as the tapered fibres have a smaller surface area, especially at the tip.

6.4 Future work to be considered

To take this study further, it would be interesting to investigate the activity of PPT/LDT glutamatergic and GABAergic neurons in relation to REM sleep and P-waves. Both glutamate and GABA transmission have been implicated in the regulation of REM sleep and glutamatergic neurons are thought to play a part in the generation of P-waves (Datta, 1997, Datta, 2002, Luppi et al., 2006, Cox et al., 2016, Saper and Fuller, 2017). This can be done by repeating the current study, but with different transgenic mice, such as vGluT2-Cre and vGAT-Cre mice. To investigate the activity dynamics of two cell-types simultaneously, the fibre photometry system could be adjusted to enable imaging of spectrally distinct GECIs, such as the XCaMP variants (Inoue et al., 2019).

The PPT/LDT nuclei have several functions in sleep, stress, reward, startle response and posture and gait regulation (Jones and Shannon, 2004, Janickova et al., 2017, Fernandez et al., 2018, Azzopardi et al., 2018, Janickova et al., 2019). Neuronal distributions and projections have also been described to have a topographical organisation, which could explain how the PPT/LDT can have many functions (Mena-Segovia et al., 2009, Martinez-Gonzalez et al., 2011, Mena-Segovia and Bolam, 2017). There are more GABAergic neurons in the rostral PPT compared to the caudal PPT, but cholinergic neurons appear to be equally spaced out across the PPT in rats (Mena-Segovia et al., 2009, Martinez-Gonzalez et al., 2011). As this topographical axis has only been assessed anatomically, it would be beneficial to carry out functional studies to investigate this further and also assess the neuronal distribution of glutamatergic neurons. Future studies should, also take this topographical axis into account.

Finally, from these experiments, it is unknown as to whether the population of cholinergic PPT/LDT neurons fire synchronously or whether increases in fluorescence signals are due to a subset of neurons. Complementary techniques, such as single cells imaging or optogenetically tagging neurons, could be used to explore this further.

Overall, the current study has provided a foundation for further investigation of P-waves in mice to be carried out. Their neurobiological underpinnings and functions would be valuable to add to our knowledge of sleep-wake regulation and REM sleep in general.

Bibliography

AASM 2005. *International classification of sleep disorders: diagnostic and coding manual (2nd Edition)*, American Academy of Sleep Medicine.

ABDELFATTAH, A. S., KAWASHIMA, T., SINGH, A., NOVAK, O., LIU, H., SHUAI, Y., HUANG, Y. C., CAMPAGNOLA, L., SEEMAN, S. C., YU, J., ZHENG, J., GRIMM, J. B., PATEL, R., FRIEDRICH, J., MENSH, B. D., PANINSKI, L., MACKLIN, J. J., MURPHY, G. J., PODGORSKI, K., LIN, B. J., CHEN, T. W., TURNER, G. C., LIU, Z., KOYAMA, M., SVOBODA, K., AHRENS, M. B., LAVIS, L. D. & SCHREITER, E. R. 2019. Bright and photostable chemigenetic indicators for extended in vivo voltage imaging. *Science,* 365**,** 699-704.

ADAM, Y., KIM, J. J., LOU, S., ZHAO, Y., XIE, M. E., BRINKS, D., WU, H., MOSTAJO-RADJI, M. A., KHEIFETS, S., PAROT, V., CHETTIH, S., WILLIAMS, K. J., GMEINER, B., FARHI, S. L., MADISEN, L., BUCHANAN, E. K., KINSELLA, I., ZHOU, D., PANINSKI, L., HARVEY, C. D., ZENG, H., ARLOTTA, P., CAMPBELL, R. E. & COHEN, A. E. 2019. Voltage imaging and optogenetics reveal behaviour-dependent changes in hippocampal dynamics. *Nature,* 569**,** 413-417.

ADAMANTIDIS, A. R., GUTIERREZ HERRERA, C. & GENT, T. C. 2019. Oscillating circuitries in the sleeping brain. *Nat Rev Neurosci,* 20**,** 746-762.

AKERBOOM, J., CARRERAS CALDERON, N., TIAN, L., WABNIG, S., PRIGGE, M., TOLO, J., GORDUS, A., ORGER, M. B., SEVERI, K. E., MACKLIN, J. J., PATEL, R., PULVER, S. R., WARDILL, T. J., FISCHER, E., SCHULER, C., CHEN, T. W., SARKISYAN, K. S., MARVIN, J. S., BARGMANN, C. I., KIM, D. S., KUGLER, S., LAGNADO, L., HEGEMANN, P., GOTTSCHALK, A., SCHREITER, E. R. & LOOGER, L. L. 2013. Genetically encoded calcium indicators for multi-color neural activity imaging and combination with optogenetics. *Front Mol Neurosci,* 6**,** 2.

AKERBOOM, J., CHEN, T. W., WARDILL, T. J., TIAN, L., MARVIN, J. S., MUTLU, S., CALDERON, N. C., ESPOSTI, F., BORGHUIS, B. G., SUN, X. R., GORDUS, A., ORGER, M. B., PORTUGUES, R., ENGERT, F., MACKLIN, J. J., FILOSA, A., AGGARWAL, A., KERR, R. A., TAKAGI, R., KRACUN, S., SHIGETOMI, E., KHAKH, B. S., BAIER, H., LAGNADO, L., WANG, S. S., BARGMANN, C. I., KIMMEL, B. E., JAYARAMAN, V., SVOBODA, K., KIM, D. S., SCHREITER, E. R. & LOOGER, L. L. 2012. Optimization of a GCaMP calcium indicator for neural activity imaging. *J Neurosci,* 32**,** 13819-40.

AMATRUDA, T. T., 3RD, BLACK, D. A., MCKENNA, T. M., MCCARLEY, R. W. & HOBSON, J. A. 1975. Sleep cycle control and cholinergic mechanisms: differential effects of carbachol injections at pontine brain stem sites. *Brain Res,* 98**,** 501-15.

ASERINSKY, E. & KLEITMAN, N. 1953. Regularly occurring periods of eye motility, and concomitant phenomena, during sleep. *Science,* 118**,** 273-4.

ATKIN, S. D., PATEL, S., KOCHARYAN, A., HOLTZCLAW, L. A., WEERTH, S. H., SCHRAM, V., PICKEL, J. & RUSSELL, J. T. 2009. Transgenic mice expressing a cameleon fluorescent Ca2+ indicator in astrocytes and Schwann cells allow study of glial cell Ca2+ signals in situ and in vivo. *J Neurosci Methods,* 181**,** 212-26.

AZZOPARDI, E., LOUTTIT, A. G., DEOLIVEIRA, C., LAVIOLETTE, S. R. & SCHMID, S. 2018. The Role of Cholinergic Midbrain Neurons in Startle and Prepulse Inhibition. *J Neurosci,* 38**,** 8798-8808.

BAGHDOYAN, H. A., MONACO, A. P., RODRIGO-ANGULO, M. L., ASSENS, F., MCCARLEY, R. W. & HOBSON, J. A. 1984a. Microinjection of neostigmine into the pontine reticular formation of cats enhances desynchronized sleep signs. *J Pharmacol Exp Ther,* 231**,** 173-80.

BAGHDOYAN, H. A., RODRIGO-ANGULO, M. L., MCCARLEY, R. W. & HOBSON, J. A. 1984b. Site-specific enhancement and suppression of desynchronized sleep signs following cholinergic stimulation of three brainstem regions. *Brain Res,* 306**,** 39-52.

BAKER, B. J., MUTOH, H., DIMITROV, D., AKEMANN, W., PERRON, A., IWAMOTO, Y., JIN, L., COHEN, L. B., ISACOFF, E. Y., PIERIBONE, V. A., HUGHES, T. & KNOPFEL, T. 2008. Genetically encoded fluorescent sensors of membrane potential. *Brain Cell Biol,* 36**,** 53-67.

BARRETTO, R. P., KO, T. H., JUNG, J. C., WANG, T. J., CAPPS, G., WATERS, A. C., ZIV, Y., ATTARDO, A., RECHT, L. & SCHNITZER, M. J. 2011. Time-lapse imaging of disease progression in deep brain areas using fluorescence microendoscopy. *Nat Med,* 17**,** 223-8.

BAZHENOV, M., TIMOFEEV, I., STERIADE, M. & SEJNOWSKI, T. 2000. Spiking-bursting Activity in the Thalamic Reticular Nucleus Initiates Sequences of Spindle Oscillations in Thalamic Networks. *Journal of neurophysiology,* 84.

BEAULIEU-BONNEAU, S. & HUDON, C. 2009. Sleep disturbances in older adults with mild cognitive impairment. *Int Psychogeriatr,* 21**,** 654-66.

BEEBE, D. W., GROESZ, L., WELLS, C., NICHOLS, A. & MCGEE, K. 2003. The neuropsychological effects of obstructive sleep apnea: a meta-analysis of norm-referenced and case-controlled data. *Sleep,* 26**,** 298-307.

BELGER, M., HARO, J. M., REED, C., HAPPICH, M., ARGIMON, J. M., BRUNO, G., DODEL, R., JONES, R. W., VELLAS, B. & WIMO, A. 2019. Determinants of time to institutionalisation and related healthcare and societal costs in a community-based cohort of patients with Alzheimer's disease dementia. *Eur J Health Econ,* 20**,** 343-355.

BERGER, H. 1929. Über das elektrenkephalogramm des menschen [German]. *European archives of psychiatry and clinical neuroscience,* 87**,** 527-570.

BERRIDGE, M. J., BOOTMAN, M. D. & RODERICK, H. L. 2003. Calcium signalling: dynamics, homeostasis and remodelling. *Nat Rev Mol Cell Biol,* 4**,** 517-29.

BIRKS, J., GRIMLEY EVANS, J., IAKOVIDOU, V. & TSOLAKI, M. 2000a. Rivastigmine for Alzheimer's disease. *Cochrane Database Syst Rev***,** Cd001191.

BIRKS, J. S., MELZER, D. & BEPPU, H. 2000b. Donepezil for mild and moderate Alzheimer's disease. *Cochrane Database Syst Rev***,** Cd001190.

BIZZI, E. & BROOKS, D. C. 1963. Functional connections between pontine reticular formation and lateral geniculate nucleus during deep sleep. *Arch Ital Biol,* 101**,** 666-80.

BLIWISE, D. L., HUGHES, M., MCMAHON, P. M. & KUTNER, N. 1995. Observed sleep/wakefulness and severity of dementia in an Alzheimer's disease special care unit. *J Gerontol A Biol Sci Med Sci,* 50**,** M303-6.

BOISSARD, R., GERVASONI, D., SCHMIDT, M. H., BARBAGLI, B., FORT, P. & LUPPI, P. H. 2002. The rat ponto-medullary network responsible for paradoxical sleep onset and maintenance: a combined microinjection and functional neuroanatomical study. *Eur J Neurosci,* 16**,** 1959-73.

BOND, M., ROGERS, G., PETERS, J., ANDERSON, R., HOYLE, M., MINERS, A., MOXHAM, T., DAVIS, S., THOKALA, P., WAILOO, A., JEFFREYS, M. & HYDE, C. 2012. The effectiveness and cost-effectiveness of donepezil, galantamine, rivastigmine and memantine for the treatment of Alzheimer's disease (review of Technology Appraisal No. 111): a systematic review and economic model. *Health Technol Assess,* 16**,** 1-470.

BORBELY, A. A. 1982. A two process model of sleep regulation. *Hum Neurobiol,* 1**,** 195-204.

BORRELL, V., YOSHIMURA, Y. & CALLAWAY, E. M. 2005. Targeted gene delivery to telencephalic inhibitory neurons by directional in utero electroporation. *J Neurosci Methods,* 143**,** 151-8.

BOUCETTA, S., CISSE, Y., MAINVILLE, L., MORALES, M. & JONES, B. E. 2014. Discharge profiles across the sleep-waking cycle of identified cholinergic, GABAergic, and glutamatergic neurons in the pontomesencephalic tegmentum of the rat. *J Neurosci,* 34**,** 4708-27.

BROOKS, D. C. & BIZZI, E. 1963. Brain stem electrical activity during deep sleep. *Arch Ital Biol,* 101**,** 648-65.

BROWN, R. E., BASHEER, R., MCKENNA, J. T., STRECKER, R. E. & MCCARLEY, R. W. 2012. Control of sleep and wakefulness. *Physiol Rev,* 92**,** 1087-187.

CALLAWAY, C. W., LYDIC, R., BAGHDOYAN, H. A. & HOBSON, J. A. 1987. Pontogeniculooccipital waves: spontaneous visual system activity during rapid eye movement sleep. *Cell Mol Neurobiol,* 7**,** 105-49.

CAO, G., PLATISA, J., PIERIBONE, V. A., RACCUGLIA, D., KUNST, M. & NITABACH, M. N. 2013. Genetically targeted optical electrophysiology in intact neural circuits. *Cell,* 154**,** 904-13.

CARSKADON, M. A. & DEMENT, W. C. 2017. Normal human sleep: An Overview. *In:* KRYGER, M. H., T., ROTH & DEMENT, W. C. (eds.) *Principles and practice of sleep medicine.* 6 ed. Philadelphia, PA: Elsevier.

CHAVARHA, M., VILLETTE, V., DIMOV, I., PRADHAN, L., EVANS, S., SHI, D., YANG, R., CHAMBERLAND, S., BRADLEY, J. & MATHIEU, B. 2018. Fast two-photon volumetric imaging of an improved voltage indicator reveals electrical activity in deeply located neurons in the awake brain. *bioRxiv***,** 445064.

CHEN, T. W., WARDILL, T. J., SUN, Y., PULVER, S. R., RENNINGER, S. L., BAOHAN, A., SCHREITER, E. R., KERR, R. A., ORGER, M. B., JAYARAMAN, V., LOOGER, L. L., SVOBODA, K. & KIM, D. S. 2013. Ultrasensitive fluorescent proteins for imaging neuronal activity. *Nature,* 499**,** 295-300.

CHO, J. R., TREWEEK, J. B., ROBINSON, J. E., XIAO, C., BREMNER, L. R., GREENBAUM, A. & GRADINARU, V. 2017. Dorsal Raphe Dopamine Neurons Modulate Arousal and Promote Wakefulness by Salient Stimuli. *Neuron,* 94**,** 1205-1219.e8.

CHROBAK, J. J. & BUZSAKI, G. 1996. High-frequency oscillations in the output networks of the hippocampal-entorhinal axis of the freely behaving rat. *J Neurosci,* 16**,** 3056-66.

CHUI, D. H., TANAHASHI, H., OZAWA, K., IKEDA, S., CHECLER, F., UEDA, O., SUZUKI, H., ARAKI, W., INOUE, H., SHIROTANI, K., TAKAHASHI, K., GALLYAS, F. & TABIRA, T. 1999. Transgenic mice with Alzheimer presenilin 1 mutations show accelerated neurodegeneration without amyloid plaque formation. *Nat Med,* 5**,** 560-4.

CHUNG, S., WEBER, F., ZHONG, P., TAN, C. L., NGUYEN, T. N., BEIER, K. T., HORMANN, N., CHANG, W. C., ZHANG, Z., DO, J. P., YAO, S., KRASHES, M. J., TASIC, B., CETIN, A., ZENG, H., KNIGHT, Z. A., LUO, L. & DAN, Y. 2017. Identification of preoptic sleep neurons using retrograde labelling and gene profiling. *Nature,* 545**,** 477-481.

CIRELLI, C. & TONONI, G. 2008. Is sleep essential? *PLoS Biol,* 6**,** e216.

CISSE, Y., TOOSSI, H., ISHIBASHI, M., MAINVILLE, L., LEONARD, C. S., ADAMANTIDIS, A. & JONES, B. E. 2018. Discharge and Role of Acetylcholine Pontomesencephalic Neurons in Cortical Activity and Sleep-Wake States Examined by Optogenetics and Juxtacellular Recording in Mice. *eNeuro,* 5.

CLEMENTS, J. R. & GRANT, S. 1990. Glutamate-like immunoreactivity in neurons of the laterodorsal tegmental and pedunculopontine nuclei in the rat. *Neurosci Lett,* 120**,** 70-3.

COLEMAN, C. G., LYDIC, R. & BAGHDOYAN, H. A. 2004. M2 muscarinic receptors in pontine reticular formation of C57BL/6J mouse contribute to rapid eye movement sleep generation. *Neuroscience,* 126**,** 821-30.

CORNWALL, J., COOPER, J. D. & PHILLIPSON, O. T. 1990. Afferent and efferent connections of the laterodorsal tegmental nucleus in the rat. *Brain Res Bull,* 25**,** 271-84.

COX, J., PINTO, L. & DAN, Y. 2016. Calcium imaging of sleep-wake related neuronal activity in the dorsal pons. *Nat Commun,* 7**,** 10763.

CRUTS, M., THEUNS, J. & VAN BROECKHOVEN, C. 2012. Locus-specific mutation databases for neurodegenerative brain diseases. *Hum Mutat,* 33**,** 1340-4.

CUMMINGS, B. J., PIKE, C. J., SHANKLE, R. & COTMAN, C. W. 1996. Beta-amyloid deposition and other measures of neuropathology predict cognitive status in Alzheimer's disease. *Neurobiol Aging,* 17**,** 921-33.

DAAN, S., BEERSMA, D. G. & BORBELY, A. A. 1984. Timing of human sleep: recovery process gated by a circadian pacemaker. *Am J Physiol,* 246**,** R161-83.

DAIGLE, T. L., MADISEN, L., HAGE, T. A., VALLEY, M. T., KNOBLICH, U., LARSEN, R. S., TAKENO, M. M., HUANG, L., GU, H., LARSEN, R., MILLS, M., BOSMA-MOODY, A., SIVERTS, L. A., WALKER, M., GRAYBUCK, L. T., YAO, Z., FONG, O., NGUYEN, T. N., GARREN, E., LENZ, G. H., CHAVARHA, M., PENDERGRAFT, J., HARRINGTON, J., HIROKAWA, K. E., HARRIS, J. A., NICOVICH, P. R., MCGRAW, M. J., OLLERENSHAW, D. R., SMITH, K. A., BAKER, C. A., TING, J. T., SUNKIN, S. M., LECOQ, J., LIN, M. Z., BOYDEN, E. S., MURPHY, G. J., DA COSTA, N. M., WATERS, J., LI, L., TASIC, B. & ZENG, H. 2018. A Suite of Transgenic Driver and Reporter Mouse Lines with Enhanced Brain-Cell-Type Targeting and Functionality. *Cell,* 174**,** 465-480.e22.

DANA, H., MOHAR, B., SUN, Y., NARAYAN, S., GORDUS, A., HASSEMAN, J. P., TSEGAYE, G., HOLT, G. T., HU, A., WALPITA, D., PATEL, R., MACKLIN, J. J., BARGMANN, C. I., AHRENS, M. B., SCHREITER, E. R., JAYARAMAN, V., LOOGER, L. L., SVOBODA, K. & KIM, D. S. 2016. Sensitive red protein calcium indicators for imaging neural activity. *Elife,* 5.

DANA, H., SUN, Y., MOHAR, B., HULSE, B. K., KERLIN, A. M., HASSEMAN, J. P., TSEGAYE, G., TSANG, A., WONG, A., PATEL, R., MACKLIN, J. J., CHEN, Y., KONNERTH, A., JAYARAMAN, V., LOOGER, L. L., SCHREITER, E. R., SVOBODA, K. & KIM, D. S. 2019. High-performance calcium sensors for imaging activity in neuronal populations and microcompartments. *Nat Methods,* 16**,** 649-657.

DATTA, S. 1995. Neuronal activity in the peribrachial area: relationship to behavioral state control. *Neurosci Biobehav Rev,* 19**,** 67-84.

DATTA, S. 1997. Cellular basis of pontine ponto-geniculo-occipital wave generation and modulation. *Cell Mol Neurobiol,* 17**,** 341-65.

DATTA, S. 2000. Avoidance task training potentiates phasic pontine-wave density in the rat: A mechanism for sleep-dependent plasticity. *J Neurosci,* 20**,** 8607-13.

DATTA, S. 2002. Evidence that REM sleep is controlled by the activation of brain stem pedunculopontine tegmental kainate receptor. *J Neurophysiol,* 87**,** 1790-8.

DATTA, S., CALVO, J. M., QUATTROCHI, J. & HOBSON, J. A. 1992. Cholinergic microstimulation of the peribrachial nucleus in the cat. I. Immediate and prolonged increases in ponto-geniculo-occipital waves. *Arch Ital Biol,* 130**,** 263-84.

DATTA, S. & HOBSON, J. A. 1994. Neuronal activity in the caudolateral peribrachial pons: relationship to PGO waves and rapid eye movements. *J Neurophysiol,* 71**,** 95-109.

DATTA, S. & HOBSON, J. A. 1995. Suppression of ponto-geniculo-occipital waves by neurotoxic lesions of pontine caudo-lateral peribrachial cells. *Neuroscience,* 67**,** 703-12.

DATTA, S., MAVANJI, V., ULLOOR, J. & PATTERSON, E. H. 2004. Activation of phasic pontine-wave generator prevents rapid eye movement sleep deprivation-induced learning impairment in the rat: a mechanism for sleep-dependent plasticity. *J Neurosci,* 24**,** 1416-27.

DATTA, S. & O'MALLEY, M. W. 2013. Fear extinction memory consolidation requires potentiation of pontine-wave activity during REM sleep. *J Neurosci,* 33**,** 4561-9.

DATTA, S. & SIWEK, D. F. 1997. Excitation of the brain stem pedunculopontine tegmentum cholinergic cells induces wakefulness and REM sleep. *J Neurophysiol,* 77**,** 2975-88.

DATTA, S. & SIWEK, D. F. 2002. Single cell activity patterns of pedunculopontine tegmentum neurons across the sleep-wake cycle in the freely moving rats. *J Neurosci Res,* 70**,** 611-21.

DATTA, S., SIWEK, D. F., PATTERSON, E. H. & CIPOLLONI, P. B. 1998. Localization of pontine PGO wave generation sites and their anatomical projections in the rat. *Synapse,* 30**,** 409-23.

DAVIS, H., DAVIS, P. A., LOOMIS, A. L., HARVEY, E. N. & HOBART, G. 1937. Changes in human brain potentials during the onset of sleep. *Science,* 86**,** 448-50.

DEMENT, W. 1958. The occurrence of low voltage, fast, electroencephalogram patterns during behavioral sleep in the cat. *Electroencephalogr Clin Neurophysiol,* 10**,** 291-6.

DEURVEILHER, S., HARS, B. & HENNEVIN, E. 1997. Pontine microinjection of carbachol does not reliably enhance paradoxical sleep in rats. *Sleep,* 20**,** 593-607.

DIEZ-GARCIA, J., MATSUSHITA, S., MUTOH, H., NAKAI, J., OHKURA, M., YOKOYAMA, J., DIMITROV, D. & KNOPFEL, T. 2005. Activation of cerebellar parallel fibers monitored in transgenic mice expressing a fluorescent Ca2+ indicator protein. *Eur J Neurosci,* 22**,** 627-35.

DIMITROV, D., HE, Y., MUTOH, H., BAKER, B. J., COHEN, L., AKEMANN, W. & KNOPFEL, T. 2007. Engineering and characterization of an enhanced fluorescent protein voltage sensor. *PLoS One,* 2**,** e440.

DUMOULIN BRIDI, M. C., ATON, S. J., SEIBT, J., RENOUARD, L., COLEMAN, T. & FRANK, M. G. 2015. Rapid eye movement sleep promotes cortical plasticity in the developing brain. *Sci Adv,* 1**,** e1500105.

EBAN-ROTHSCHILD, A., ROTHSCHILD, G., GIARDINO, W. J., JONES, J. R. & DE LECEA, L. 2016. VTA dopaminergic neurons regulate ethologically relevant sleep-wake behaviors. *Nat Neurosci,* 19**,** 1356-66.

EDGAR, D., DEMENT, W. & FULLER, C. 1993. Effect of SCN Lesions on Sleep in Squirrel Monkeys: Evidence for Opponent Processes in Sleep-Wake Regulation. *The Journal of neuroscience : the official journal of the Society for Neuroscience,* 13.

EGGERS, C., SZELIES, B., BAUER, B., WIENHARD, K., SCHRODER, H., HERHOLZ, K. & HEISS, W. D. 2007. Imaging of acetylcholine esterase activity in brainstem nuclei involved in regulation of sleep and wakefulness. *Eur J Neurol,* 14**,** 690-3.

EL MANSARI, M., SAKAI, K. & JOUVET, M. 1989. Unitary characteristics of presumptive cholinergic tegmental neurons during the sleep-waking cycle in freely moving cats. *Exp Brain Res,* 76**,** 519-29.

FARBER, J., MARKS, G. A. & ROFFWARG, H. P. 1980. Rapid eye movement sleep PGO-type waves are present in the dorsal pons of the albino rat. *Science,* 209**,** 615-7.

FENDT, M., LI, L. & YEOMANS, J. S. 2001. Brain stem circuits mediating prepulse inhibition of the startle reflex. *Psychopharmacology (Berl),* 156**,** 216-24.

FERNANDEZ, S. P., BROUSSOT, L., MARTI, F., CONTESSE, T., MOUSKA, X., SOIZA-REILLY, M., MARIE, H., FAURE, P. & BARIK, J. 2018. Mesopontine cholinergic inputs to midbrain dopamine neurons drive stress-induced depressive-like behaviors. *Nat Commun,* 9**,** 4449.

FERRARELLI, F., HUBER, R., PETERSON, M. J., MASSIMINI, M., MURPHY, M., RIEDNER, B. A., WATSON, A., BRIA, P. & TONONI, G. 2007. Reduced sleep spindle activity in schizophrenia patients. *Am J Psychiatry,* 164**,** 483-92.

FLOOD, D. G., REAUME, A. G., DORFMAN, K. S., LIN, Y. G., LANG, D. M., TRUSKO, S. P., SAVAGE, M. J., ANNAERT, W. G., DE STROOPER, B., SIMAN, R. & SCOTT, R. W. 2002. FAD mutant PS-1 gene-targeted mice: increased A beta 42 and A beta deposition without APP overproduction. *Neurobiol Aging,* 23**,** 335-48.

FORD, B., HOLMES, C. J., MAINVILLE, L. & JONES, B. E. 1995. GABAergic neurons in the rat pontomesencephalic tegmentum: codistribution with cholinergic and other tegmental neurons projecting to the posterior lateral hypothalamus. *J Comp Neurol,* 363**,** 177-96.

FRIEDRICH, J., ZHOU, P. & PANINSKI, L. 2017. Fast online deconvolution of calcium imaging data. *PLoS Comput Biol,* 13.

GAGNON, J. F., BEDARD, M. A., FANTINI, M. L., PETIT, D., PANISSET, M., ROMPRE, S., CARRIER, J. & MONTPLAISIR, J. 2002. REM sleep behavior disorder and REM sleep without atonia in Parkinson's disease. *Neurology,* 59**,** 585-9.

GAGNON, J. F., PETIT, D., FANTINI, M. L., ROMPRE, S., GAUTHIER, S., PANISSET, M., ROBILLARD, A. & MONTPLAISIR, J. 2006. REM sleep behavior disorder and REM sleep without atonia in probable Alzheimer disease. *Sleep,* 29**,** 1321-5.

GALBIATI, A., VERGA, L., GIORA, E., ZUCCONI, M. & FERINI-STRAMBI, L. 2019. The risk of neurodegeneration in REM sleep behavior disorder: A systematic review and meta-analysis of longitudinal studies. *Sleep Med Rev,* 43**,** 37-46.

GARCIA-RILL, E., SAPER, C. B., RYE, D. B., KOFLER, M., NONNEKES, J., LOZANO, A., VALLS-SOLE, J. & HALLETT, M. 2019. Focus on the pedunculopontine nucleus. Consensus review from the May 2018 brainstem society meeting in Washington, DC, USA. *Clin Neurophysiol,* 130**,** 925-940.

GEORGE, R., HASLETT, W. L. & JENDEN, D. J. 1964. A Cholinergic Mechanism in the Brainstem Reticular Formation: Induction of Paradoxical Sleep. *Int J Neuropharmacol,* 3**,** 541-52.

GNADT, J. W. & PEGRAM, G. V. 1986. Cholinergic brainstem mechanisms of REM sleep in the rat. *Brain Res,* 384**,** 29-41.

GONG, Y., HUANG, C., LI, J. Z., GREWE, B. F., ZHANG, Y., EISMANN, S. & SCHNITZER, M. J. 2015. High-speed recording of neural spikes in awake mice and flies with a fluorescent voltage sensor. *Science,* 350**,** 1361-6.

GOTT, J. A., LILEY, D. T. J. & HOBSON, J. A. 2017. Towards a Functional Understanding of PGO Waves. *Front Hum Neurosci,* 11.

GOTZ, J., BODEA, L. G. & GOEDERT, M. 2018. Rodent models for Alzheimer disease. *Nat Rev Neurosci,* 19**,** 583-598.

GRACE, K. P. 2015. How useful is optogenetic activation in determining neuronal function within dynamic circuits? *Proc Natl Acad Sci U S A,* 112**,** E3755.

GRACE, K. P. & HORNER, R. L. 2015. Evaluating the Evidence Surrounding Pontine Cholinergic Involvement in REM Sleep Generation. *Front Neurol,* 6**,** 190.

GREWE, B. F., LANGER, D., KASPER, H., KAMPA, B. M. & HELMCHEN, F. 2010. High-speed in vivo calcium imaging reveals neuronal network activity with near-millisecond precision. *Nat Methods,* 7**,** 399-405.

GROTHE, M., HEINSEN, H. & TEIPEL, S. J. 2012. Atrophy of the cholinergic Basal forebrain over the adult age range and in early stages of Alzheimer's disease. *Biol Psychiatry,* 71**,** 805-13.

GUNAYDIN, L. A., GROSENICK, L., FINKELSTEIN, J. C., KAUVAR, I. V., FENNO, L. E., ADHIKARI, A., LAMMEL, S., MIRZABEKOV, J. J., AIRAN, R. D., ZALOCUSKY, K. A., TYE, K. M., ANIKEEVA, P., MALENKA, R. C. & DEISSEROTH, K. 2014. Natural neural projection dynamics underlying social behavior. *Cell,* 157**,** 1535-51.

GUO, Q., ZHOU, J., FENG, Q., LIN, R., GONG, H., LUO, Q., ZENG, S., LUO, M. & FU, L. 2015. Multi-channel fiber photometry for population neuronal activity recording. *Biomed Opt Express,* 6**,** 3919-31.

HAHN, E. A., WANG, H. X., ANDEL, R. & FRATIGLIONI, L. 2014. A change in sleep pattern may predict Alzheimer disease. *Am J Geriatr Psychiatry,* 22**,** 1262-71.

HALASSA, M., SIEGLE, J., RITT, J., TING, J., FENG, G. & MOORE, C. 2011. Selective Optical Drive of Thalamic Reticular Nucleus Generates Thalamic Bursts and Cortical Spindles. *Nature neuroscience,* 14.

HASAN, S., DAUVILLIERS, Y., MONGRAIN, V., FRANKEN, P. & TAFTI, M. 2012. Age-related changes in sleep in inbred mice are genotype dependent. *Neurobiol Aging,* 33**,** 195.e13-26.

HATFIELD, C. F., HERBERT, J., VAN SOMEREN, E. J., HODGES, J. R. & HASTINGS, M. H. 2004. Disrupted daily activity/rest cycles in relation to daily cortisol rhythms of home-dwelling patients with early Alzheimer's dementia. *Brain,* 127**,** 1061-74.

HELMCHEN, F. & DENK, W. 2005. Deep tissue two-photon microscopy. *Nat Methods,* 2**,** 932-40.

HELMCHEN, F., FEE, M. S., TANK, D. W. & DENK, W. 2001. A miniature head-mounted two-photon microscope. high-resolution brain imaging in freely moving animals. *Neuron,* 31**,** 903-12.

HELMCHEN, F., IMOTO, K. & SAKMANN, B. 1996. Ca2+ buffering and action potential-evoked Ca2+ signaling in dendrites of pyramidal neurons. *Biophys J,* 70**,** 1069-81.

HERICE, C., PATEL, A. A. & SAKATA, S. 2019. Circuit mechanisms and computational models of REM sleep. *Neurosci Res,* 140**,** 77-92.

HILLMAN, D., MITCHELL, S., STREATFEILD, J., BURNS, C., BRUCK, D. & PEZZULLO, L. 2018. The economic cost of inadequate sleep. *Sleep,* 41.

HOCHBAUM, D. R., ZHAO, Y., FARHI, S. L., KLAPOETKE, N., WERLEY, C. A., KAPOOR, V., ZOU, P., KRALJ, J. M., MACLAURIN, D., SMEDEMARK-MARGULIES, N., SAULNIER, J. L., BOULTING, G. L., STRAUB, C., CHO, Y. K., MELKONIAN, M., WONG, G. K., HARRISON, D. J., MURTHY, V. N., SABATINI, B. L., BOYDEN, E. S., CAMPBELL, R. E. & COHEN, A. E. 2014. All-optical electrophysiology in mammalian neurons using engineered microbial rhodopsins. *Nat Methods,* 11**,** 825-33.

HORIKAWA, K., YAMADA, Y., MATSUDA, T., KOBAYASHI, K., HASHIMOTO, M., MATSU-URA, T., MIYAWAKI, A., MICHIKAWA, T., MIKOSHIBA, K. & NAGAI, T. 2010. Spontaneous network activity visualized by ultrasensitive Ca(2+) indicators, yellow Cameleon-Nano. *Nat Methods,* 7**,** 729-32.

HSIAO, K. 1998. Transgenic mice expressing Alzheimer amyloid precursor proteins. *Exp Gerontol,* 33**,** 883-9.

HSIAO, K., CHAPMAN, P., NILSEN, S., ECKMAN, C., HARIGAYA, Y., YOUNKIN, S., YANG, F. & COLE, G. 1996. Correlative memory deficits, Abeta elevation, and amyloid plaques in transgenic mice. *Science,* 274**,** 99-102.

HUANG, Z. J. & ZENG, H. 2013. Genetic approaches to neural circuits in the mouse. *Annu Rev Neurosci,* 36**,** 183-215.

IBER, C., S, A.-I., A, C. & SF, Q. 2007. *The AASM manual for the scoring of sleep and associated events: Rules,* Westchester, IL, American Academy of Sleep Medicine.

IBUKA, N. 1984. Ontogenesis of circadian sleep-wakefulness rhythms and developmental changes of sleep in the altricial rat and in the precocial guinea pig. *Behav Brain Res,* 11**,** 185-96.

INGRAM, D. K., LONDON, E. D. & REYNOLDS, M. A. 1982. Circadian rhythmicity and sleep: effects of aging in laboratory animals. *Neurobiol Aging,* 3**,** 287-97.

INOUE, M., TAKEUCHI, A., HORIGANE, S., OHKURA, M., GENGYO-ANDO, K., FUJII, H., KAMIJO, S., TAKEMOTO-KIMURA, S., KANO, M., NAKAI, J., KITAMURA, K. & BITO, H. 2015. Rational design of a high-affinity, fast, red calcium indicator R-CaMP2. *Nat Methods,* 12**,** 64-70.

INOUE, M., TAKEUCHI, A., MANITA, S., HORIGANE, S. I., SAKAMOTO, M., KAWAKAMI, R., YAMAGUCHI, K., OTOMO, K., YOKOYAMA, H., KIM, R., YOKOYAMA, T., TAKEMOTO-KIMURA, S., ABE, M., OKAMURA, M., KONDO, Y., QUIRIN, S., RAMAKRISHNAN, C., IMAMURA, T., SAKIMURA, K., NEMOTO, T., KANO, M., FUJII, H., DEISSEROTH, K., KITAMURA, K. & BITO, H. 2019. Rational Engineering of XCaMPs, a Multicolor GECI Suite for In Vivo Imaging of Complex Brain Circuit Dynamics. *Cell,* 177**,** 1346-1360.e24.

IRWIN, M. & VITIELLO, M. 2019. Implications of Sleep Disturbance and Inflammation for Alzheimer's Disease Dementia. *The Lancet. Neurology,* 18.

JACQUES, S. L. 2013. Optical properties of biological tissues: a review. *Phys Med Biol,* 58**,** R37-61.

JANICKOVA, H., KLJAKIC, O., ROSBOROUGH, K., RAULIC, S., MATOVIC, S., GROS, R., SAKSIDA, L. M., BUSSEY, T. J., INOUE, W., PRADO, V. F. & PRADO, M. A. M. 2019. Selective decrease of cholinergic signaling from pedunculopontine and laterodorsal tegmental nuclei has little impact on cognition but markedly increases susceptibility to stress. *Faseb j,* 33**,** 7018-7036.

JANICKOVA, H., ROSBOROUGH, K., AL-ONAIZI, M., KLJAKIC, O., GUZMAN, M. S., GROS, R., PRADO, M. A. & PRADO, V. F. 2017. Deletion of the vesicular acetylcholine transporter from pedunculopontine/laterodorsal tegmental neurons modifies gait. *J Neurochem,* 140**,** 787-798.

JARES-ERIJMAN, E. A. & JOVIN, T. M. 2003. FRET imaging. *Nat Biotechnol,* 21**,** 1387-95.

JONES, B. E. 1990. Immunohistochemical study of choline acetyltransferase-immunoreactive processes and cells innervating the pontomedullary reticular formation in the rat. *J Comp Neurol,* 295**,** 485-514.

JONES, C. K. & SHANNON, H. E. 2004. Lesions of the laterodorsal tegmental nucleus disrupt prepulse inhibition of the acoustic startle reflex. *Pharmacol Biochem Behav,* 78**,** 229-37.

JOUVET, M. 1962. Research on the neural structures and responsible mechanisms in different phases of physiological sleep. *Arch Ital Biol,* 100**,** 125-206.

JOUVET, M. 1972. The role of monoamines and acetylcholine-containing neurons in the regulation of the sleep-waking cycle. *Ergeb Physiol,* 64**,** 166-307.

JOUVET, M., MICHEL, F. & COURJON, J. 1959. On a stage of rapid cerebral electrical activity in the course of physiological sleep. *C R Seances Soc Biol Fil,* 153**,** 1024-8.

JOUVET-MOUNIER, D., ASTIC, L. & LACOTE, D. 1970. Ontogenesis of the states of sleep in rat, cat, and guinea pig during the first postnatal month. *Dev Psychobiol,* 2**,** 216-39.

JU, Y. E., MCLELAND, J. S., TOEDEBUSCH, C. D., XIONG, C., FAGAN, A. M., DUNTLEY, S. P., MORRIS, J. C. & HOLTZMAN, D. M. 2013. Sleep quality and preclinical Alzheimer disease. *JAMA Neurol,* 70**,** 587-93.

JU, Y. E. S., LUCEY, B. P. & HOLTZMAN, D. M. 2014. Sleep and Alzheimer disease pathology—a bidirectional relationship. *Nat Rev Neurol,* 10**,** 115-9.

JUNG, J. C., MEHTA, A. D., AKSAY, E., STEPNOSKI, R. & SCHNITZER, M. J. 2004. In vivo mammalian brain imaging using one- and two-photon fluorescence microendoscopy. *J Neurophysiol,* 92**,** 3121-33.

JYOTI, A., PLANO, A., RIEDEL, G. & PLATT, B. 2010. EEG, activity, and sleep architecture in a transgenic AbetaPPswe/PSEN1A246E Alzheimer's disease mouse. *J Alzheimers Dis,* 22**,** 873-87.

KANG, J. E., LIM, M. M., BATEMAN, R. J., LEE, J. J., SMYTH, L. P., CIRRITO, J. R., FUJIKI, N., NISHINO, S. & HOLTZMAN, D. M. 2009. Amyloid-beta dynamics are regulated by orexin and the sleep-wake cycle. *Science,* 326**,** 1005-7.

KANNAN, M., VASAN, G., HUANG, C., HAZIZA, S., LI, J. Z., INAN, H., SCHNITZER, M. J. & PIERIBONE, V. A. 2018. Fast, in vivo voltage imaging using a red fluorescent indicator. *Nat Methods,* 15**,** 1108-1116.

KENT, B. A., STRITTMATTER, S. M. & NYGAARD, H. B. 2018. Sleep and EEG Power Spectral Analysis in Three Transgenic Mouse Models of Alzheimer's Disease: APP/PS1, 3xTgAD, and Tg2576. *J Alzheimers Dis,* 64**,** 1325-1336.

KERLIN, A., BOAZ, M., FLICKINGER, D., MACLENNAN, B. J., DEAN, M. B., DAVIS, C., SPRUSTON, N. & SVOBODA, K. 2019. Functional clustering of dendritic activity during decision-making. *Elife,* 8.

KHODAGHOLY, D., GELINAS, J. N. & BUZSAKI, G. 2017. Learning-enhanced coupling between ripple oscillations in association cortices and hippocampus. *Science,* 358**,** 369-372.

KIM, C., ADHIKARI, A. & DEISSEROTH, K. 2017. Integration of Optogenetics With Complementary Methodologies in Systems Neuroscience. *Nature reviews. Neuroscience,* 18.

KIM, C. K., YANG, S. J., PICHAMOORTHY, N., YOUNG, N. P., KAUVAR, I., JENNINGS, J. H., LERNER, T. N., BERNDT, A., LEE, S. Y., RAMAKRISHNAN, C., DAVIDSON, T. J., INOUE, M., BITO, H. & DEISSEROTH, K. 2016. Simultaneous fast measurement of circuit dynamics at multiple sites across the mammalian brain. *Nat Methods,* 13**,** 325-8.

KLINZING, J. G., MOLLE, M., WEBER, F., SUPP, G., HIPP, J. F., ENGEL, A. K. & BORN, J. 2016. Spindle activity phase-locked to sleep slow oscillations. *Neuroimage,* 134**,** 607-616.

KNAPP, M., PRINCE, M., ALBANESE, E., BANERJEE, S., DHANASIRI, S., FERNANDEZ, J., FERRI, C., KNAPP, M., MCCRONE, P., PRINCE, M. & SNELL, T. 2007. Dementia UK: the full report. London: Alzheimer's Society.

KNOPFEL, T. 2012. Genetically encoded optical indicators for the analysis of neuronal circuits. *Nat Rev Neurosci,* 13**,** 687-700.

KNUTSON, K. L., SPIEGEL, K., PENEV, P. & VAN CAUTER, E. 2007. The metabolic consequences of sleep deprivation. *Sleep Med Rev,* 11**,** 163-78.

KOESTER, H. J. & SAKMANN, B. 2000. Calcium dynamics associated with action potentials in single nerve terminals of pyramidal cells in layer 2/3 of the young rat neocortex. *J Physiol,* 529 Pt 3**,** 625-46.

KOVÁCS, K. 1998. c-Fos as a Transcription Factor: A Stressful (Re)view From a Functional Map. *Neurochemistry international,* 33.

KOVÁCS, K. 2008. Measurement of Immediate-Early Gene Activation- C-Fos and Beyond. *Journal of neuroendocrinology,* 20.

KOYAMA, Y., JODO, E. & KAYAMA, Y. 1994. Sensory responsiveness of "broad-spike" neurons in the laterodorsal tegmental nucleus, locus coeruleus and dorsal raphe of awake rats: implications for cholinergic and monoaminergic neuron-specific responses. *Neuroscience,* 63**,** 1021-31.

KRALJ, J. M., DOUGLASS, A. D., HOCHBAUM, D. R., MACLAURIN, D. & COHEN, A. E. 2011. Optical recording of action potentials in mammalian neurons using a microbial rhodopsin. *Nat Methods,* 9**,** 90-5.

KRENZER, M., ANACLET, C., VETRIVELAN, R., WANG, N., VONG, L., LOWELL, B. B., FULLER, P. M. & LU, J. 2011. Brainstem and spinal cord circuitry regulating REM sleep and muscle atonia. *PLoS One,* 6**,** e24998.

KROEGER, D., ABSI, G., GAGLIARDI, C., BANDARU, S. S., MADARA, J. C., FERRARI, L. L., ARRIGONI, E., MUNZBERG, H., SCAMMELL, T. E., SAPER, C. B. & VETRIVELAN, R. 2018. Galanin neurons in the ventrolateral preoptic area promote sleep and heat loss in mice. *Nat Commun,* 9**,** 4129.

KROEGER, D., FERRARI, L. L., PETIT, G., MAHONEY, C. E., FULLER, P. M., ARRIGONI, E. & SCAMMELL, T. E. 2017. Cholinergic, Glutamatergic, and GABAergic Neurons of the Pedunculopontine Tegmental Nucleus Have Distinct Effects on Sleep/Wake Behavior in Mice. *J Neurosci,* 37**,** 1352-1366.

KUMAR, S., BHATIA, M. & BEHARI, M. 2002. Sleep disorders in Parkinson's disease. *Mov Disord,* 17**,** 775-81.

L, G., MC, K., M, D. & FP, B. 2014. Light Sleep Versus Slow Wave Sleep in Memory Consolidation: A Question of Global Versus Local Processes? *Trends in neurosciences,* 37.

LEE, J. E. & HAN, P. L. 2013. An update of animal models of Alzheimer disease with a reevaluation of plaque depositions. *Exp Neurobiol,* 22**,** 84-95.

LI, W., MA, L., YANG, G. & GAN, W. B. 2017. REM sleep selectively prunes and maintains new synapses in development and learning. *Nat Neurosci,* 20**,** 427-437.

LI, Y., ZHONG, W., WANG, D., FENG, Q., LIU, Z., ZHOU, J., JIA, C., HU, F., ZENG, J., GUO, Q., FU, L. & LUO, M. 2016. Serotonin neurons in the dorsal raphe nucleus encode reward signals. *Nat Commun,* 7**,** 10503.

LIM, A. S., KOWGIER, M., YU, L., BUCHMAN, A. S. & BENNETT, D. A. 2013. Sleep Fragmentation and the Risk of Incident Alzheimer's Disease and Cognitive Decline in Older Persons. *Sleep,* 36**,** 1027-1032.

LIM, A. S., LOZANO, A. M., MORO, E., HAMANI, C., HUTCHISON, W. D., DOSTROVSKY, J. O., LANG, A. E., WENNBERG, R. A. & MURRAY, B. J. 2007. Characterization of REM-Sleep Associated Ponto-Geniculo-Occipital Waves in the Human Pons. *Sleep,* 30**,** 823-7.

LIN, M. Z. & SCHNITZER, M. J. 2016. Genetically encoded indicators of neuronal activity. *Nat Neurosci,* 19**,** 1142-53.

LIU, C. C., KANEKIYO, T., XU, H. & BU, G. 2013. Apolipoprotein E and Alzheimer disease: risk, mechanisms, and therapy. *Nat Rev Neurol,* 9**,** 106-18.

LOOMIS, A. L., HARVEY, E. N. & HOBART, G. 1935a. Further observations on the potential rhythms of the cerebral cortex during sleep. *Science,* 82**,** 198-200.

LOOMIS, A. L., HARVEY, E. N. & HOBART, G. 1935b. Potential rhythms of the cerebral cortex during sleep. *Science,* 81**,** 597-8.

LORINCZ, M. L., GUNNER, D., BAO, Y., CONNELLY, W. M., ISAAC, J. T., HUGHES, S. W. & CRUNELLI, V. 2015. A distinct class of slow (~0.2-2 Hz) intrinsically bursting layer 5 pyramidal neurons determines UP/DOWN state dynamics in the neocortex. *J Neurosci,* 35**,** 5442-58.

LOUIS, J., CANNARD, C., BASTUJI, H. & CHALLAMEL, M. J. 1997. Sleep ontogenesis revisited: a longitudinal 24-hour home polygraphic study on 15 normal infants during the first two years of life. *Sleep,* 20**,** 323-33.

LU, J., SHERMAN, D., DEVOR, M. & SAPER, C. B. 2006. A putative flip-flop switch for control of REM sleep. *Nature,* 441**,** 589-94.

LUCAS, E. A. & STERMAN, M. B. 1974. The polycyclic sleep-wake cycle in the cat: effects produced by sensorimotor rhythm conditioning. *Exp Neurol,* 42**,** 347-68.

LUPPI, P. H., ASTON-JONES, G., AKAOKA, H., CHOUVET, G. & JOUVET, M. 1995. Afferent projections to the rat locus coeruleus demonstrated by retrograde and anterograde tracing with cholera-toxin B subunit and Phaseolus vulgaris leucoagglutinin. *Neuroscience,* 65**,** 119-60.

LUPPI, P. H., GERVASONI, D., VERRET, L., GOUTAGNY, R., PEYRON, C., SALVERT, D., LEGER, L. & FORT, P. 2006. Paradoxical (REM) sleep genesis: the switch from an aminergic-cholinergic to a GABAergic-glutamatergic hypothesis. *J Physiol Paris,* 100**,** 271-83.

LUTCKE, H., MURAYAMA, M., HAHN, T., MARGOLIS, D. J., ASTORI, S., ZUM ALTEN BORGLOH, S. M., GOBEL, W., YANG, Y., TANG, W., KUGLER, S., SPRENGEL, R., NAGAI, T., MIYAWAKI, A., LARKUM, M. E., HELMCHEN, F. & HASAN, M. T. 2010. Optical recording of neuronal activity with a genetically-encoded calcium indicator in anesthetized and freely moving mice. *Front Neural Circuits,* 4**,** 9.

LYAMIN, O. I., MANGER, P. R., RIDGWAY, S. H., MUKHAMETOV, L. M. & SIEGEL, J. M. 2008. Cetacean sleep: an unusual form of mammalian sleep. *Neurosci Biobehav Rev,* 32**,** 1451-84.

MADISEN, L., GARNER, A. R., SHIMAOKA, D., CHUONG, A. S., KLAPOETKE, N. C., LI, L., VAN DER BOURG, A., NIINO, Y., EGOLF, L., MONETTI, C., GU, H., MILLS, M., CHENG, A., TASIC, B., NGUYEN, T. N., SUNKIN, S. M., BENUCCI, A., NAGY, A., MIYAWAKI, A., HELMCHEN, F., EMPSON, R. M., KNOPFEL, T., BOYDEN, E. S., REID, R. C., CARANDINI, M. & ZENG, H. 2015. Transgenic mice for intersectional targeting of neural sensors and effectors with high specificity and performance. *Neuron,* 85**,** 942-58.

MALONEY, K. J., MAINVILLE, L. & JONES, B. E. 1999. Differential c-Fos expression in cholinergic, monoaminergic, and GABAergic cell groups of the pontomesencephalic tegmentum after paradoxical sleep deprivation and recovery. *J Neurosci,* 19**,** 3057-72.

MANDER, B. A., WINER, J. R., JAGUST, W. J. & WALKER, M. P. 2016. Sleep: A Novel Mechanistic Pathway, Biomarker, and Treatment Target in the Pathology of Alzheimer's Disease? *Trends Neurosci,* 39**,** 552-566.

MANDER, B. A., WINER, J. R. & WALKER, M. P. 2017. Sleep and Human Aging. *Neuron,* 94**,** 19-36.

MANGER, P. R., CORT, J., EBRAHIM, N., GOODMAN, A., HENNING, J., KAROLIA, M., RODRIGUES, S. L. & STRKALJ, G. 2008. Is 21st century neuroscience too focussed on the rat/mouse model of brain function and dysfunction? *Front Neuroanat,* 2**,** 5.

MARKS, G. A., FARBER, J., RUBINSTEIN, M. & ROFFWARG, H. P. 1980. Demonstration of ponto-geniculo-occipital waves in the albino rat. *Exp Neurol,* 69**,** 648-66.

MARKS, G. A., SHAFFERY, J. P., OKSENBERG, A., SPECIALE, S. G. & ROFFWARG, H. P. 1995. A functional role for REM sleep in brain maturation. *Behav Brain Res,* 69**,** 1-11.

MARSHALL, J. D., LI, J. Z., ZHANG, Y., GONG, Y., ST-PIERRE, F., LIN, M. Z. & SCHNITZER, M. J. 2016. Cell-Type-Specific Optical Recording of Membrane Voltage Dynamics in Freely Moving Mice. *Cell,* 167**,** 1650-1662.e15.

MARTINEZ-GONZALEZ, C., BOLAM, J. P. & MENA-SEGOVIA, J. 2011. Topographical organization of the pedunculopontine nucleus. *Front Neuroanat,* 5**,** 22.

MATTHEWS, F. & BRAYNE, C. 2005. The incidence of dementia in England and Wales: findings from the five identical sites of the MRC CFA Study. *PLoS Med,* 2**,** e193.

MATTSON, M. P. 2004. Pathways towards and away from Alzheimer's disease. *Nature,* 430**,** 631-9.

MAVANJI, V. & DATTA, S. 2003. Activation of the phasic pontine-wave generator enhances improvement of learning performance: a mechanism for sleep-dependent plasticity. *Eur J Neurosci,* 17**,** 359-70.

MAVANJI, V., ULLOOR, J., SAHA, S. & DATTA, S. 2004. Neurotoxic lesions of phasic pontine-wave generator cells impair retention of 2-way active avoidance memory. *Sleep,* 27**,** 1282-92.

MCCARLEY, R. W. 2007. Neurobiology of REM and NREM sleep. *Sleep Med,* 8**,** 302-30.

MCCARLEY, R. W. & HOBSON, J. A. 1971. Single neuron activity in cat gigantocellular tegmental field: selectivity of discharge in desynchronized sleep. *Science,* 174**,** 1250-2.

MCCARLEY, R. W., NELSON, J. P. & HOBSON, J. A. 1978. Ponto-geniculo-occipital (PGO) burst neurons: correlative evidence for neuronal generators of PGO waves. *Science,* 201**,** 269-72.

MCCURRY, S. M., REYNOLDS, C. F., ANCOLI-ISRAEL, S., TERI, L. & VITIELLO, M. V. 2000. Treatment of sleep disturbance in Alzheimer's disease. *Sleep Med Rev,* 4**,** 603-628.

MCKILLOP, L. E., FISHER, S. P., CUI, N., PEIRSON, S. N., FOSTER, R. G., WAFFORD, K. A. & VYAZOVSKIY, V. V. 2018. Effects of Aging on Cortical Neural Dynamics and Local Sleep Homeostasis in Mice. *J Neurosci,* 38**,** 3911-3928.

MCKILLOP, L. E. & VYAZOVSKIY, V. V. 2020. Sleep and ageing: from human studies to rodent models. 15**,** 210-216.

MENA-SEGOVIA, J. & BOLAM, J. P. 2017. Rethinking the Pedunculopontine Nucleus: From Cellular Organization to Function. *Neuron,* 94**,** 7-18.

MENA-SEGOVIA, J., MICKLEM, B. R., NAIR-ROBERTS, R. G., UNGLESS, M. A. & BOLAM, J. P. 2009. GABAergic neuron distribution in the pedunculopontine nucleus defines functional subterritories. *J Comp Neurol,* 515**,** 397-408.

MENA-SEGOVIA, J., SIMS, H. M., MAGILL, P. J. & BOLAM, J. P. 2008. Cholinergic brainstem neurons modulate cortical gamma activity during slow oscillations. *J Physiol,* 586**,** 2947-60.

MENDRELA, A. E., KIM, K., ENGLISH, D., MCKENZIE, S., SEYMOUR, J. P., BUZSAKI, G. & YOON, E. 2018. A High-Resolution Opto-Electrophysiology System With a Miniature Integrated Headstage. *IEEE Trans Biomed Circuits Syst*.

MENG, C., ZHOU, J., PAPANERI, A., PEDDADA, T., XU, K. & CUI, G. 2018. Spectrally Resolved Fiber Photometry for Multi-component Analysis of Brain Circuits. *Neuron,* 98**,** 707-717.e4.

MIKITEN, T. M., NIEBYL, P. H. & HENDLEY, C. D. 1961. EEG desynchronization during behavioral sleep associated with spike discharges from the thalamus of the cat. *Fed. Proc,* 20:327.

MINAKAWA, E. N., MIYAZAKI, K., MARUO, K., YAGIHARA, H., FUJITA, H., WADA, K. & NAGAI, Y. 2017. Chronic sleep fragmentation exacerbates amyloid beta deposition in Alzheimer's disease model mice. *Neurosci Lett,* 653**,** 362-369.

MISTLBERGER, R., BERGMANN, B., WALDENAR, W. & RECHTSCHAFFEN, A. 1983. Recovery Sleep Following Sleep Deprivation in Intact and Suprachiasmatic Nuclei-Lesioned Rats. *Sleep,* 6.

MIYAWAKI, A., GRIESBECK, O., HEIM, R. & TSIEN, R. Y. 1999. Dynamic and quantitative Ca2+ measurements using improved cameleons. *Proc Natl Acad Sci U S A,* 96**,** 2135-40.

MORAES WDOS, S., POYARES, D. R., GUILLEMINAULT, C., RAMOS, L. R., BERTOLUCCI, P. H. & TUFIK, S. 2006. The effect of donepezil on sleep and REM sleep EEG in patients with Alzheimer disease: a double-blind placebo-controlled study. *Sleep,* 29**,** 199-205.

MOSER, D., ANDERER, P., GRUBER, G., PARAPATICS, S., LORETZ, E., BOECK, M., KLOESCH, G., HELLER, E., SCHMIDT, A., DANKER-HOPFE, H., SALETU, B., ZEITLHOFER, J. & DORFFNER, G. 2009. Sleep classification according to AASM and Rechtschaffen & Kales: effects on sleep scoring parameters. *Sleep,* 32**,** 139-49.

MOTTS, S. D. & SCHOFIELD, B. R. 2009. Sources of cholinergic input to the inferior colliculus. *Neuroscience,* 160**,** 103-14.

MOURET, J., JEANNEROD, M. & JOUVET, M. 1963. Electrical activity of the visual system during the paradoxical phase of sleep in the cat. *J Physiol (Paris),* 55**,** 305-6.

MUSIEK, E. S., XIONG, D. D. & HOLTZMAN, D. M. 2015. Sleep, circadian rhythms, and the pathogenesis of Alzheimer disease. *Exp Mol Med,* 47**,** e148.

NAGAI, T., YAMADA, S., TOMINAGA, T., ICHIKAWA, M. & MIYAWAKI, A. 2004. Expanded dynamic range of fluorescent indicators for Ca(2+) by circularly permuted yellow fluorescent proteins. *Proc Natl Acad Sci U S A,* 101**,** 10554-9.

NALBANTOGLU, J., GILFIX, B. M., BERTRAND, P., ROBITAILLE, Y., GAUTHIER, S., ROSENBLATT, D. S. & POIRIER, J. 1994. Predictive value of apolipoprotein E genotyping in Alzheimer's disease: results of an autopsy series and an analysis of several combined studies. *Ann Neurol,* 36**,** 889-95.

NELSON, J. P., MCCARLEY, R. W. & HOBSON, J. A. 1983. REM sleep burst neurons, PGO waves, and eye movement information. *J Neurophysiol,* 50**,** 784-97.

OAKLEY, H., COLE, S. L., LOGAN, S., MAUS, E., SHAO, P., CRAFT, J., GUILLOZET-BONGAARTS, A., OHNO, M., DISTERHOFT, J., VAN ELDIK, L., BERRY, R. & VASSAR, R. 2006. Intraneuronal beta-amyloid aggregates, neurodegeneration, and neuron loss in transgenic mice with five familial Alzheimer's disease mutations: potential factors in amyloid plaque formation. *J Neurosci,* 26**,** 10129-40.

OLSON, E. J., BOEVE, B. F. & SILBER, M. H. 2000. Rapid eye movement sleep behaviour disorder: demographic, clinical and laboratory findings in 93 cases. *Brain,* 123 (Pt 2)**,** 331-9.

OTT, A., BRETELER, M. M., VAN HARSKAMP, F., CLAUS, J. J., VAN DER CAMMEN, T. J., GROBBEE, D. E. & HOFMAN, A. 1995. Prevalence of Alzheimer's disease and vascular dementia: association with education. The Rotterdam study. *Bmj,* 310**,** 970-3.

PANAGIOTOU, M., VYAZOVSKIY, V. V., MEIJER, J. H. & DEBOER, T. 2017. Differences in electroencephalographic non-rapid-eye movement sleep slow-wave characteristics between young and old mice. *Sci Rep,* 7**,** 43656.

PARE, D., SMITH, Y., PARENT, A. & STERIADE, M. 1988. Projections of brainstem core cholinergic and non-cholinergic neurons of cat to intralaminar and reticular thalamic nuclei. *Neuroscience,* 25**,** 69-86.

PATEL, A. A., MCALINDEN, N., MATHIESON, K. & SAKATA, S. 2020. Simultaneous Electrophysiology and Fiber Photometry in Freely Behaving Mice. *Frontiers in Neuroscience,* 14.

PAXINOS, G. & FRANKLIN, K. B. 2012. *The Mouse Brain in Stereotaxic Coordinates, 4th Edition*, Academic Press.

PETER-DEREX, L., YAMMINE, P., BASTUJI, H. & CROISILE, B. 2015. Sleep and Alzheimer's disease. *Sleep Med Rev,* 19**,** 29-38.

PETROVIC, J., CIRIC, J., LAZIC, K., KALAUZI, A. & SAPONJIC, J. 2013. Lesion of the pedunculopontine tegmental nucleus in rat augments cortical activation and disturbs sleep/wake state transitions structure. *Exp Neurol,* 247**,** 562-71.

PIATKEVICH, K. D., BENSUSSEN, S., TSENG, H. A., SHROFF, S. N., LOPEZ-HUERTA, V. G., PARK, D., JUNG, E. E., SHEMESH, O. A., STRAUB, C., GRITTON, H. J., ROMANO, M. F., COSTA, E., SABATINI, B. L., FU, Z., BOYDEN, E. S. & HAN, X. 2019. Population imaging of neural activity in awake behaving mice. *Nature,* 574**,** 413-417.

PISANO, F., PISANELLO, M., LEE, S. J., LEE, J., MAGLIE, E., BALENA, A., SILEO, L., SPAGNOLO, B., BIANCO, M., HYUN, M., DE VITTORIO, M., SABATINI, B. L. & PISANELLO, F. 2019. Depth-resolved fiber photometry with a single tapered optical fiber implant. *Nat Methods,* 16**,** 1185-1192.

PNEVMATIKAKIS, E. A., SOUDRY, D., GAO, Y., MACHADO, T. A., MEREL, J., PFAU, D., REARDON, T., MU, Y., LACEFIELD, C., YANG, W., AHRENS, M., BRUNO, R., JESSELL, T. M., PETERKA, D. S., YUSTE, R. & PANINSKI, L. 2016. Simultaneous Denoising, Deconvolution, and Demixing of Calcium Imaging Data. *Neuron,* 89**,** 285-99.

POLLOCK, M. S. & MISTLBERGER, R. E. 2005. Microinjection of neostigmine into the pontine reticular formation of the mouse: further evaluation of a proposed REM sleep enhancement technique. *Brain Res,* 1031**,** 253-67.

PUNJABI, N. M., CAFFO, B. S., GOODWIN, J. L., GOTTLIEB, D. J., NEWMAN, A. B., O'CONNOR, G. T., RAPOPORT, D. M., REDLINE, S., RESNICK, H. E., ROBBINS, J. A., SHAHAR, E., UNRUH, M. L. & SAMET, J. M. 2009. Sleep-disordered breathing and mortality: a prospective cohort study. *PLoS Med,* 6**,** e1000132.

QUATTROCHI, J. J. & HOBSON, J. A. 1999. Carbachol microinjection into the caudal peribrachial area induces long-term enhancement of PGO wave activity but not REM sleep. *J Sleep Res,* 8**,** 281-90.

RADULOVACKI, M., VIRUS, R. M., DJURICIC-NEDELSON, M. & GREEN, R. D. 1984. Adenosine analogs and sleep in rats. *J Pharmacol Exp Ther,* 228**,** 268-74.

RASCH, B. & BORN, J. 2013. About sleep's role in memory. *Physiol Rev,* 93**,** 681-766.

RASKIND, M. A., PESKIND, E. R., WESSEL, T. & YUAN, W. 2000. Galantamine in AD: A 6-month randomized, placebo-controlled trial with a 6-month extension. The Galantamine USA-1 Study Group. *Neurology,* 54**,** 2261-8.

RATTENBORG, N. C., AMLANER, C. J. & LIMA, S. L. 2000. Behavioral, neurophysiological and evolutionary perspectives on unihemispheric sleep. *Neurosci Biobehav Rev,* 24**,** 817-42.

RECHTSCHAFFEN, A. 1998. Current perspectives on the function of sleep. *Perspect Biol Med,* 41**,** 359-90.

RECHTSCHAFFEN, A. & BERGMANN, B. M. 1995. Sleep deprivation in the rat by the disk-over-water method. *Behav Brain Res,* 69**,** 55-63.

RECHTSCHAFFEN, A. & BERGMANN, B. M. 2002. Sleep deprivation in the rat: an update of the 1989 paper. *Sleep,* 25**,** 18-24.

RECHTSCHAFFEN, A. & KALES, A. 1968. *A manual of standardized terminology, technique and scoring system for sleep stages of human sleep,* Los Angeles, Brain Information Service/Brain Research Institute.

REDLINE, S., YENOKYAN, G., GOTTLIEB, D. J., SHAHAR, E., O'CONNOR, G. T., RESNICK, H. E., DIENER-WEST, M., SANDERS, M. H., WOLF, P. A., GERAGHTY, E. M., ALI, T., LEBOWITZ, M. & PUNJABI, N. M. 2010. Obstructive sleep apnea-hypopnea and incident stroke: the sleep heart health study. *Am J Respir Crit Care Med,* 182**,** 269-77.

RESENDEZ, S. L., JENNINGS, J. H., UNG, R. L., NAMBOODIRI, V. M., ZHOU, Z. C., OTIS, J. M., NOMURA, H., MCHENRY, J. A., KOSYK, O. & STUBER, G. D. 2016. Visualization of cortical, subcortical and deep brain neural circuit dynamics during naturalistic mammalian behavior with head-mounted microscopes and chronically implanted lenses. *Nat Protoc,* 11**,** 566-97.

ROFFWARG, H. P., MUZIO, J. N. & DEMENT, W. C. 1966. Ontogenetic development of the human sleep-dream cycle. *Science,* 152**,** 604-19.

ROH, J. H., HUANG, Y., BERO, A. W., KASTEN, T., STEWART, F. R., BATEMAN, R. J. & HOLTZMAN, D. M. 2012. Disruption of the sleep-wake cycle and diurnal fluctuation of beta-amyloid in mice with Alzheimer's disease pathology. *Sci Transl Med,* 4**,** 150ra122.

ROTHMAN, S. M. & MATTSON, M. P. 2012. Sleep disturbances in Alzheimer's and Parkinson's diseases. *Neuromolecular Med,* 14**,** 194-204.

SAITO, H., SAKAI, K. & JOUVET, M. 1977. Discharge patterns of the nucleus parabrachialis lateralis neurons of the cat during sleep and waking. *Brain Res,* 134**,** 59-72.

SAKAI, K. & JOUVET, M. 1980. Brain stem PGO-on cells projecting directly to the cat dorsal lateral geniculate nucleus. *Brain Res,* 194**,** 500-5.

SAKAI, K., PETITJEAN, F. & JOUVET, M. 1976. Effects of ponto-mesencephalic lesions and electrical stimulation upon PGO waves and EMPs in unanesthetized cats. *Electroencephalogr Clin Neurophysiol,* 41**,** 49-63.

SAKAI, R., REPUNTE-CANONIGO, V., RAJ, C. D. & KNOPFEL, T. 2001. Design and characterization of a DNA-encoded, voltage-sensitive fluorescent protein. *Eur J Neurosci,* 13**,** 2314-8.

SALATINO, J. W., LUDWIG, K. A., KOZAI, T. D. Y. & PURCELL, E. K. 2017. Glial responses to implanted electrodes in the brain. *Nat Biomed Eng,* 1**,** 862-877.

SANCHEZ-VIVES, M. V. & MCCORMICK, D. A. 2000. Cellular and network mechanisms of rhythmic recurrent activity in neocortex. *Nat Neurosci,* 3**,** 1027-34.

SAPER, C. B., CHOU, T. C. & SCAMMELL, T. E. 2001. The sleep switch: hypothalamic control of sleep and wakefulness. *Trends Neurosci,* 24**,** 726-31.

SAPER, C. B. & FULLER, P. M. 2017. Wake-sleep circuitry: an overview. *Curr Opin Neurobiol,* 44**,** 186-192.

SAPER, C. B., FULLER, P. M., PEDERSEN, N. P., LU, J. & SCAMMELL, T. E. 2010. Sleep state switching. *Neuron,* 68**,** 1023-42.

SAPER, C. B. & LOEWY, A. D. 1982. Projections of the pedunculopontine tegmental nucleus in the rat: evidence for additional extrapyramidal circuitry. *Brain Res,* 252**,** 367-72.

SAPIN, E., LAPRAY, D., BEROD, A., GOUTAGNY, R., LEGER, L., RAVASSARD, P., CLEMENT, O., HANRIOT, L., FORT, P. & LUPPI, P. H. 2009. Localization of the brainstem GABAergic neurons controlling paradoxical (REM) sleep. *PLoS One,* 4**,** e4272.

SASTRE, J. P., SAKAI, K. & JOUVET, M. 1981. Are the gigantocellular tegmental field neurons responsible for paradoxical sleep? *Brain Res,* 229**,** 147-61.

SAUNDERS, A. M., STRITTMATTER, W. J., SCHMECHEL, D., GEORGE-HYSLOP, P. H., PERICAK-VANCE, M. A., JOO, S. H., ROSI, B. L., GUSELLA, J. F., CRAPPER-MACLACHLAN, D. R., ALBERTS, M. J. & ET AL. 1993. Association of apolipoprotein E allele epsilon 4 with late-onset familial and sporadic Alzheimer's disease. *Neurology,* 43**,** 1467-72.

SCAMMELL, T. E., ARRIGONI, E. & LIPTON, J. O. 2017. Neural Circuitry of Wakefulness and Sleep. *Neuron,* 93**,** 747-765.

SCHENCK, C. H., BOEVE, B. F. & MAHOWALD, M. W. 2013. Delayed emergence of a parkinsonian disorder or dementia in 81% of older men initially diagnosed with idiopathic rapid eye movement sleep behavior disorder: a 16-year update on a previously reported series. *Sleep Med,* 14**,** 744-8.

SCHLIEBS, R. & ARENDT, T. 2006. The significance of the cholinergic system in the brain during aging and in Alzheimer's disease. *J Neural Transm (Vienna),* 113**,** 1625-44.

SCHNEIDER, F., BALDAUF, K., WETZEL, W. & REYMANN, K. G. 2014. Behavioral and EEG changes in male 5xFAD mice. *Physiol Behav,* 135**,** 25-33.

SCHOFIELD, B. R. & MOTTS, S. D. 2009. Projections from auditory cortex to cholinergic cells in the midbrain tegmentum of guinea pigs. *Brain Res Bull,* 80**,** 163-70.

SEMBA, K. & FIBIGER, H. C. 1992. Afferent connections of the laterodorsal and the pedunculopontine tegmental nuclei in the rat: a retro- and antero-grade transport and immunohistochemical study. *J Comp Neurol,* 323**,** 387-410.

SEMBA, K., REINER, P. B. & FIBIGER, H. C. 1990. Single cholinergic mesopontine tegmental neurons project to both the pontine reticular formation and the thalamus in the rat. *Neuroscience,* 38**,** 643-54.

SETHI, M., JOSHI, S. S., WEBB, R. L., BECKETT, T. L., DONOHUE, K. D., MURPHY, M. P., O'HARA, B. F. & DUNCAN, M. J. 2015. Increased fragmentation of sleep-wake cycles in the 5XFAD mouse model of Alzheimer's disease. *Neuroscience,* 290**,** 80-9.

SHAFFERY, J. P., SINTON, C. M., BISSETTE, G., ROFFWARG, H. P. & MARKS, G. A. 2002. Rapid eye movement sleep deprivation modifies expression of long-term potentiation in visual cortex of immature rats. *Neuroscience,* 110**,** 431-43.

SHOUSE, M. N. & SIEGEL, J. M. 1992. Pontine regulation of REM sleep components in cats: integrity of the pedunculopontine tegmentum (PPT) is important for phasic events but unnecessary for atonia during REM sleep. *Brain Res,* 571**,** 50-63.

SIEGEL, J. M. 2005. Clues to the functions of mammalian sleep. *Nature,* 437**,** 1264-71.

SIEGEL, J. M. 2008. Do all animals sleep? *Trends Neurosci,* 31**,** 208-13.

SIEGEL, J. M. 2009. Sleep viewed as a state of adaptive inactivity. *Nat Rev Neurosci,* 10**,** 747-53.

SIEGEL, M. S. & ISACOFF, E. Y. 1997. A genetically encoded optical probe of membrane voltage. *Neuron,* 19**,** 735-41.

SLOANE, P. D., ZIMMERMAN, S., SUCHINDRAN, C., REED, P., WANG, L., BOUSTANI, M. & SUDHA, S. 2002. The public health impact of Alzheimer's disease, 2000-2050: potential implication of treatment advances. *Annu Rev Public Health,* 23**,** 213-31.

SOLTANI, S., CHAUVETTE, S., BUKHTIYAROVA, O., LINA, J. M., DUBE, J., SEIGNEUR, J., CARRIER, J. & TIMOFEEV, I. 2019. Sleep-Wake Cycle in Young and Older Mice. *Front Syst Neurosci,* 13**,** 51.

STEPHAN, F. K. & ZUCKER, I. 1972. Circadian rhythms in drinking behavior and locomotor activity of rats are eliminated by hypothalamic lesions. *Proc Natl Acad Sci U S A,* 69**,** 1583-6.

STEPHENSON, R., LIM, J., FAMINA, S., CARON, A. M. & DOWSE, H. B. 2012. Sleep-wake behavior in the rat: ultradian rhythms in a light-dark cycle and continuous bright light. *J Biol Rhythms,* 27**,** 490-501.

STERIADE, M. 1993. Electroencephalography:
Basic Principles, Clinical Applications, and Related Fields. *In:* NIEDERMEYER, E. & LOPES DA SILVA, F. (eds.). Baltimore: Williams
& Wilkins.

STERIADE, M. 2000. Corticothalamic resonance, states of vigilance and mentation. *Neuroscience,* 101**,** 243-76.

STERIADE, M., DATTA, S., PARE, D., OAKSON, G. & CURRO DOSSI, R. C. 1990a. Neuronal activities in brain-stem cholinergic nuclei related to tonic activation processes in thalamocortical systems. *J Neurosci,* 10**,** 2541-59.

STERIADE, M., DESCHÊNES, M., DOMICH, L. & MULLE, C. 1985. Abolition of Spindle Oscillations in Thalamic Neurons Disconnected From Nucleus Reticularis Thalami. *Journal of neurophysiology,* 54.

STERIADE, M., NUNEZ, A. & AMZICA, F. 1993. A novel slow (< 1 Hz) oscillation of neocortical neurons in vivo: depolarizing and hyperpolarizing components. *J Neurosci,* 13**,** 3252-65.

STERIADE, M., PARE, D., DATTA, S., OAKSON, G. & CURRO DOSSI, R. 1990b. Different cellular types in mesopontine cholinergic nuclei related to ponto-geniculo-occipital waves. *J Neurosci,* 10**,** 2560-79.

STERIADE, M. & TIMOFEEV, I. 2003. Neuronal Plasticity in Thalamocortical Networks During Sleep and Waking Oscillations. *Neuron,* 37.

STERIADE, M., TIMOFEEV, I. & GRENIER, F. 2001. Natural Waking and Sleep States: A View From Inside Neocortical Neurons. *Journal of neurophysiology,* 85.

STERMAN, M. B., KNAUSS, T., LEHMANN, D. & CLEMENTE, C. D. 1965. Circadian sleep and waking patterns in the laboratory cat. *Electroencephalogr Clin Neurophysiol,* 19**,** 509-17.

STICKGOLD, R. & WALKER, M. P. 2005. Memory consolidation and reconsolidation: what is the role of sleep? *Trends Neurosci,* 28**,** 408-15.

STURCHLER-PIERRAT, C., ABRAMOWSKI, D., DUKE, M., WIEDERHOLD, K. H., MISTL, C., ROTHACHER, S., LEDERMANN, B., BURKI, K., FREY, P., PAGANETTI, P. A., WARIDEL, C., CALHOUN, M. E., JUCKER, M., PROBST, A., STAUFENBIEL, M. & SOMMER, B. 1997. Two amyloid precursor protein transgenic mouse models with Alzheimer disease-like pathology. *Proc Natl Acad Sci U S A,* 94**,** 13287-92.

SYCH, Y., CHERNYSHEVA, M., SUMANOVSKI, L. T. & HELMCHEN, F. 2019. High-density multi-fiber photometry for studying large-scale brain circuit dynamics. *Nat Methods,* 16**,** 553-560.

TABATA, H. & NAKAJIMA, K. 2001. Efficient in utero gene transfer system to the developing mouse brain using electroporation: visualization of neuronal migration in the developing cortex. *Neuroscience,* 103**,** 865-72.

THAKKAR, M., PORTAS, C. & MCCARLEY, R. W. 1996. Chronic low-amplitude electrical stimulation of the laterodorsal tegmental nucleus of freely moving cats increases REM sleep. *Brain Res,* 723**,** 223-7.

THEIS, L., BERENS, P., FROUDARAKIS, E., REIMER, J., ROMAN ROSON, M., BADEN, T., EULER, T., TOLIAS, A. S. & BETHGE, M. 2016. Benchmarking Spike Rate Inference in Population Calcium Imaging. *Neuron,* 90**,** 471-82.

THESTRUP, T., LITZLBAUER, J., BARTHOLOMAUS, I., MUES, M., RUSSO, L., DANA, H., KOVALCHUK, Y., LIANG, Y., KALAMAKIS, G., LAUKAT, Y., BECKER, S., WITTE, G., GEIGER, A., ALLEN, T., ROME, L. C., CHEN, T. W., KIM, D. S., GARASCHUK, O., GRIESINGER, C. & GRIESBECK, O. 2014. Optimized ratiometric calcium sensors for functional in vivo imaging of neurons and T lymphocytes. *Nat Methods,* 11**,** 175-82.

THOMAS, J. & BENOIT, O. 1967. Individualization of a sleep stage with slow waves and phasic activity. *Brain Res,* 5**,** 221-35.

TOBLER, I., DEBOER, T. & FISCHER, M. 1997. Sleep and sleep regulation in normal and prion protein-deficient mice. *J Neurosci,* 17**,** 1869-79.

TORTEROLO, P., YAMUY, J., SAMPOGNA, S., MORALES, F. R. & CHASE, M. H. 2001. GABAergic neurons of the laterodorsal and pedunculopontine tegmental nuclei of the cat express c-fos during carbachol-induced active sleep. *Brain Res,* 892**,** 309-19.

TSUNEMATSU, T., PATEL, A. A., ONKEN, A. & SAKATA, S. 2020. State-dependent brainstem ensemble dynamics and their interactions with hippocampus across sleep states. *Elife,* 9**,** e52244.

TSUTSUI, H., KARASAWA, S., OKAMURA, Y. & MIYAWAKI, A. 2008. Improving membrane voltage measurements using FRET with new fluorescent proteins. *Nat Methods,* 5**,** 683-5.

VAN DAM, D. & DE DEYN, P. P. 2011. Animal models in the drug discovery pipeline for Alzheimer's disease. *Br J Pharmacol,* 164**,** 1285-300.

VAN DORT, C. J., ZACHS, D. P., KENNY, J. D., ZHENG, S., GOLDBLUM, R. R., GELWAN, N. A., RAMOS, D. M., NOLAN, M. A., WANG, K., WENG, F. J., LIN, Y., WILSON, M. A. & BROWN, E. N. 2015. Optogenetic activation of cholinergic neurons in the PPT or LDT induces REM sleep. *Proc Natl Acad Sci U S A,* 112**,** 584-9.

VANDEPUTTE, M. & DE WEERD, A. 2003. Sleep disorders and depressive feelings: a global survey with the Beck depression scale. *Sleep Med,* 4**,** 343-5.

VANDERHEYDEN, W. M., LIM, M. M., MUSIEK, E. S. & GERSTNER, J. R. 2018. Alzheimer's Disease and Sleep-Wake Disturbances: Amyloid, Astrocytes, and Animal Models. *J Neurosci,* 38**,** 2901-2910.

VERRET, L., LEGER, L., FORT, P. & LUPPI, P. H. 2005. Cholinergic and noncholinergic brainstem neurons expressing Fos after paradoxical (REM) sleep deprivation and recovery. *Eur J Neurosci,* 21**,** 2488-504.

WAMSLEY, E. J., SHINN, A. K., TUCKER, M. A., ONO, K. E., MCKINLEY, S. K., ELY, A. V., GOFF, D. C., STICKGOLD, R. & MANOACH, D. S. 2013. The effects of eszopiclone on sleep spindles and memory consolidation in schizophrenia: a randomized placebo-controlled trial. *Sleep,* 36**,** 1369-76.

WAMSLEY, E. J., TUCKER, M. A., SHINN, A. K., ONO, K. E., MCKINLEY, S. K., ELY, A. V., GOFF, D. C., STICKGOLD, R. & MANOACH, D. S. 2012. Reduced sleep spindles and spindle coherence in schizophrenia: mechanisms of impaired memory consolidation? *Biol Psychiatry,* 71**,** 154-61.

WANG, H. L. & MORALES, M. 2009. Pedunculopontine and laterodorsal tegmental nuclei contain distinct populations of cholinergic, glutamatergic and GABAergic neurons in the rat. *Eur J Neurosci,* 29**,** 340-58.

WEBER, F., CHUNG, S., BEIER, K. T., XU, M., LUO, L. & DAN, Y. 2015. Control of REM sleep by ventral medulla GABAergic neurons. *Nature,* 526**,** 435-8.

WEBER, F. & DAN, Y. 2016. Circuit-based interrogation of sleep control. *Nature,* 538**,** 51-59.

WEBER, F., HOANG DO, J. P., CHUNG, S., BEIER, K. T., BIKOV, M., SAFFARI DOOST, M. & DAN, Y. 2018. Regulation of REM and Non-REM Sleep by Periaqueductal GABAergic Neurons. *Nat Commun,* 9**,** 354.

WEBSTER, H. H. & JONES, B. E. 1988. Neurotoxic lesions of the dorsolateral pontomesencephalic tegmentum-cholinergic cell area in the cat. II. Effects upon sleep-waking states. *Brain Res,* 458**,** 285-302.

WELSH, D. K., TAKAHASHI, J. S. & KAY, S. A. 2010. Suprachiasmatic nucleus: cell autonomy and network properties. *Annu Rev Physiol,* 72**,** 551-77.

WESTERBERG, C. E., LUNDGREN, E. M., FLORCZAK, S. M., MESULAM, M. M., WEINTRAUB, S., ZEE, P. C. & PALLER, K. A. 2010. Sleep influences the severity of memory disruption in amnestic mild cognitive impairment: results from sleep self-assessment and continuous activity monitoring. *Alzheimer Dis Assoc Disord,* 24**,** 325-33.

WETTER, T. C., COLLADO-SEIDEL, V., POLLMACHER, T., YASSOURIDIS, A. & TRENKWALDER, C. 2000. Sleep and periodic leg movement patterns in drug-free patients with Parkinson's disease and multiple system atrophy. *Sleep,* 23**,** 361-7.

WILLIAMS, J. A., COMISAROW, J., DAY, J., FIBIGER, H. C. & REINER, P. B. 1994. State-dependent release of acetylcholine in rat thalamus measured by in vivo microdialysis. *J Neurosci,* 14**,** 5236-42.

WIMO, A., GUERCHET, M., ALI, G. C., WU, Y. T., PRINA, A. M., WINBLAD, B., JONSSON, L., LIU, Z. & PRINCE, M. 2017. The worldwide costs of dementia 2015 and comparisons with 2010. *Alzheimers Dement,* 13**,** 1-7.

WISOR, J. P., EDGAR, D. M., YESAVAGE, J., RYAN, H. S., MCCORMICK, C. M., LAPUSTEA, N. & MURPHY, G. M., JR. 2005. Sleep and circadian abnormalities in a transgenic mouse model of Alzheimer's disease: a role for cholinergic transmission. *Neuroscience,* 131**,** 375-85.

WOOLF, N. J. & BUTCHER, L. L. 1986. Cholinergic systems in the rat brain: III. Projections from the pontomesencephalic tegmentum to the thalamus, tectum, basal ganglia, and basal forebrain. *Brain Res Bull,* 16**,** 603-37.

WORLD HEALTH ORGANIZATION. 2019a. *Dementia Key Facts* [Online]. Available: https://www.who.int/news-room/fact-sheets/detail/dementia [Accessed 2019, November 4].

WORLD HEALTH ORGANIZATION. 2019b. *Dementia Key Facts* [Online]. https://www.who.int/news-room/fact-sheets/detail/dementia. Available: https://www.who.int/news-room/fact-sheets/detail/dementia [Accessed 2019, November 4 2019].

WU, J., LIU, L., MATSUDA, T., ZHAO, Y., REBANE, A., DROBIZHEV, M., CHANG, Y. F., ARAKI, S., ARAI, Y., MARCH, K., HUGHES, T. E., SAGOU, K., MIYATA, T., NAGAI, T., LI, W. H. & CAMPBELL, R. E. 2013. Improved orange and red Ca(2)+/- indicators and photophysical considerations for optogenetic applications. *ACS Chem Neurosci,* 4**,** 963-72.

WULFF, K., GATTI, S., WETTSTEIN, J. G. & FOSTER, R. G. 2010. Sleep and circadian rhythm disruption in psychiatric and neurodegenerative disease. *Nat Rev Neurosci,* 11**,** 589-99.

WURTS, S. & EDGAR, D. 2000. Circadian and Homeostatic Control of Rapid Eye Movement (REM) Sleep: Promotion of REM Tendency by the Suprachiasmatic Nucleus. *The Journal of neuroscience : the official journal of the Society for Neuroscience,* 20.

XU, W., TAN, C., ZOU, J., CAO, X. & TAN, L. 2020. Sleep Problems and Risk of All-Cause Cognitive Decline or Dementia: An Updated Systematic Review and Meta-Analysis. *Journal of neurology, neurosurgery, and psychiatry,* 91.

YAKSI, E. & FRIEDRICH, R. W. 2006. Reconstruction of firing rate changes across neuronal populations by temporally deconvolved Ca2+ imaging. *Nat Methods,* 3**,** 377-83.

YANG, H. H., ST-PIERRE, F., SUN, X., DING, X., LIN, M. Z. & CLANDININ, T. R. 2016. Subcellular Imaging of Voltage and Calcium Signals Reveals Neural Processing In Vivo. *Cell,* 166**,** 245-57.

YANG, Y., LIU, N., HE, Y., LIU, Y., GE, L., ZOU, L., SONG, S., XIONG, W. & LIU, X. 2018. Improved calcium sensor GCaMP-X overcomes the calcium channel perturbations induced by the calmodulin in GCaMP. *Nat Commun,* 9**,** 1504.

YLINEN, A., BRAGIN, A., NADASDY, Z., JANDO, G., SZABO, I., SIK, A. & BUZSAKI, G. 1995. Sharp wave-associated high-frequency oscillation (200 Hz) in the intact hippocampus: network and intracellular mechanisms. *J Neurosci,* 15**,** 30-46.

ZALOCUSKY, K. A., RAMAKRISHNAN, C., LERNER, T. N., DAVIDSON, T. J., KNUTSON, B. & DEISSEROTH, K. 2016. Nucleus accumbens D2R cells signal prior outcomes and control risky decision-making. *Nature,* 531**,** 642-6.

ZARIWALA, H. A., BORGHUIS, B. G., HOOGLAND, T. M., MADISEN, L., TIAN, L., DE ZEEUW, C. I., ZENG, H., LOOGER, L. L., SVOBODA, K. & CHEN, T. W. 2012. A Cre-dependent GCaMP3 reporter mouse for neuronal imaging in vivo. *J Neurosci,* 32**,** 3131-41.

ZENG, H. & MADISEN, L. 2012. Mouse transgenic approaches in optogenetics. *Prog Brain Res,* 196**,** 193-213.

ZHANG, B., VEASEY, S. C., WOOD, M. A., LENG, L. Z., KAMINSKI, C., LEIGHT, S., ABEL, T., LEE, V. M. & TROJANOWSKI, J. Q. 2005. Impaired rapid eye movement sleep in the Tg2576 APP murine model of Alzheimer's disease with injury to pedunculopontine cholinergic neurons. *Am J Pathol,* 167**,** 1361-9.

ZHANG, Z., FERRETTI, V., GUNTAN, I., MORO, A., STEINBERG, E. A., YE, Z., ZECHARIA, A. Y., YU, X., VYSSOTSKI, A. L., BRICKLEY, S. G., YUSTOS, R., PILLIDGE, Z. E., HARDING, E.

C., WISDEN, W. & FRANKS, N. P. 2015. Neuronal ensembles sufficient for recovery sleep and the sedative actions of alpha2 adrenergic agonists. *Nat Neurosci,* 18**,** 553-561.

ZHAO, Y., ARAKI, S., WU, J., TERAMOTO, T., CHANG, Y. F., NAKANO, M., ABDELFATTAH, A. S., FUJIWARA, M., ISHIHARA, T., NAGAI, T. & CAMPBELL, R. E. 2011. An expanded palette of genetically encoded Ca(2)(+) indicators. *Science,* 333**,** 1888-91.